Erasmus+ PROGRAMME,

KEY ACTION: Cooperation for innovation and the exchange of good practices,

ACTION: Strategic Partnerships

FIELD: Strategic Partnerships for higher education, CALL: 2015

INNOVATIVE EUROPEAN STUDIES ON RENEWABLE ENERGY SYSTEMS

2015-1-TR01-KA203-021342

Partners:

- GAZI UNIVERSITESI, Turkey
- UNIVERSITATEA DIN PITESTI, Romania
- KLAIPEDA UNIVERSITY, Lithuania
- UNIVERSITA DEGLI STUDI DI PERUGIA, Italy
- UNIVERSIDAD DEL PAIS VASCO, Spain

Erasmus+

INNOVATIVE EUROPEAN STUDIES ON RENEWABLE ENERGY SYSTEMS

Hybrid Power Sources

Mitigation techniques of the fuel cell current ripple

Extremum Seeking Control Schemes

Global Maximum Power Point Tracking algorithms for Photovoltaic arrays under Partially Shaded Conditions

Nicu BIZON

University of Pitesti,

Pitesti, Romania

Fuel Cell Hybrid Power Source: Part I

The first part of presentation is focused on:

- ✓**Techniques of passive mitigation for the low frequency (LF) fuel cell current ripple;**
- ✓**Analysis of the appropriate structures for inverter system powered by Fuel Cell (FC);**
- ✓**Comparison of the filtering results obtained by passive filters on high voltage (HV) and/or low voltage (LV) bus;**
- ✓**Evaluation of the LF fuel cell current ripple in the Fuel Cell Hybrid Power Sources (FCHPS).**
- ✓**Validation of the modelling by measurements performed in different experiments.**

Fuel Cell Hybrid Power Source: Part I

The presentation is organized as follows:

- **Section 1 briefly presents the main concepts related to Hybrid Power Source (HPS) supplied by a Proton Exchange Membrane Fuel Cell (PEMFC) stack. The FCHPS architecture proposed to be analyzed is shown, too.**
- **Section 2 is focused in the ripple evaluation on fuel cell (FC) HPS.**
  - **The current ripple will be measured by Ripple Factor (RF);**
  - **The power spectrum is shown to evaluate the FC current ripple.**
  - **The behavior of the FCHPS subsystems under dynamic load is presented, too.**
- **Section 3 presents few Matlab-Simulink© simulations to be compared with the experimental results obtained. The use of the Low Pass Passive Filter on both HV DC and LV DC buses is analyzed by simulation and experiment.**
- **Last section concludes the presentation.**

INTRODUCTION

The Polymer Electrolyte Membrane Fuel Cell (PEMFC) is one of the most promising solutions to be utilized in Energy Generation System (EGS) and portable applications because of its relatively lightweight and small size, ease of construction, fast start-up and low operating temperature. Unfortunately, the relatively short PEMFC's life represents for moment a major obstacle to their commercialization.

Inverter current ripple represents the main factor responsible for performance degradation of PEMFC energy efficiency and PEMFC life cycle. The PEMFC low frequency (LF) current ripple affects in much measure the PEMFC life cycle, causes hysteretic losses and subsequently more fuel consumption. Recent experimental results shown that LF inverter current ripple contributes with up to 10% reduction in the available output power

- The USA National Energy Technology Laboratory published the following guidelines for fuel cell current ripple:
- *100/120 Hz ripple < 15% from 10% to 100% load, not to exceed 0.6 A for lighter loads;*
- *50/60 Hz ripple: < 10% from 10% to 100% load, not to exceed 0.4 A for lighter loads;*
- *10 kHz and above: < 60% from 10% to 100% load, not to exceed 2.4 A for lighter loads;*
- *>100/120 Hz to <10 kHz, limit linearly interpolated between the 120 Hz and 10 kHz limits;*
- *Transients below 50/60 Hz represent "load following" action of the system, and should track the maximum available current signal from the fuel cell to within 1% for purposes of both fuel cell integrity and efficiency.*

INTRODUCTION

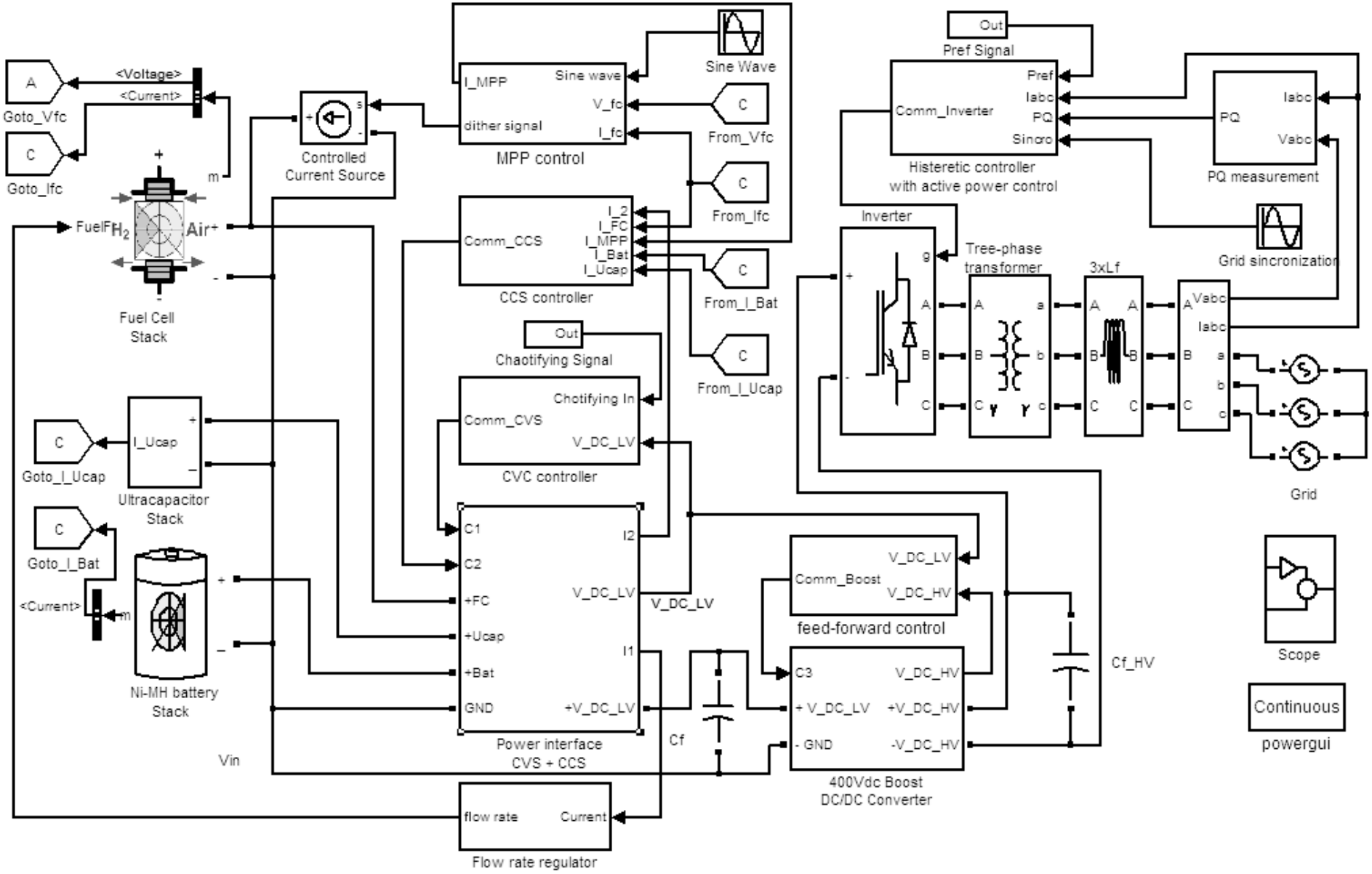

Figure 1. A typical EGS topology

INTRODUCTION

The new current ripple limits are given experimentally as Ripple Factor (RF) for different frequency bands (for example, LF RF must be up to 5% from 10% to 100% load, not to exceed 0.5 A for lighter loads; HF RF must be up to 40% from 10% to 100% load, not to exceed 2 A for lighter loads).

Usually, 100Hz fuel cell current ripple and other LF harmonics appear in operation of grid inverter system and HF harmonics are generated by PWM switching control of DC-DC converter.

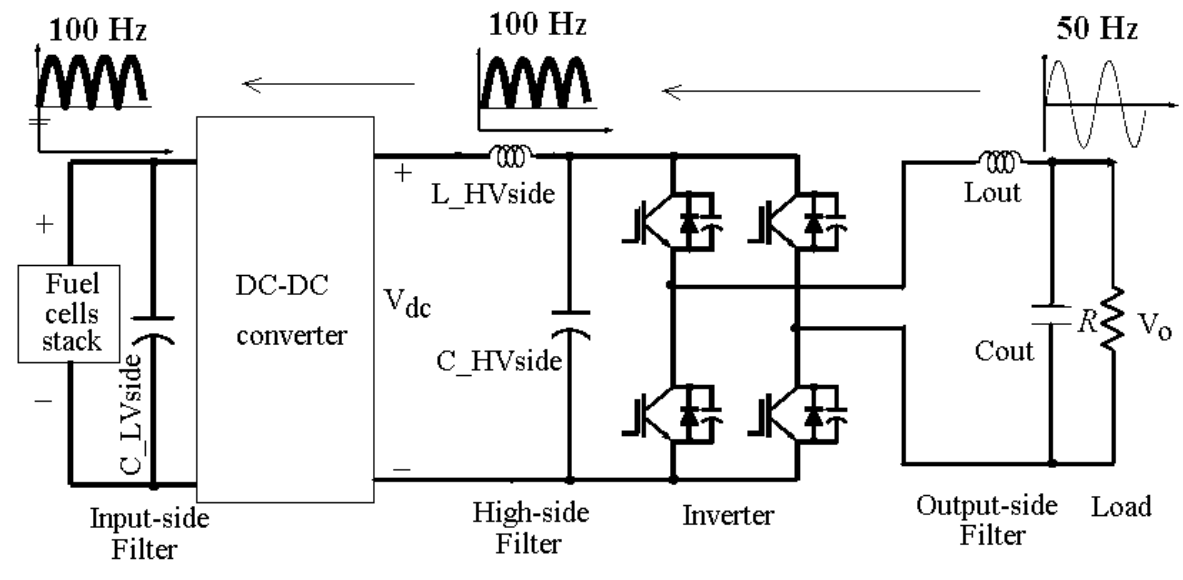

Figure 2. Back propagation of the current ripple through the fuel cell inverter system

Transients below grid frequency (50/60 Hz) represent "load following" action of the EGS control, and should track the Maximum Power Point (MPP) signal from the PEMFC to within 1% for purposes of both PEMFC reliability and efficiency (see figure 1)

INTRODUCTION

Fuel cell current ripple could be mitigated by passive filtering on the HV DC and LV DC buses or/and by an adequate active control techniques applied to different energy conversion stages. Typical structures of the basic EGS are presented in figures 3 a-c.

Figure 3a. Basic EGS topology with the inverter system powered by a fuel cell HPS

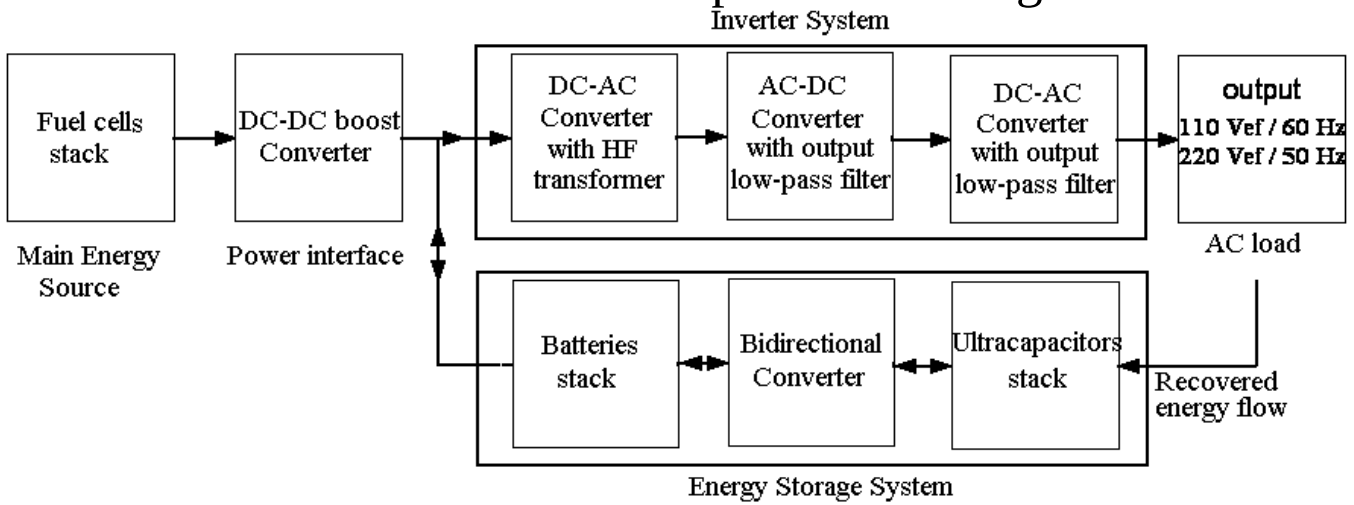

Figure 3b. Inverter system powered directly from the fuel cell stack

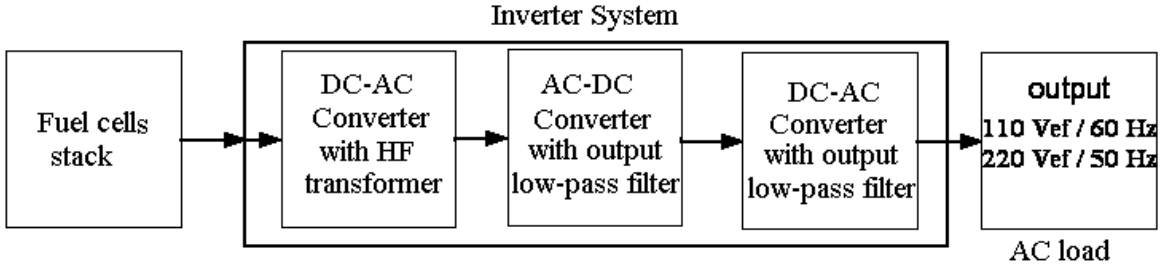

Figure 3c. Two-stage inverter system powered directly from the fuel cell stack

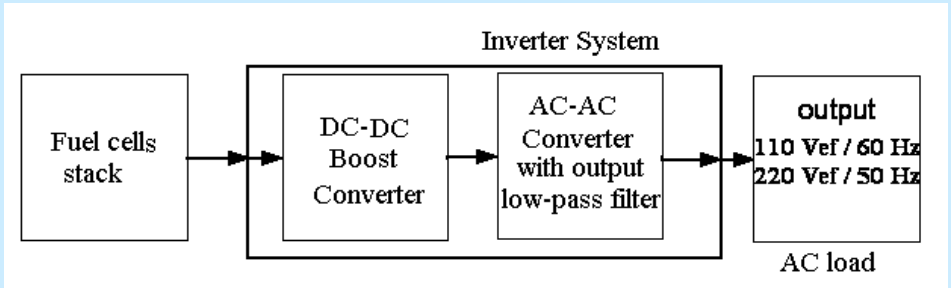

INTRODUCTION

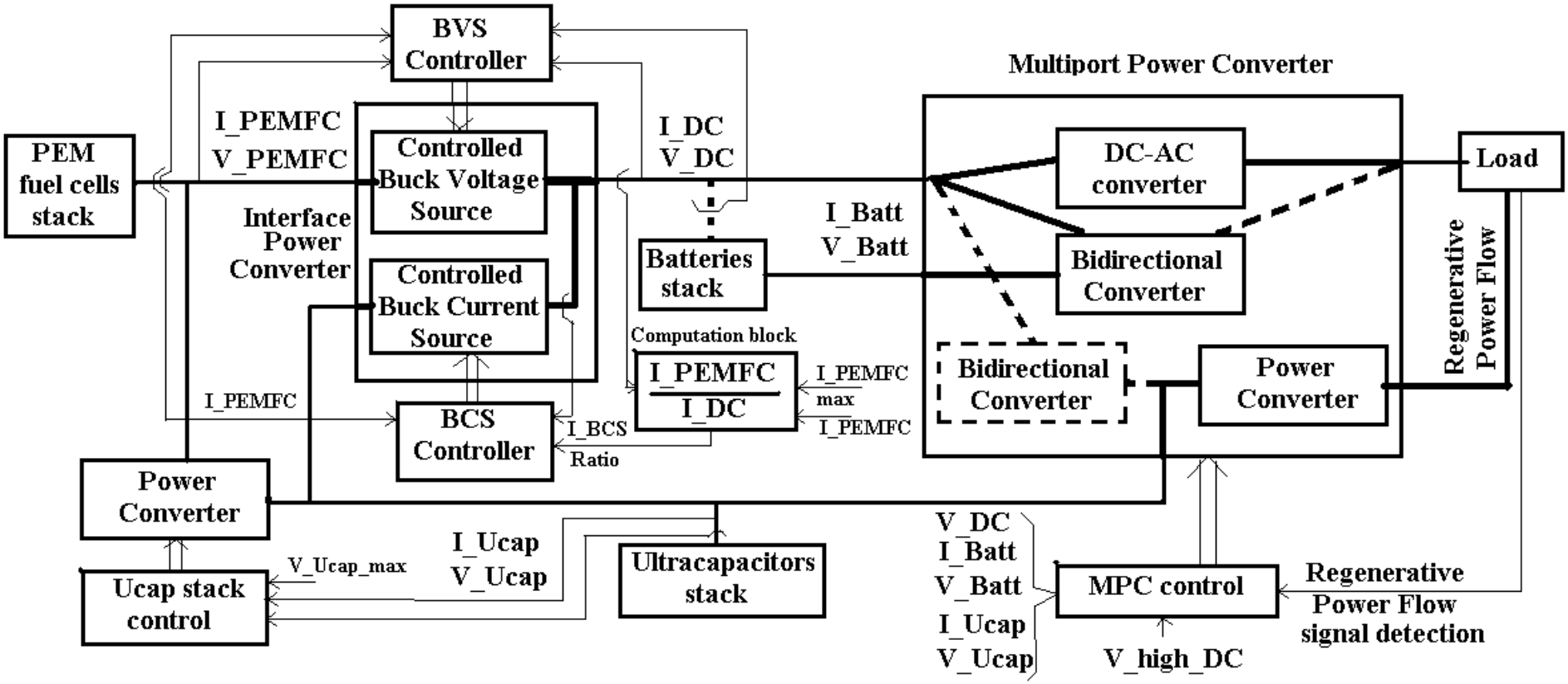

Figure 4. Multiport EGS topology with power interface for ripple mitigation

INTRODUCTION

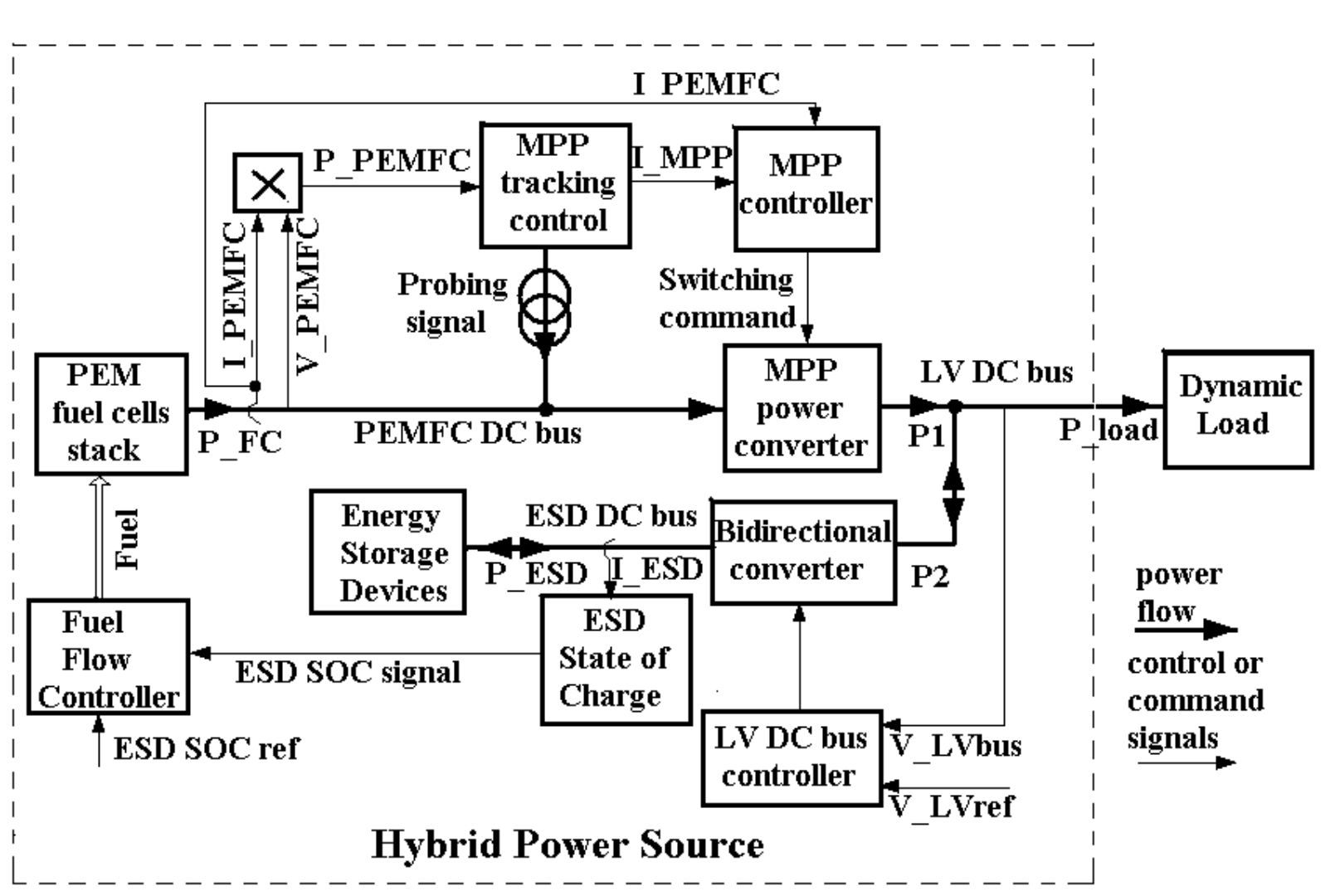

Figure 5. Hybrid power source topology with MPP tracking control

INTRODUCTION

$$V_{cell} = V_{cell\_o} - \left(j_{fc} + j_n\right) \cdot A \cdot R_{ohmic} - A_{act} \cdot \ln\left(\frac{j_{fc} + j_n}{j_0}\right) + B_{conc} \cdot \ln\left(1 - \frac{j_{fc} + j_n}{j_{\max}}\right)$$

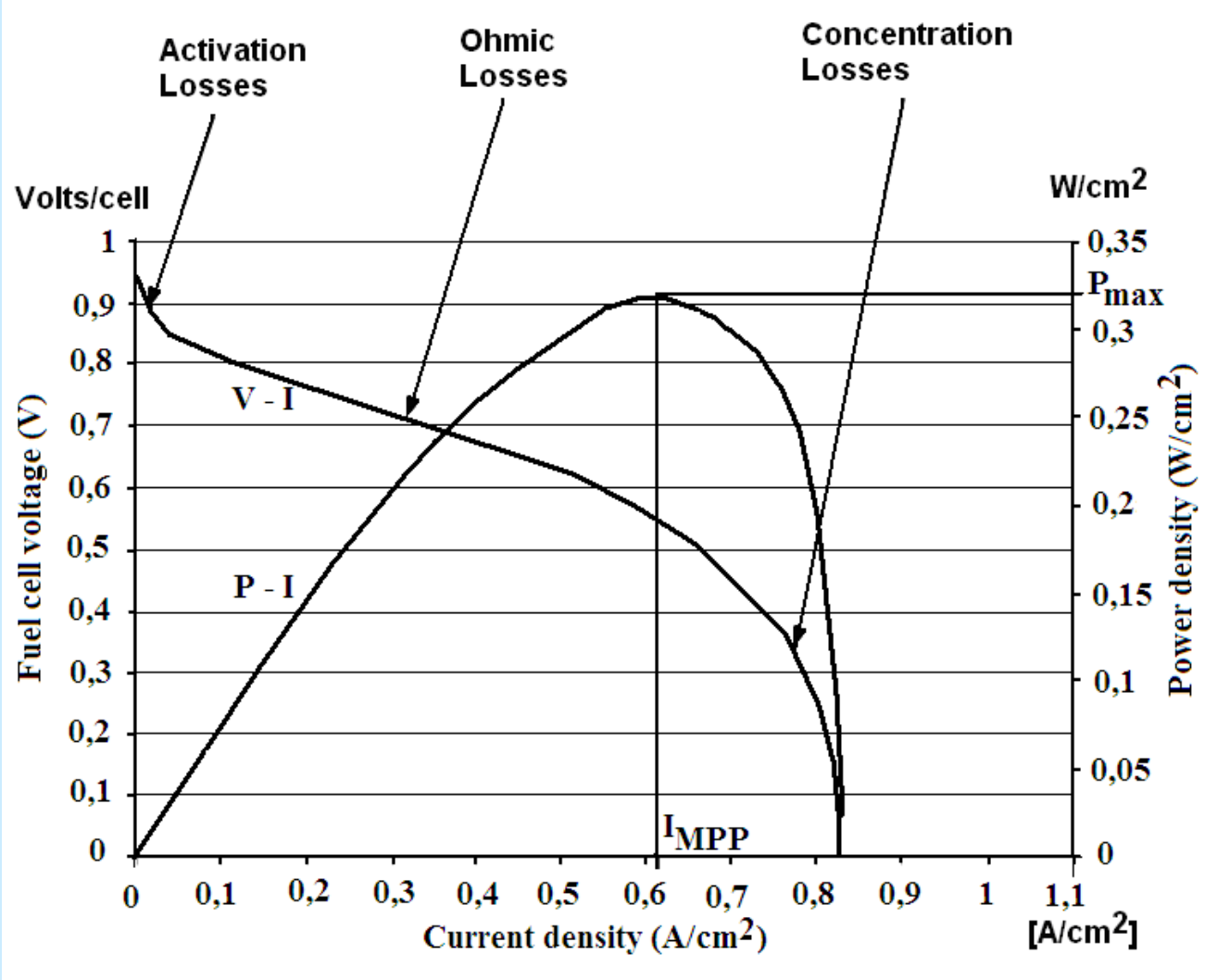

Figure 6. Polarization and power characteristics for a PEMFC (a single cell)

INTRODUCTION

$$v_{fc}(t) = N_{fc} \cdot v_{cell}(u),\ u = j(t) = \frac{i(t)}{A},\ \frac{I(s)}{I_{fc}(s)} = \frac{\exp(-s \cdot \tau_{fc})}{1 + T_{fc} \cdot s}$$

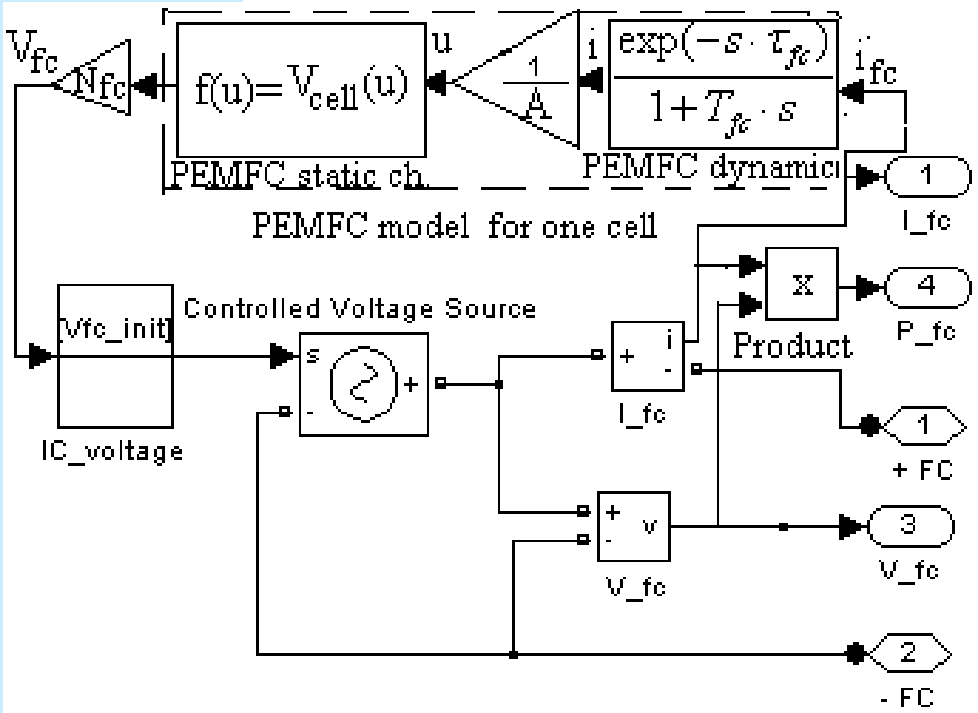

Parameter (*for* $\lambda = 1$ *and* $P_{sys} = 2$ *atm*)	Relation (2)
E^o [Volts]	1.2
j_n [mA/cm^2]	2
j_0 [mA/cm^2]	0.067
j_{max} [A/cm^2]	0.9
R_{Ohmic} [Ω]	0.03
A_{act} [Volts]	0.06
B_{conc} [Volts]	0.05

Relation (3):

f(u)=(1.2-(u+0.002)*A*0.03-0.06*log((u+0.002)/0.000067)+0.05*log(1-(u+0.002)/0.9))

where u=i/A, i[A] and A[cm^2]

Figure 7a. Proposed PEMFC macro-model that uses a transfer function for modelling the PEMFC dynamic

INTRODUCTION

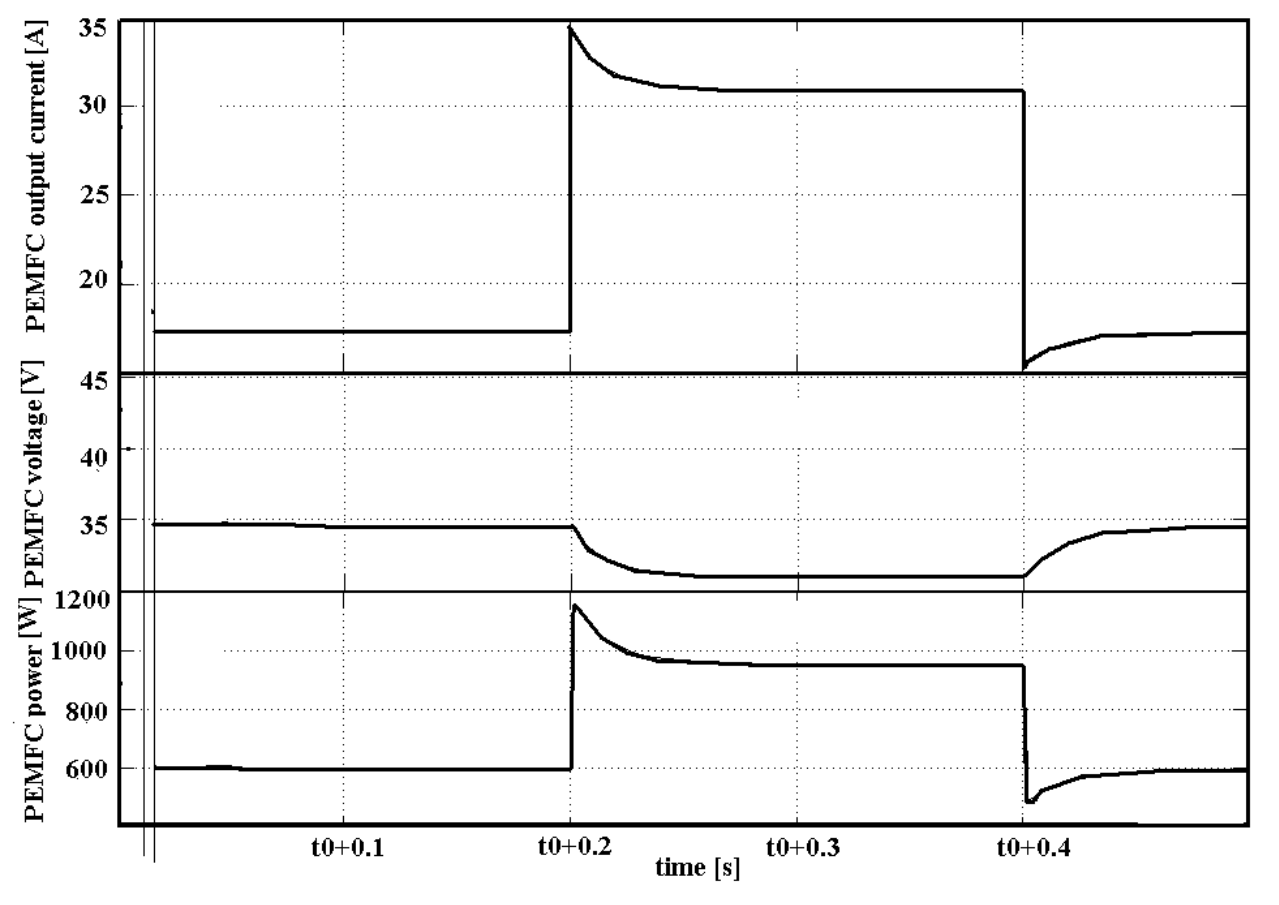

Figure 7b. Behaviour under load pulse for Nexa PEMFC model that uses a transfer function to model its dynamic

RIPPLE EVALUATION ON FUEL CELL EGS

The current ripple will be measured by the Ripple Factor (RF): $RF_I = \frac{I_{Max} - I_{Min}}{I_{(AV)}}$

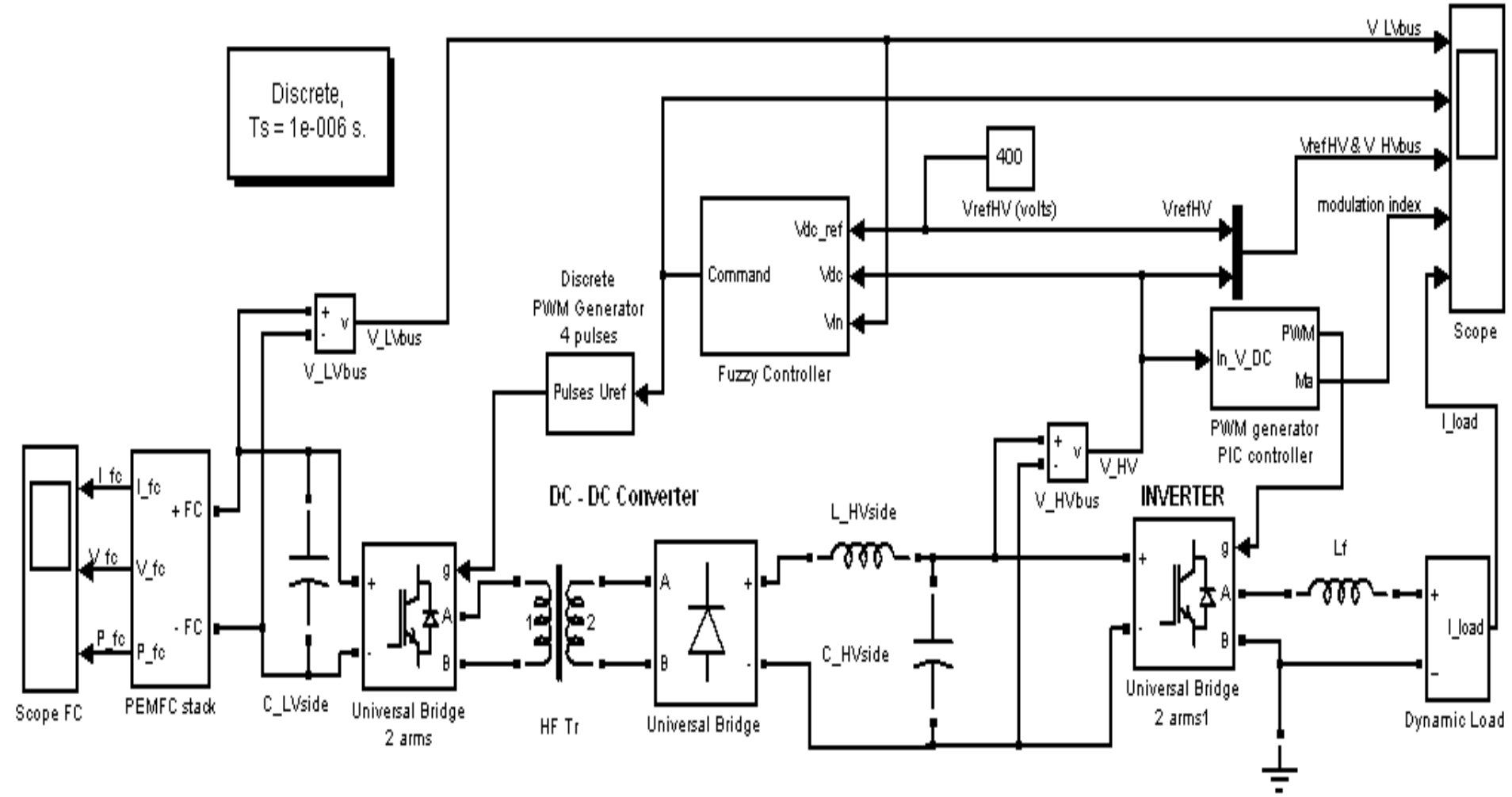

Figure 8. Matlab-Simulink diagram of the analyzed EGS that use a mono-phase inverter and a full-bridge DC-DC converter

RIPPLE EVALUATION ON FUEL CELL EGS

Power Spectrum of the Inverter System: output voltage and current

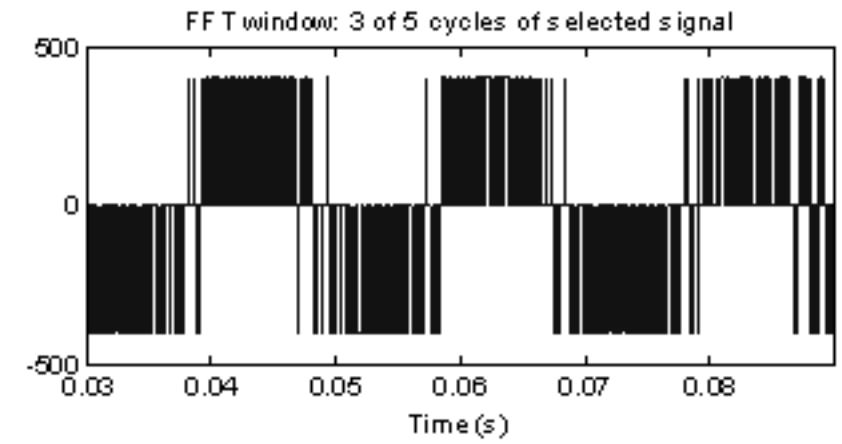

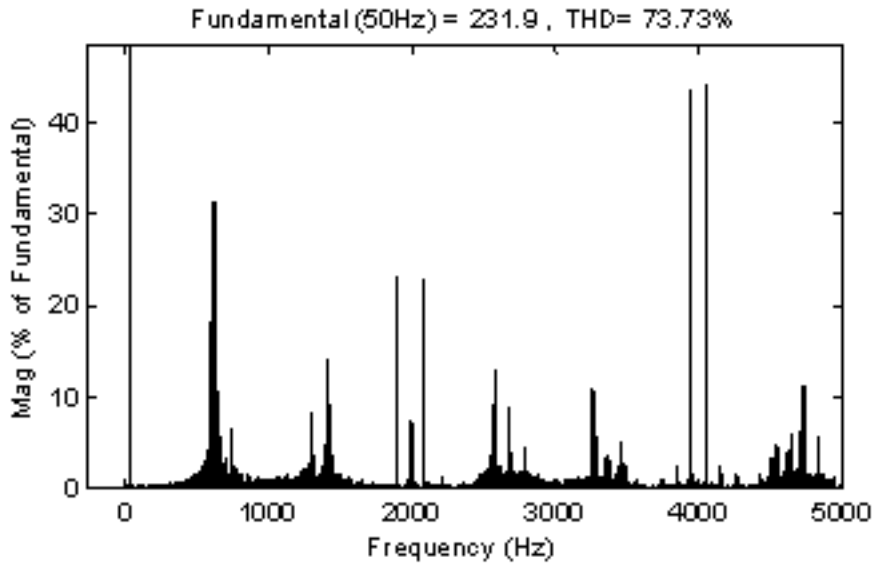

Figure 9. Output voltage of the inverter with pure sine PWM command: signal in time (top) and associate power spectrum (bottom)

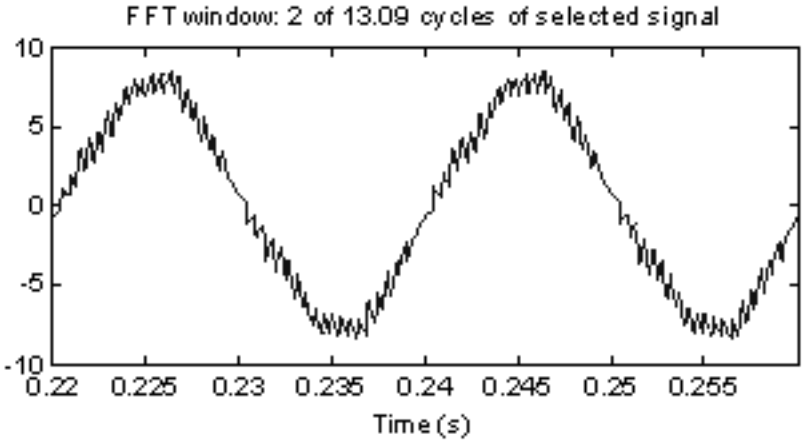

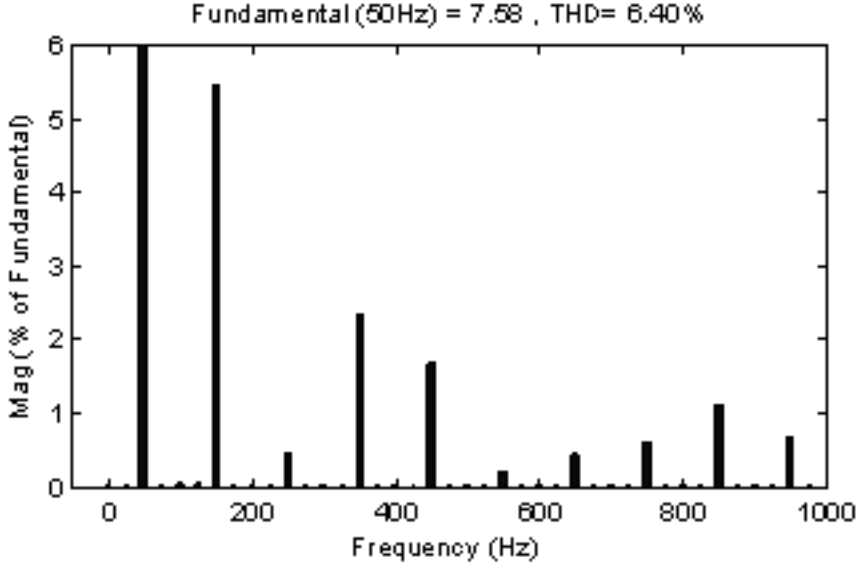

Figure 10. Output current of the inverter with pure sine PWM command: signal in time (top) and associate power spectrum (bottom)

RIPPLE EVALUATION ON FUEL CELL EGS

Power Spectrum of the Inverter System – input voltage and current

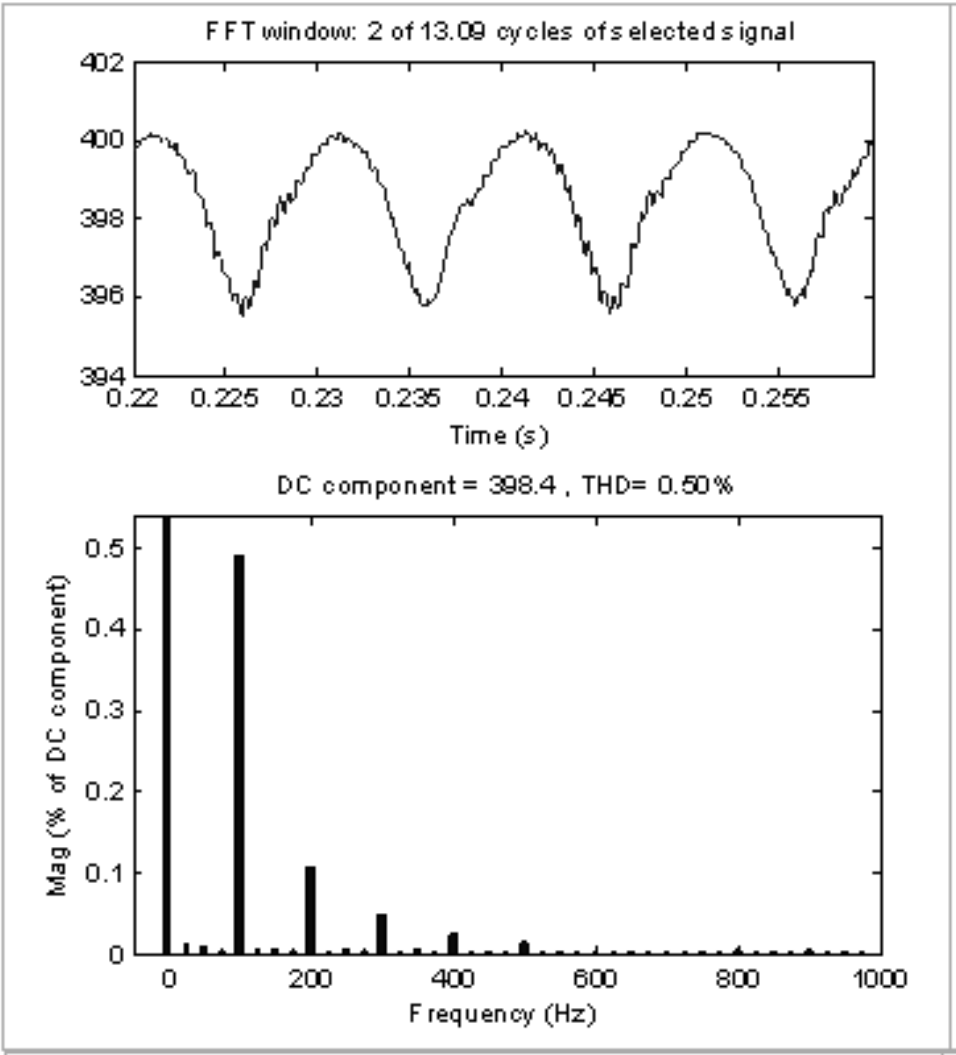

Figure 11. Input voltage of the inverter with pure sine PWM command: signal in time (top) and associate power spectrum (bottom)

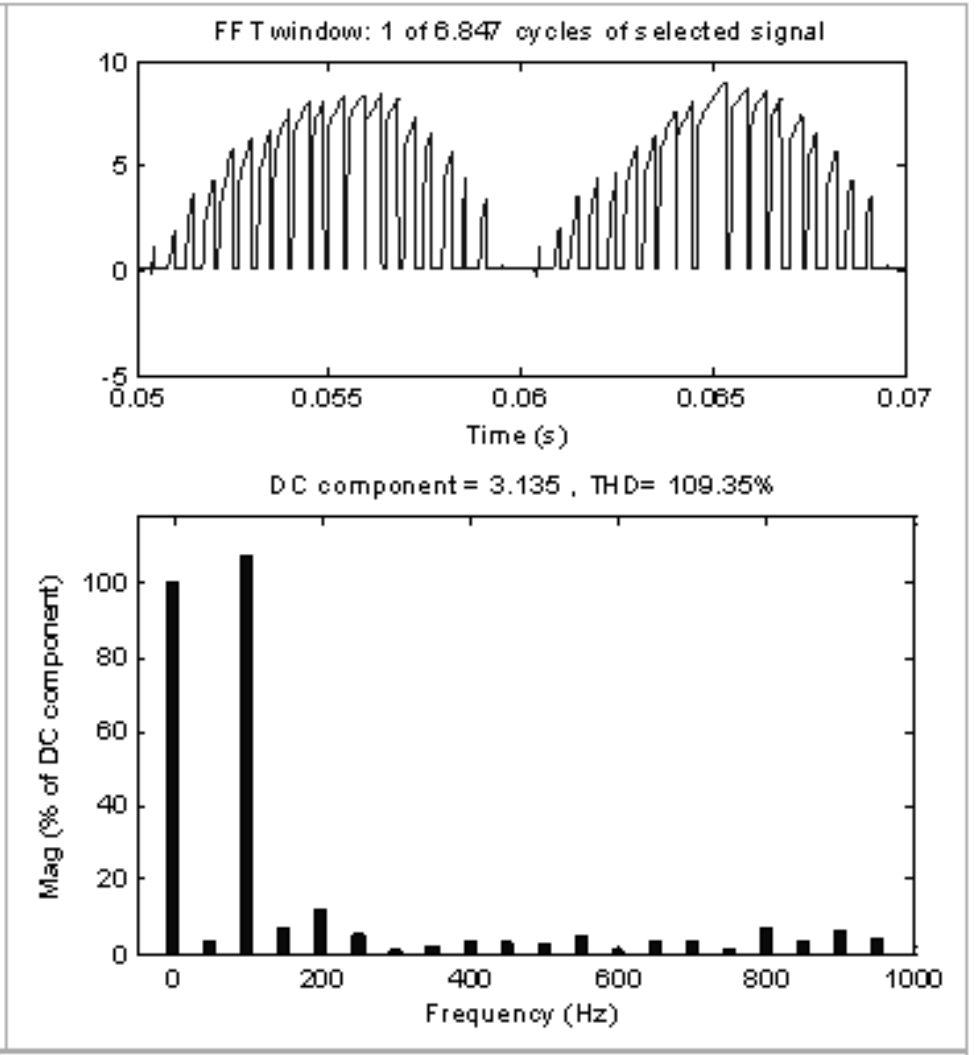

Figure 12. Input current of the inverter with pure sine PWM command: signal in time (top) and associate power spectrum (bottom)

RIPPLE EVALUATION ON FUEL CELL EGS

Power Spectrum of the Inverter System – output voltage and input current

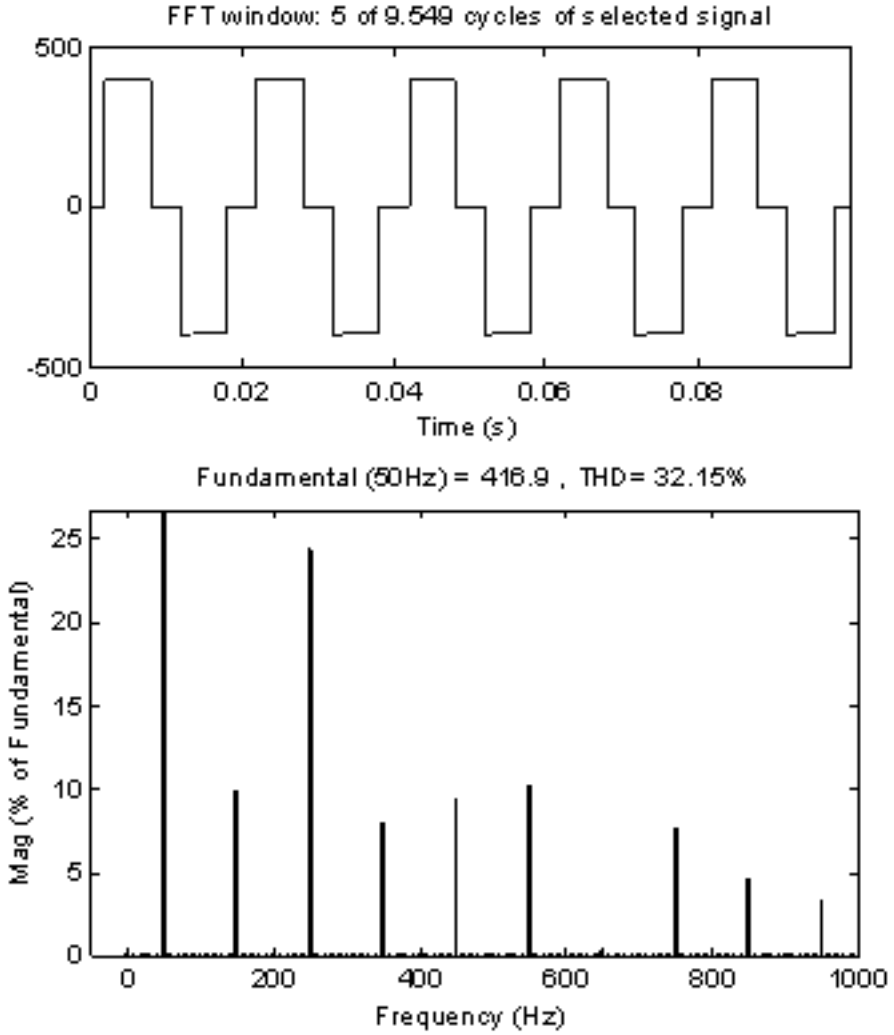

Figure 13. Output voltage of the inverter with modified sine PWM command: signal in time (top) and associate power spectrum (bottom)

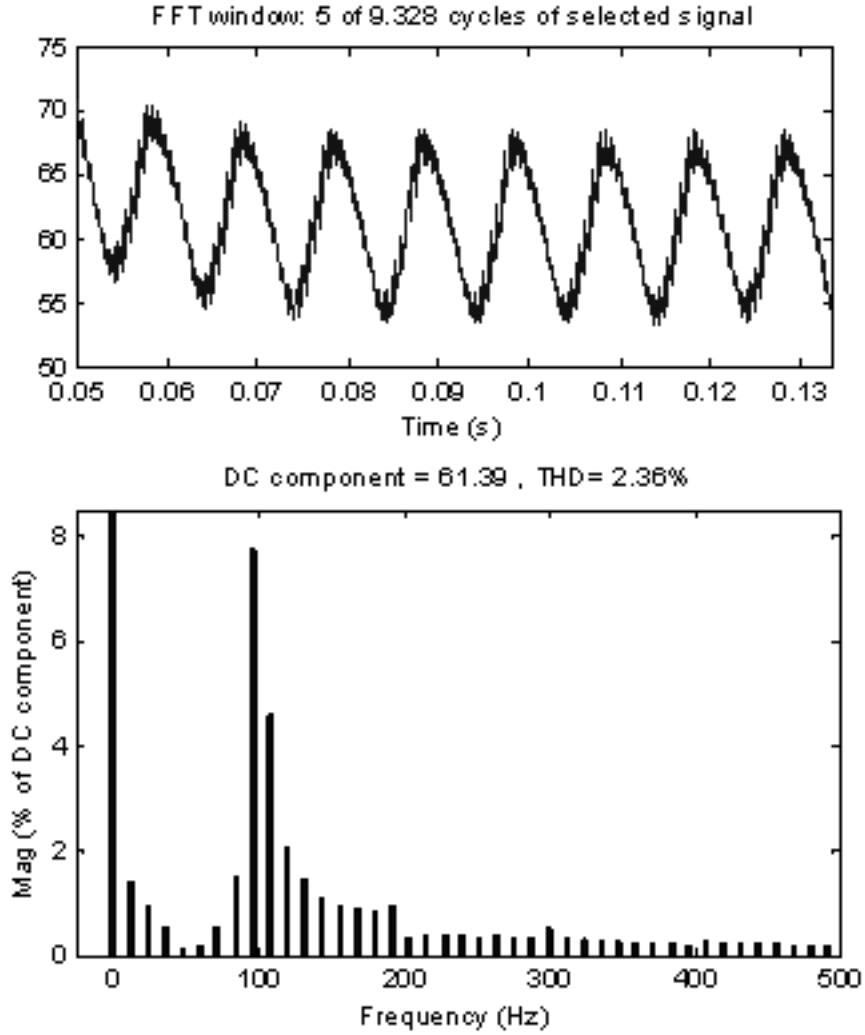

Figure 14. Input current of the inverter with modified sine PWM command: signal in time (top) and associate power spectrum (bottom)

RIPPLE EVALUATION ON FUEL CELL EGS

Behaviour of the Inverter System under dynamic load: output voltage and input current

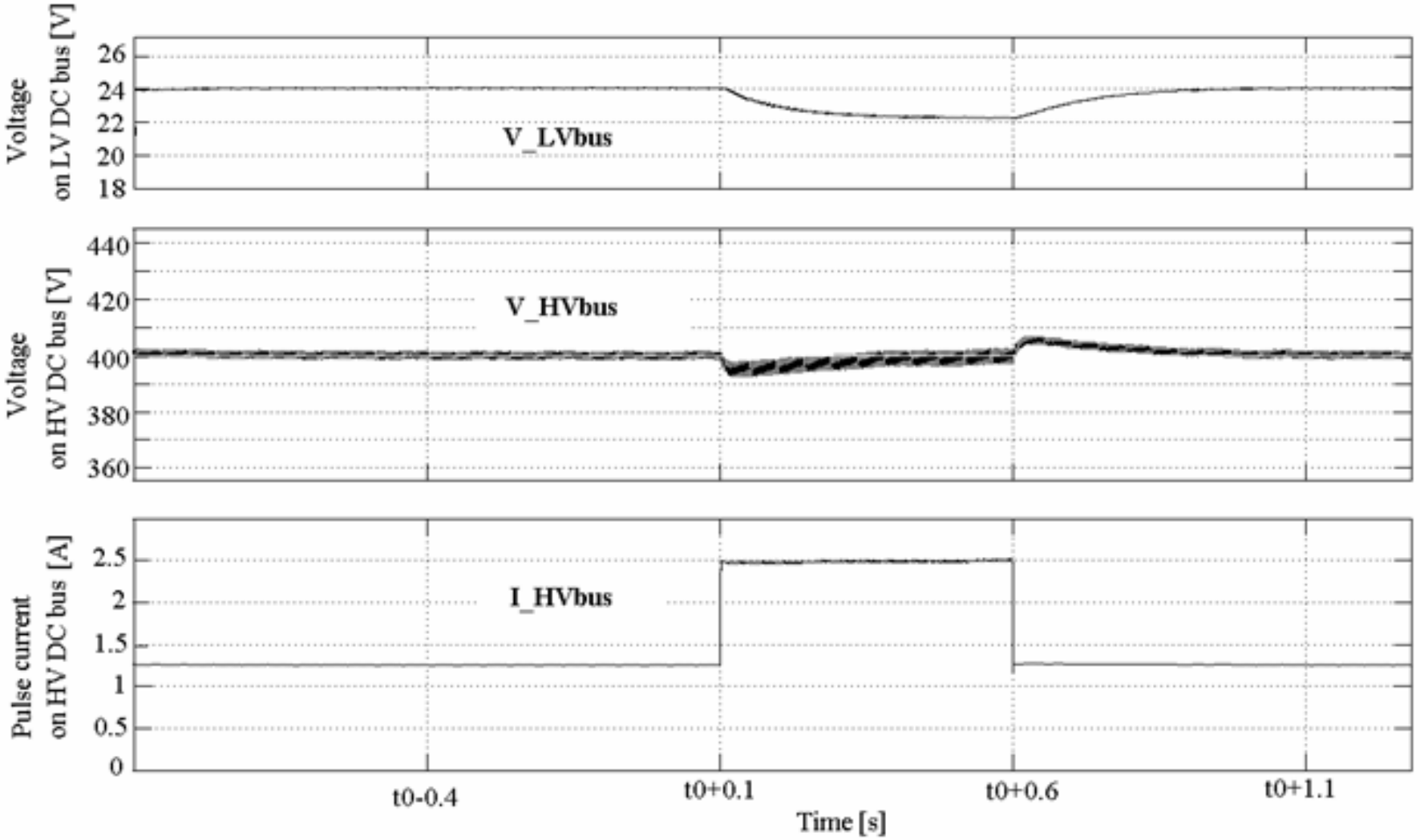

Figure 15. The effect of the current pulse, I_HVbus (bottom), on HV DC voltage, V_HVbus (middle), and LV DC voltage, V_LVbus (top)

RIPPLE EVALUATION ON FUEL CELL EGS

Behaviour of the Fuel Cell System under dynamic load

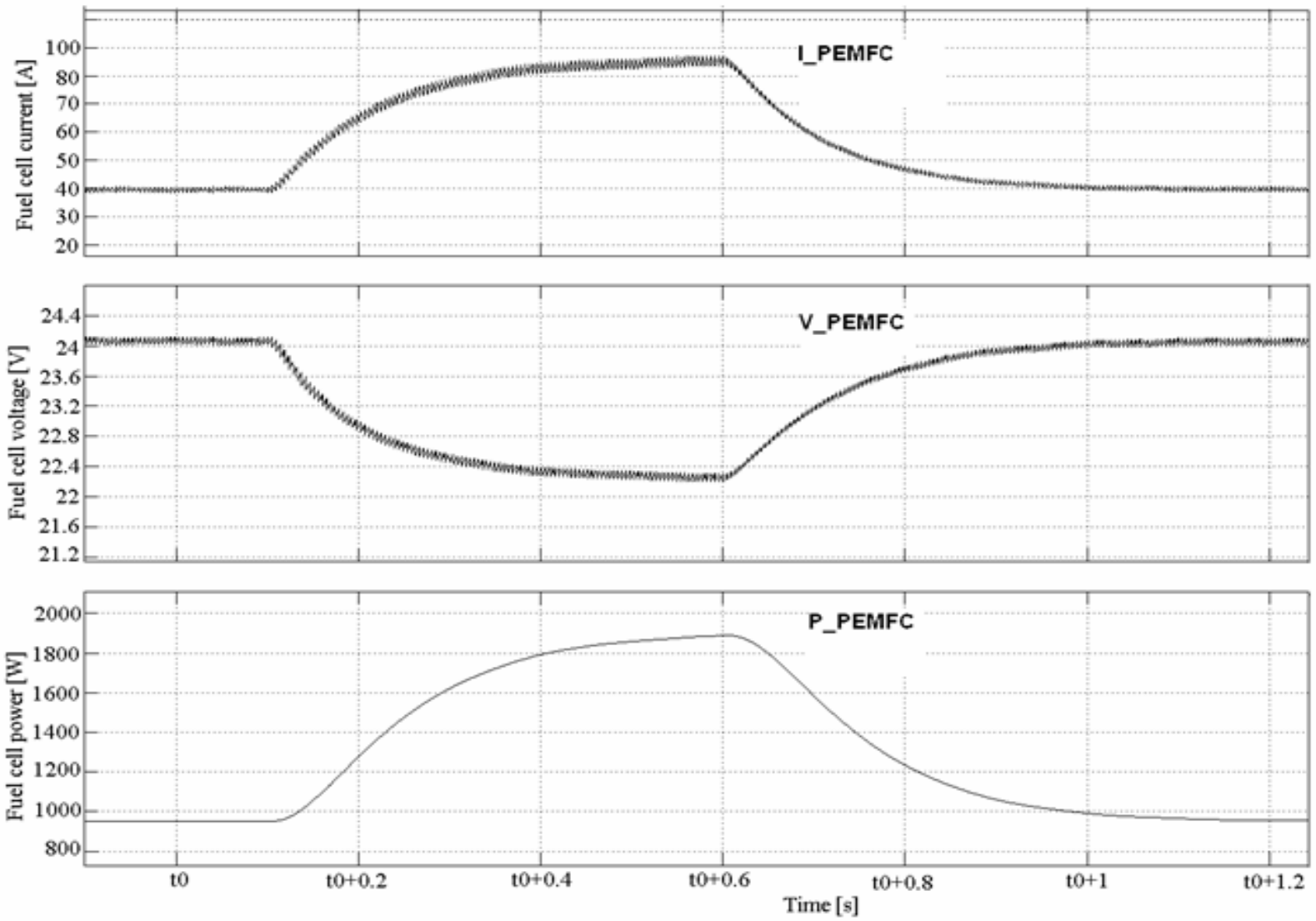

Figure 16. PEMFC stack behaviour under load pulse: power, P_PEMFC (bottom), voltage, V_ PEMFC (middle), and LV DC voltage, I_ PEMFC (top)

RIPPLE EVALUATION ON FUEL CELL EGS

Use of the Low Pass Passive Filter on HV DC bus

$$C_{HVside} = \frac{I_{1(RMS)HVside}}{4\pi f_{100}\Delta V_{HVside}}$$

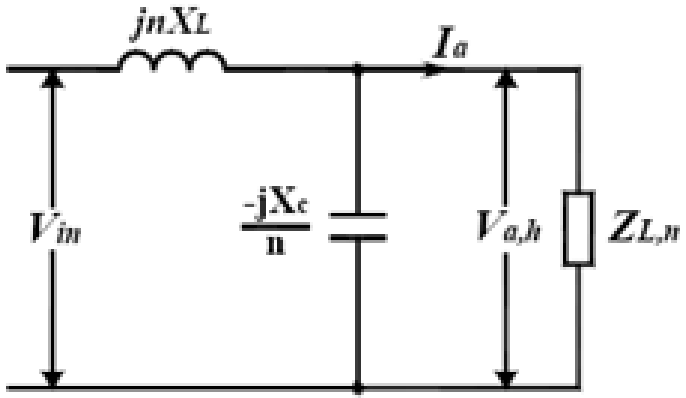

Figure 33 Low pass passive filter for harmonic number *n*

The LF current harmonics normally appears on the LV DC bus. Without use of other power interfaces (likes boost converter or passive/active filter) to mitigate the ripple, this represents the fuel cell current ripple. The PEMFC current ripple factor is about of (20A/70A)·100≅28%, much higher than the new value required (5% or even 3%). For example, considering $I_{1(p\text{-}p)HVside}$ =17A and an imposed voltage ripple value ΔV_{HVside}= 5V (see figure 15), these lead to a capacity of about 2mF. For this value of capacity, the influence of the inductance value on current ripple mitigation was tested for values in range 0.1 mH-10 mH.

If not otherwise stated, then L_{HVside}=0.5 mH.

Some simulations are shown in next slides

RIPPLE EVALUATION ON FUEL CELL EGS

Use of the Low Pass Passive Filter on HV DC bus under dynamic load

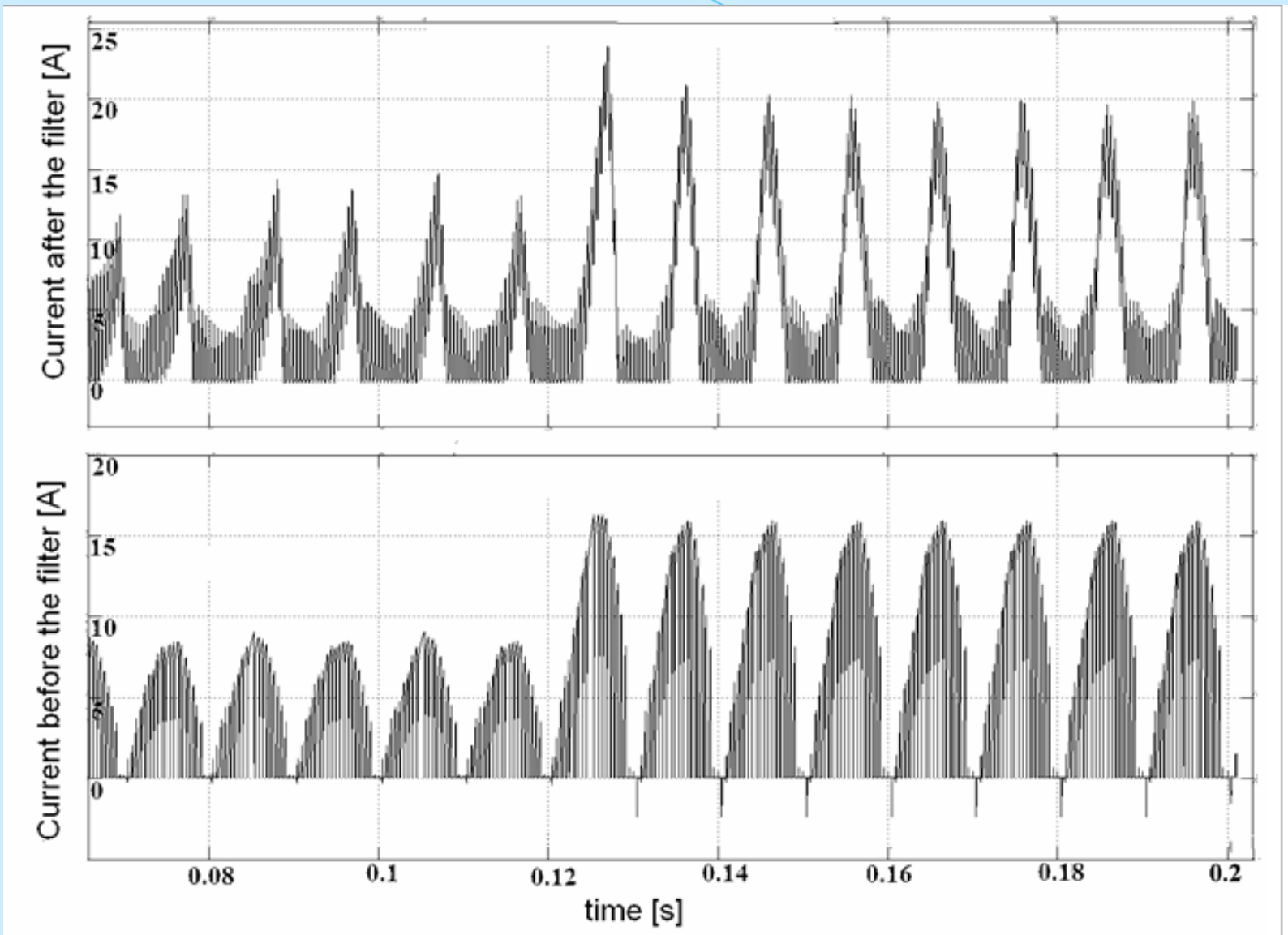

Figure 34. The current on the HV DC bus, I_{HVside}, after (top) and before (bottom) the passive filter

RIPPLE EVALUATION ON FUEL CELL EGS

Use of the Low Pass Passive Filter on HV DC bus under dynamic load

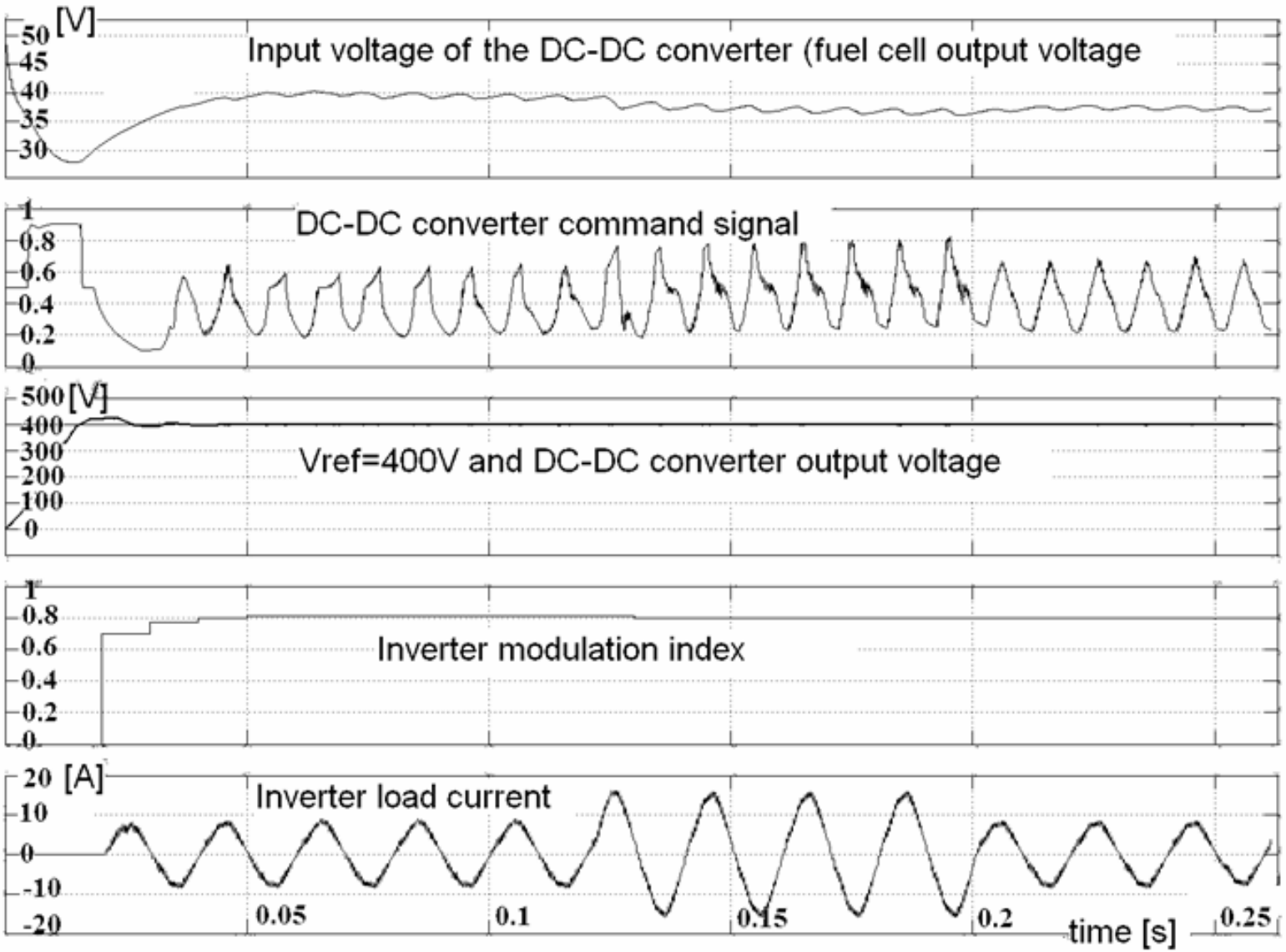

Figure 35. Significant waveforms for function of the DC-DC converter and inverter

RIPPLE EVALUATION ON FUEL CELL EGS

Use of the Low Pass Passive Filter on HV DC bus under dynamic load

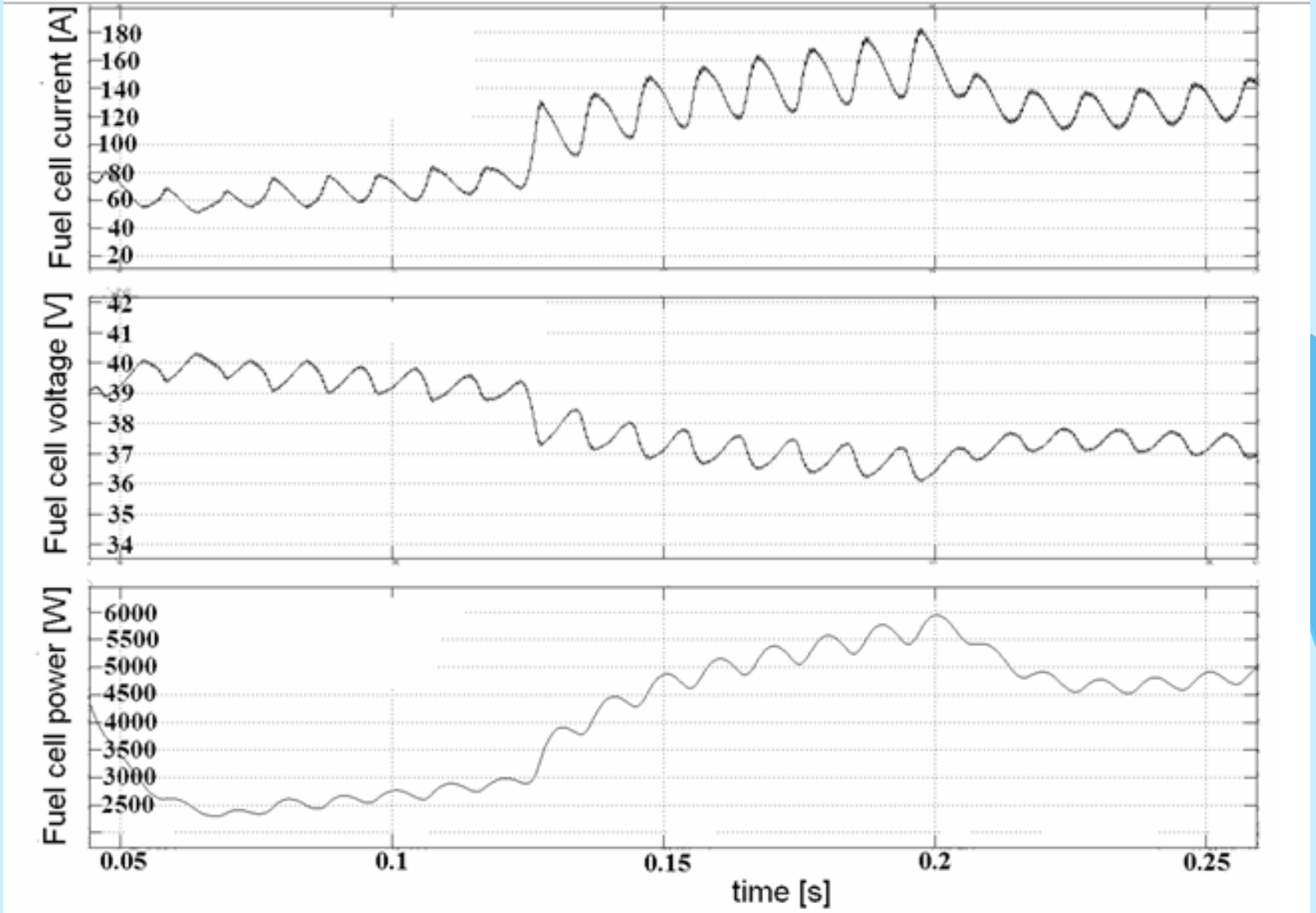

Figure 36. Fuel cell current, voltage and power

RIPPLE EVALUATION ON FUEL CELL EGS

Use of the Low Pass Passive Filter on HV DC bus: power spectrum

We can remark that 100Hz current harmonic is less dependent of the load power level.

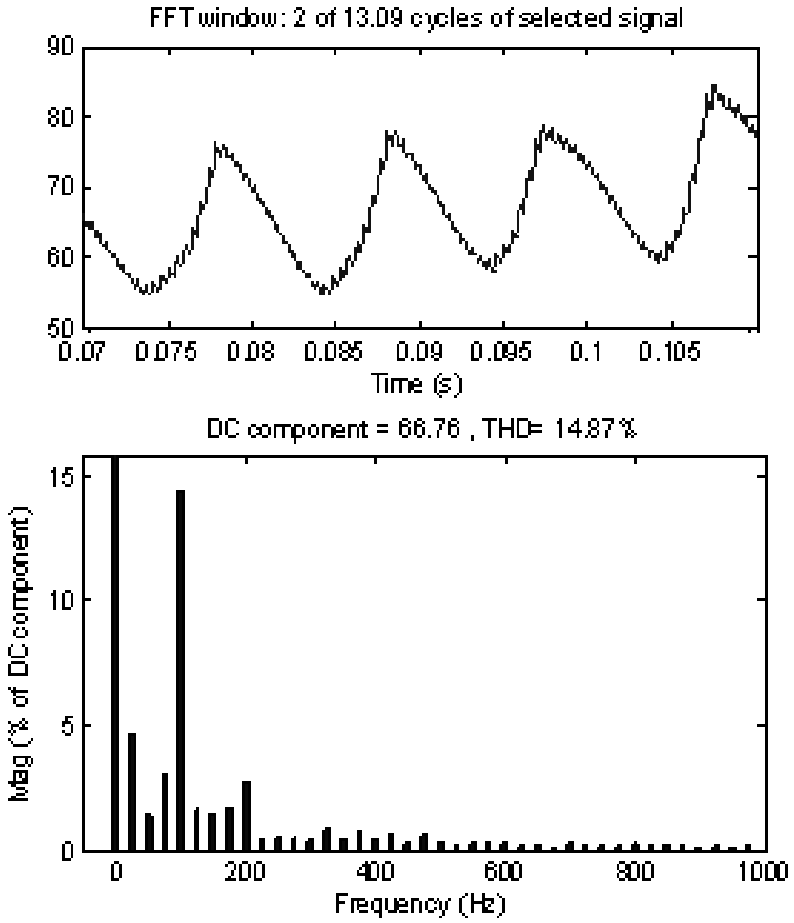

Figure 37. Fuel cell current (top) and its power spectrum (bottom) for 2.5kW load (L_{HVside}=0.2mH, C_{HVside}=2mF)

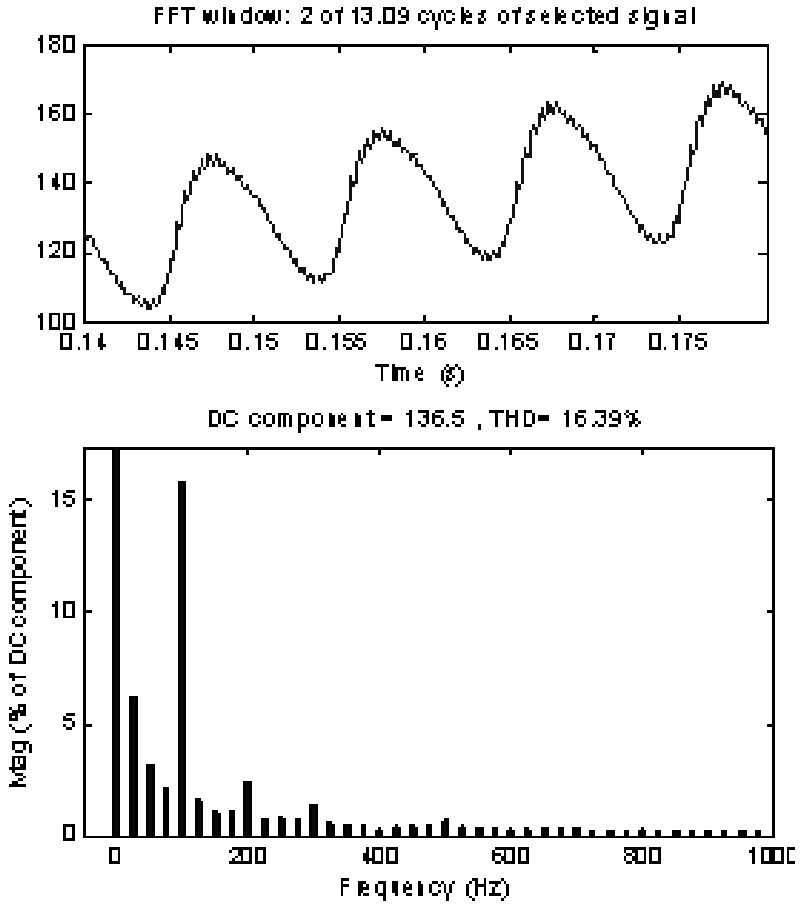

Figure 38. Fuel cell current (top) and its power spectrum (bottom) for 5kW load (L_{HVside}=0.2mH, C_{HVside}=2mF)

RIPPLE EVALUATION ON FUEL CELL EGS

Use of the Low Pass Passive Filter on HV DC bus: power spectrum

Note that a passive filter of 2nd order in comparison with one of first order type not brings major improvements

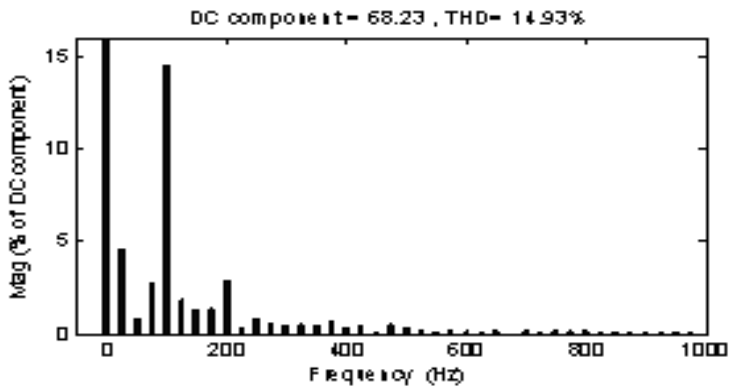

Figure 39. Power spectrum of the fuel cell current for 2.5kW load (L_{HVside} =2mH, C_{HVside} =2mF)

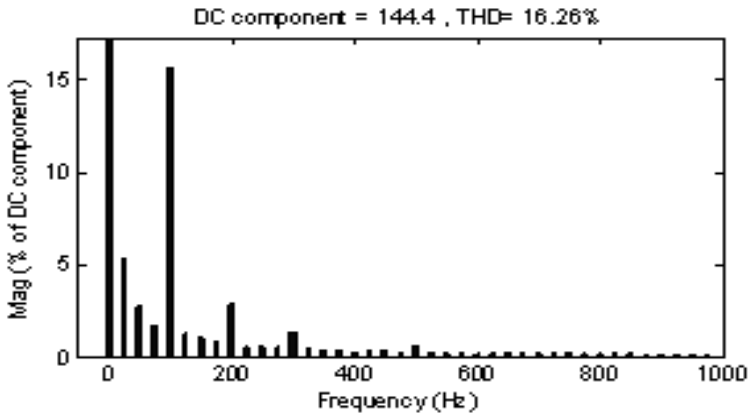

Figure 40. Power spectrum of the fuel cell current for 5kW load (L_{HVside} =2mH, C_{HVside} =2mF)

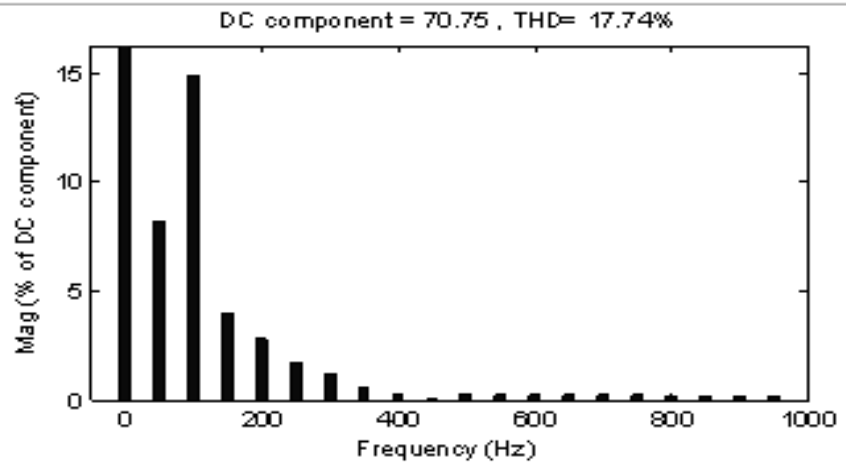

Figure 41. Power spectrum of the fuel cell current for 2.5kW load (L_{HVside} =20mH, C_{HVside} =2mF)

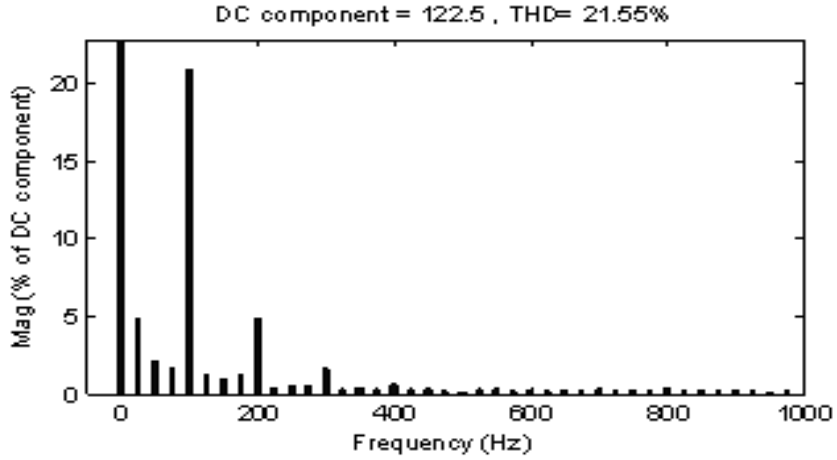

Figure 42. Power spectrum of the fuel cell current for 5kW load (L_{HVside} =20mH, C_{HVside} =2mF)

RIPPLE EVALUATION ON FUEL CELL EGS

Use of the Low Pass Passive Filter on LV DC Bus

Note that ripple factor for FC current could be about 5% for high values of passive components: L_{HVside}=0.5 mH C_{HVside}=2 mF and C_{LVside} = 70 mF (bulky components)

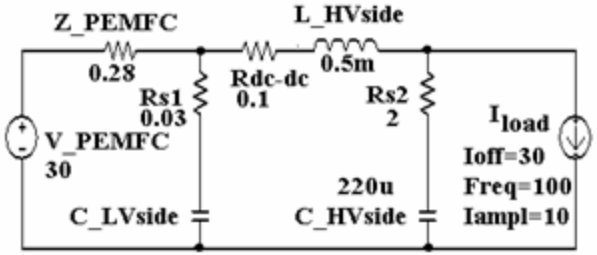

Figure 44. Current ripple model of DC-DC converter

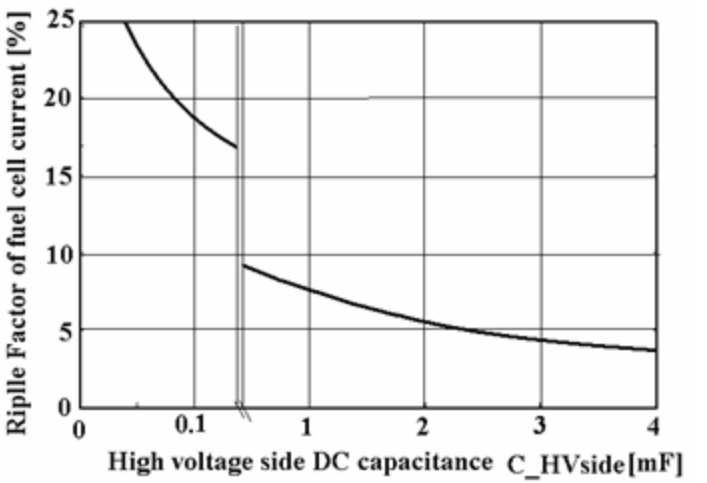

Figure 43. RF of PEMFC current vs. C_{HVside}

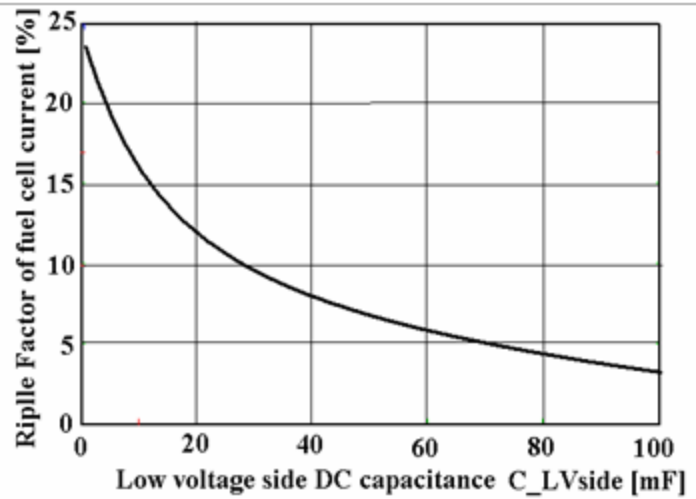

Figure 45. RF of PEMFC current vs. C_{LVside}

RIPPLE EVALUATION ON FUEL CELL EGS

Use of the Low Pass Passive Filters - EXPERIMENTAL RESULTS

- In this section the experimental results concerning the current ripple mitigation are presented for the inverter systems with different command: full wave (figure 46), modified sine PWM (figure 47) and pure sine PWM (figure 48), respectively.
- Firstly, the laboratory tests were performed using as DC power souce a lead-sealed battery (instead of PEMFC stack) and a variable resistive load, with maximum power of 1 kW. It is know that battery has characteristics and behaviour operation similar to the PEMFC stack, because both DC sources are based on specific but appropriate electro-chemical processes.
- To validate the above results, some experiments were repeated on a 2kW PEMFC stack, available at the National Research and Development Institute for Cryogenics and Isotopic Technologies - ICSI Rm.Valcea, Romania.
- Experimental results are presented in figure 49, 50 and 51 for inverters system without passive filter at input, which use a command type of full wave, modified sine PWM (with phase-shifted) and pure sine PWM, respectively.

RIPPLE EVALUATION ON FUEL CELL EGS

Use of the Low Pass Passive Filters - EXPERIMENTAL RESULTS

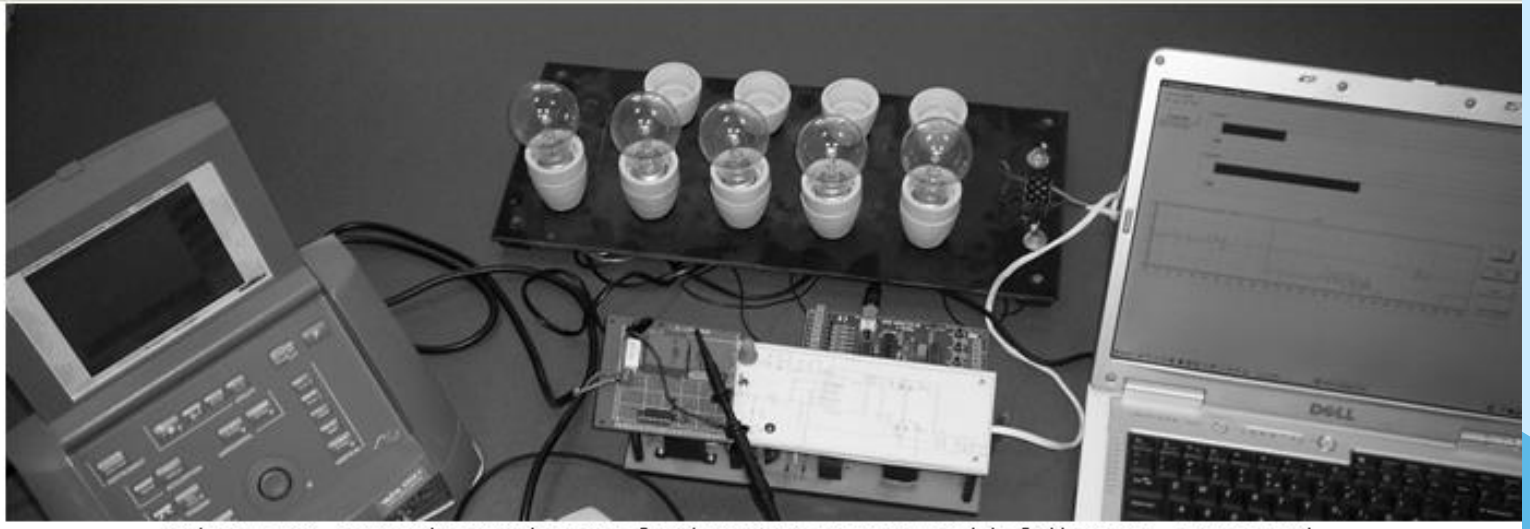

Figure 46. Experimental setup for inverter systems with full wave command

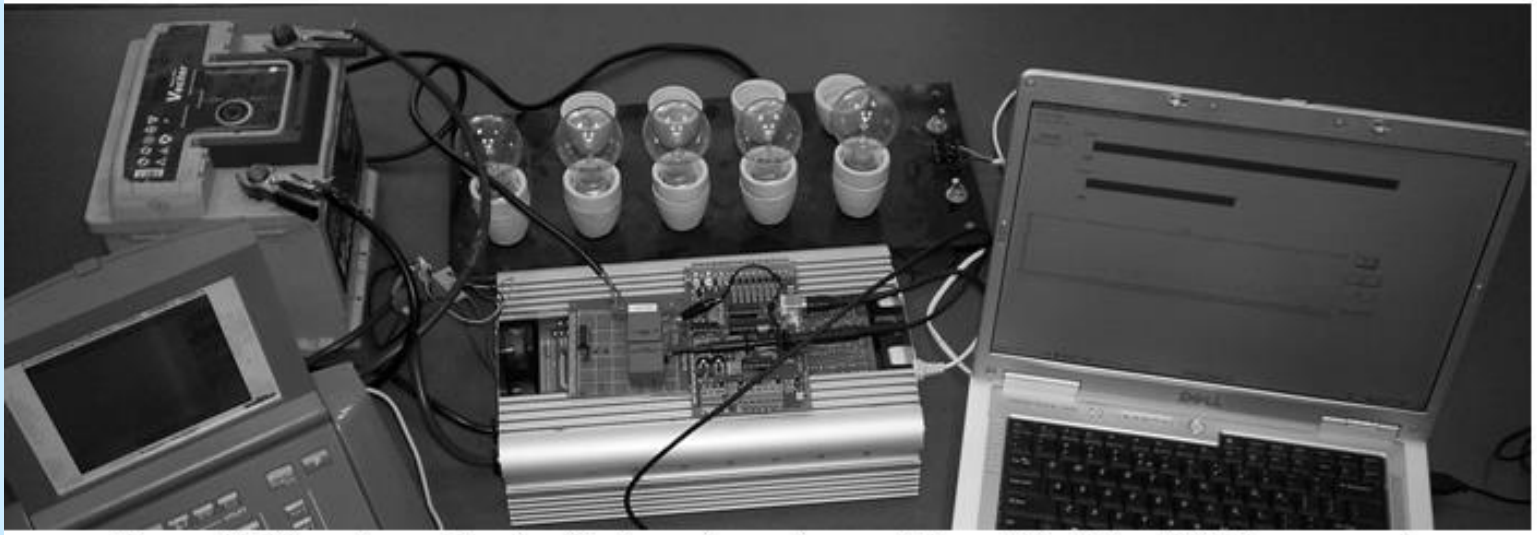

Figure 47. Experimental setup for inverter systems with modified sine PWM command

RIPPLE EVALUATION ON FUEL CELL EGS

Use of the Low Pass Passive Filters - EXPERIMENTAL RESULTS

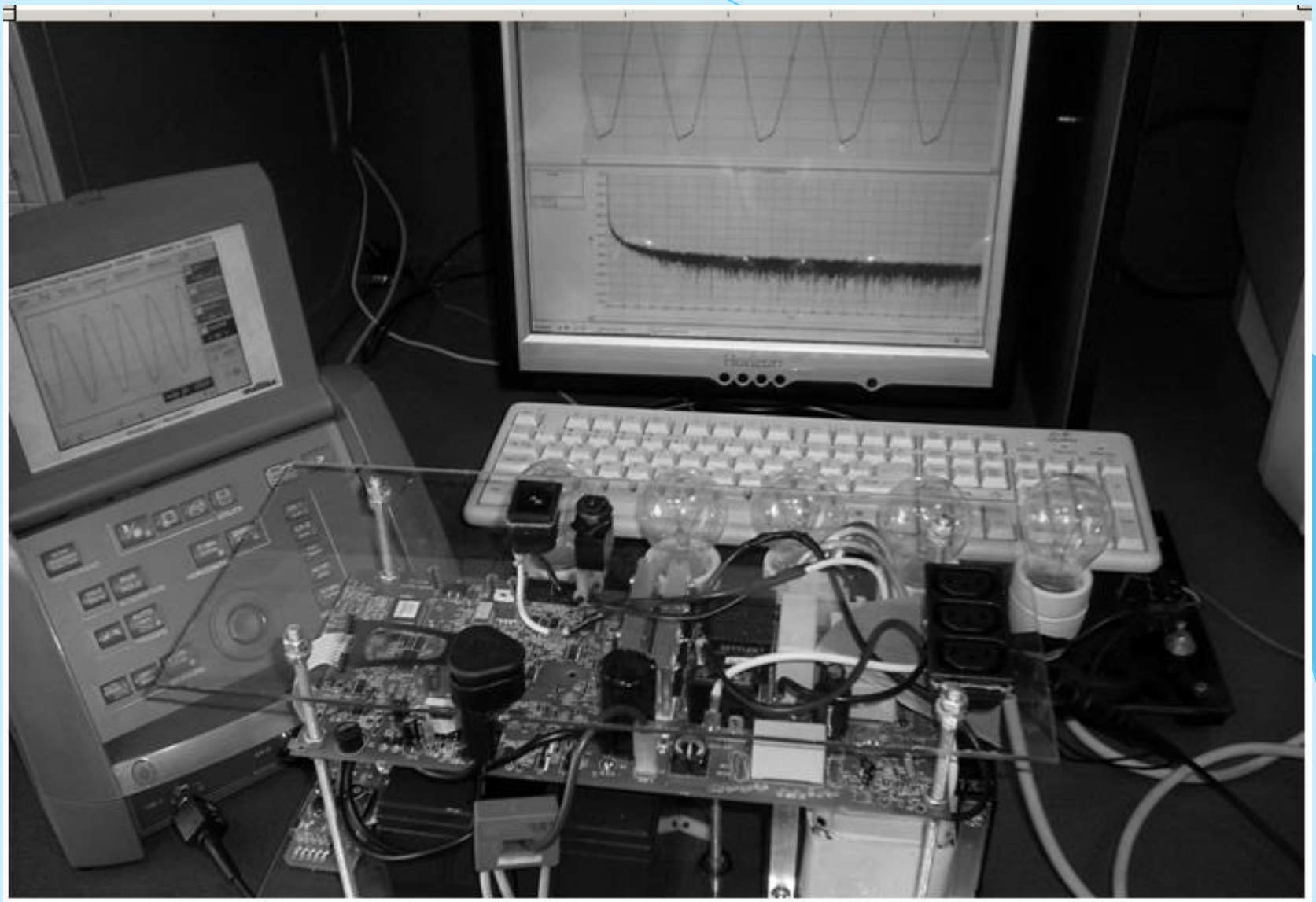

Figure 48. Experimental setup for inverter systems with pure sine PWM command

RIPPLE EVALUATION ON FUEL CELL EGS

Use of the Low Pass Passive Filters - EXPERIMENTAL RESULTS

Inverter system with full wave command

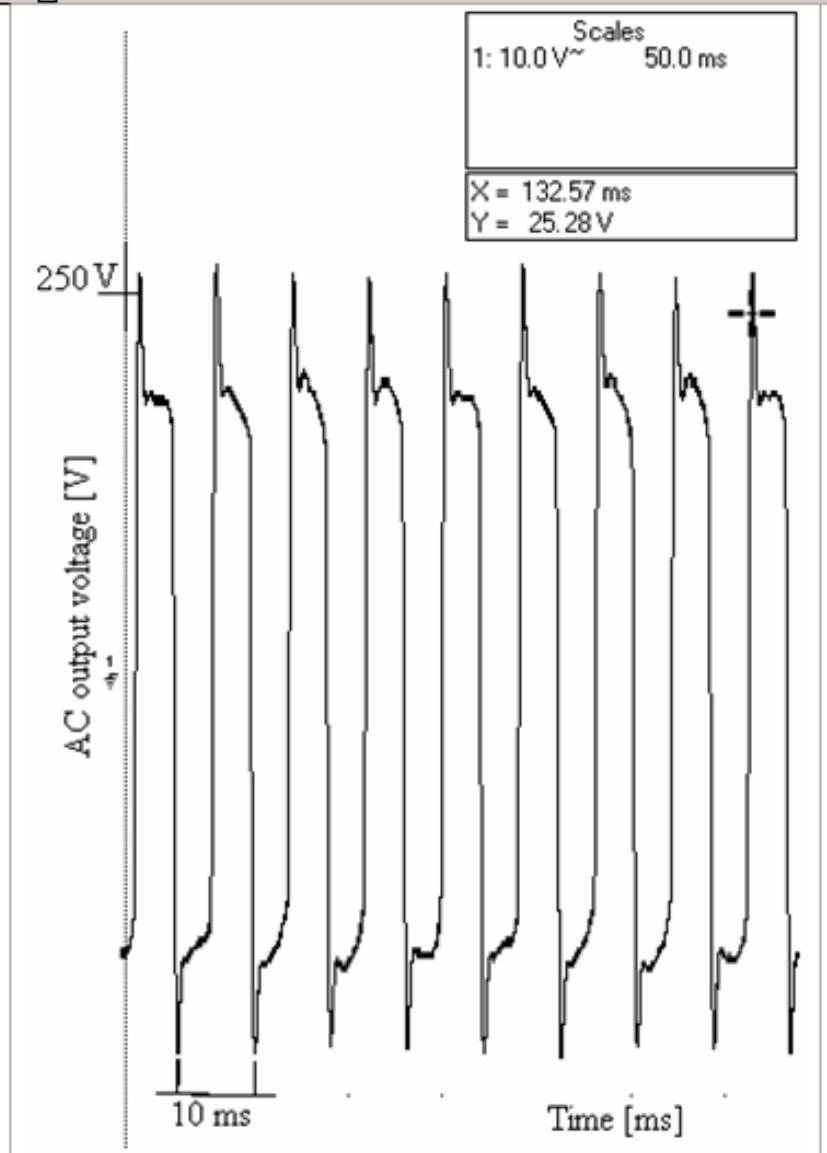

a) Output voltage

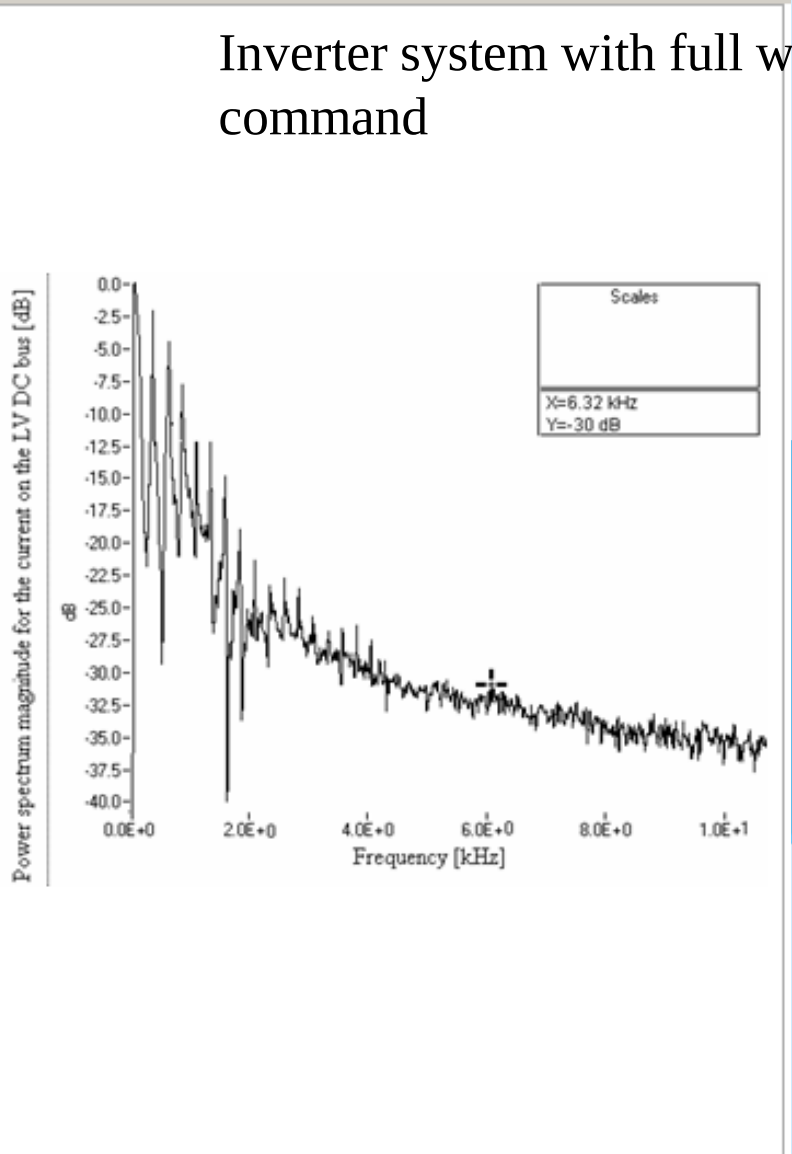

b) Power spectrum of the output voltage

RIPPLE EVALUATION ON FUEL CELL EGS

Use of the Low Pass Passive Filters - EXPERIMENTAL RESULTS

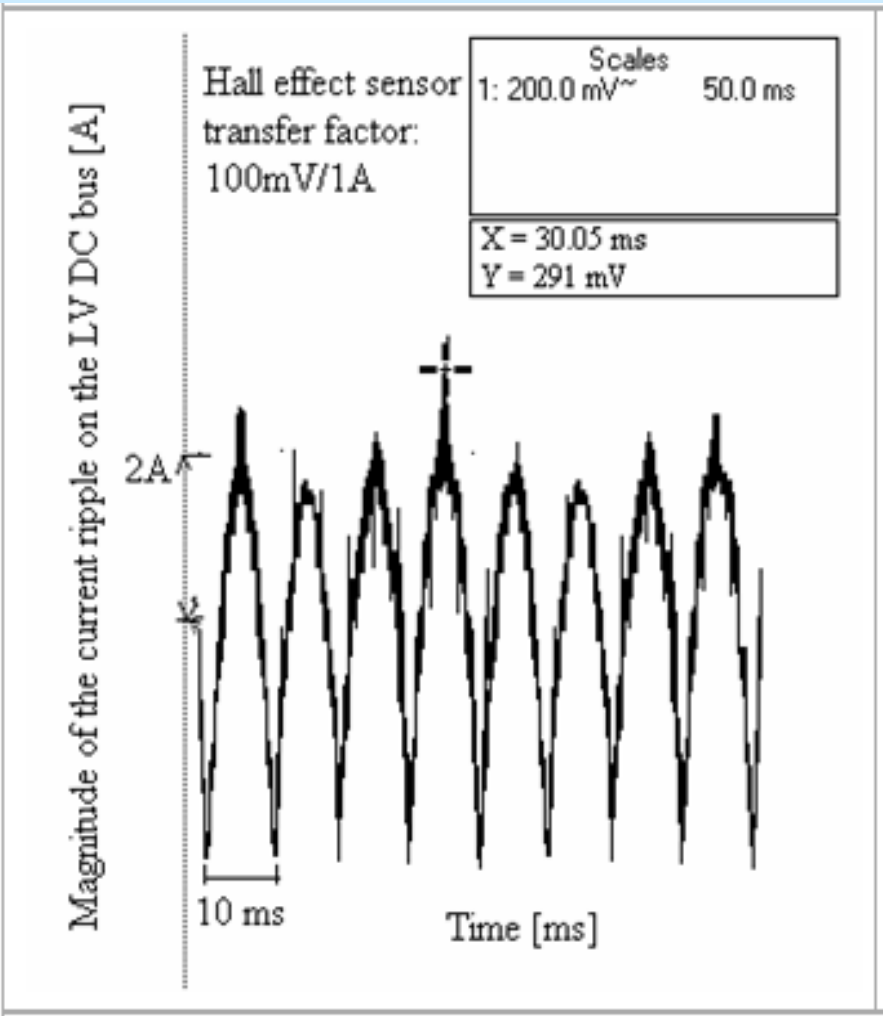

c) Input current ripple on LV DC bus

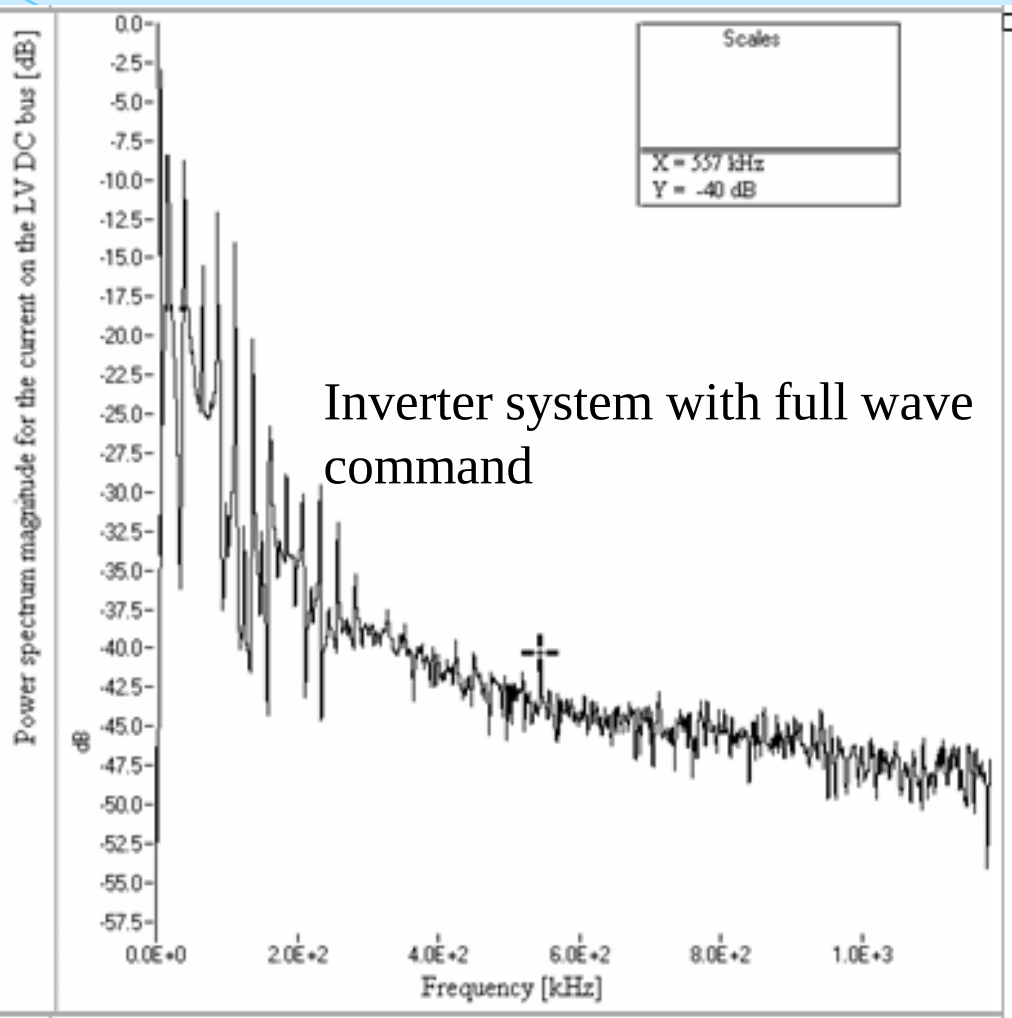

d) Power spectrum of the input current

Figure 49. Inverter system operation with full wave command

RIPPLE EVALUATION ON FUEL CELL EGS

Use of the Low Pass Passive Filters - EXPERIMENTAL RESULTS

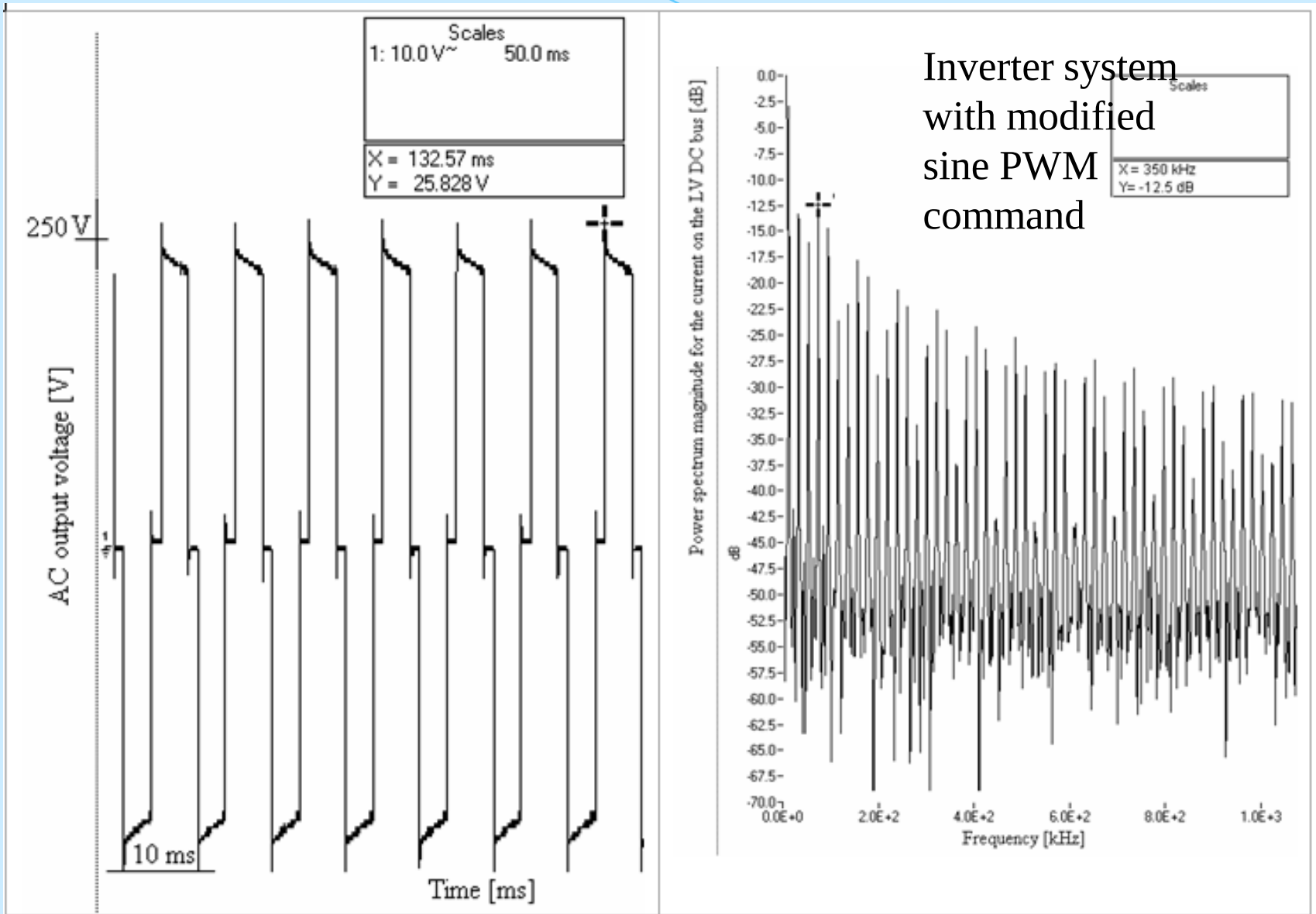

a) Output voltage

b) Power spectrum of the output voltage

RIPPLE EVALUATION ON FUEL CELL EGS

Use of the Low Pass Passive Filters - EXPERIMENTAL RESULTS

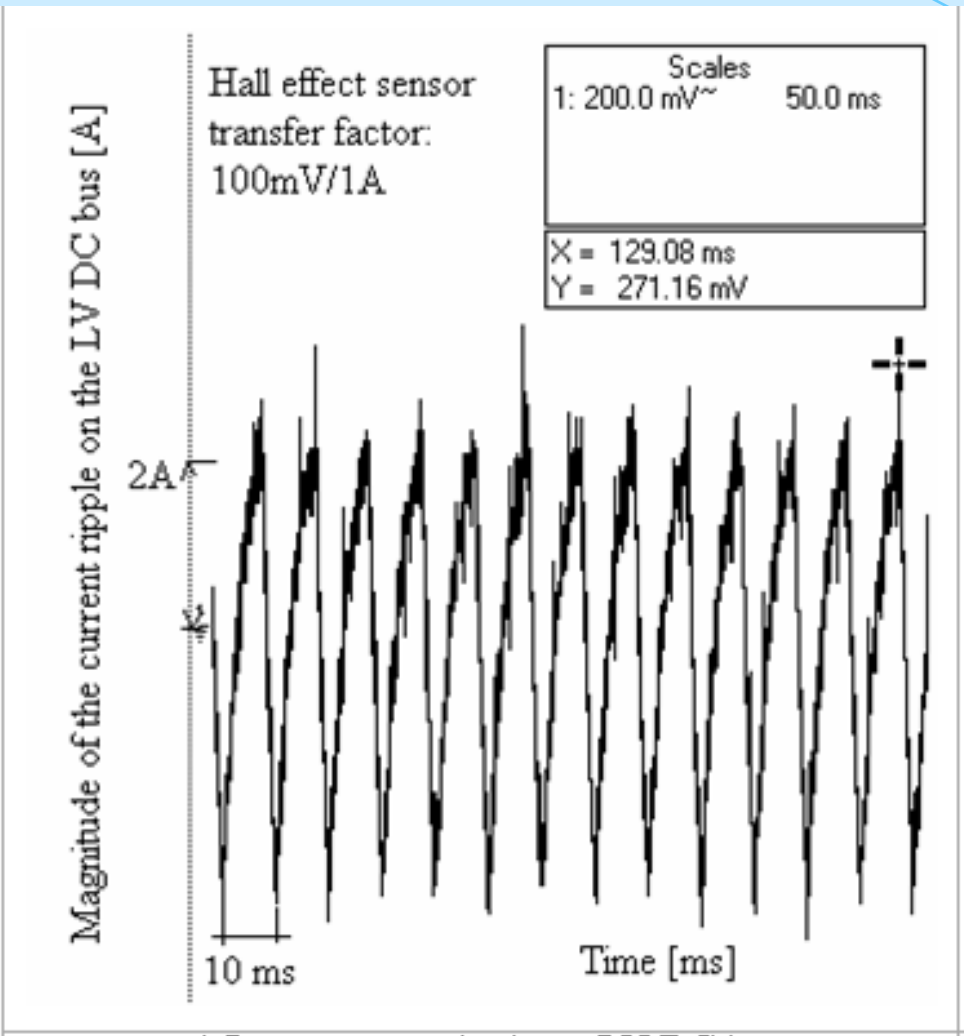

c) Input current ripple on LV DC bus

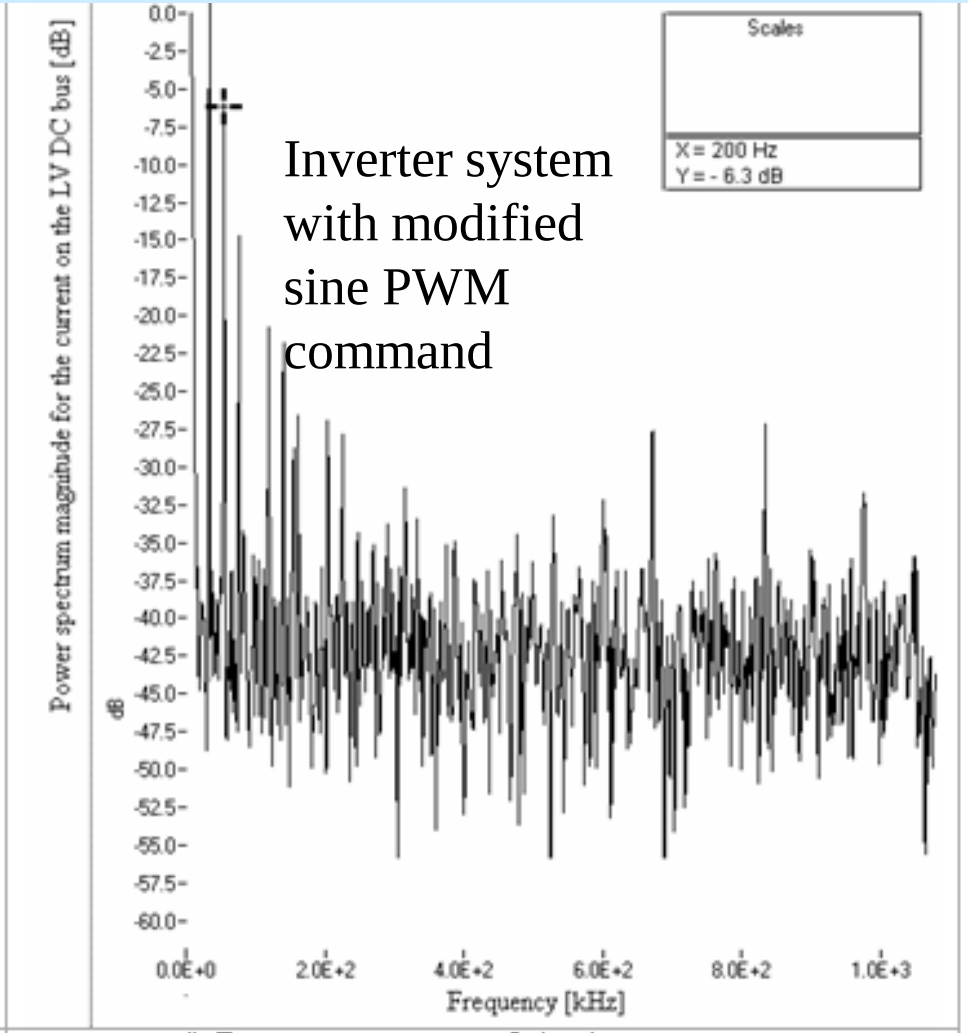

d) Power spectrum of the input current

Figure 50. Inverter system operation with modified sine PWM command

RIPPLE EVALUATION ON FUEL CELL EGS

Use of the Low Pass Passive Filters - EXPERIMENTAL RESULTS

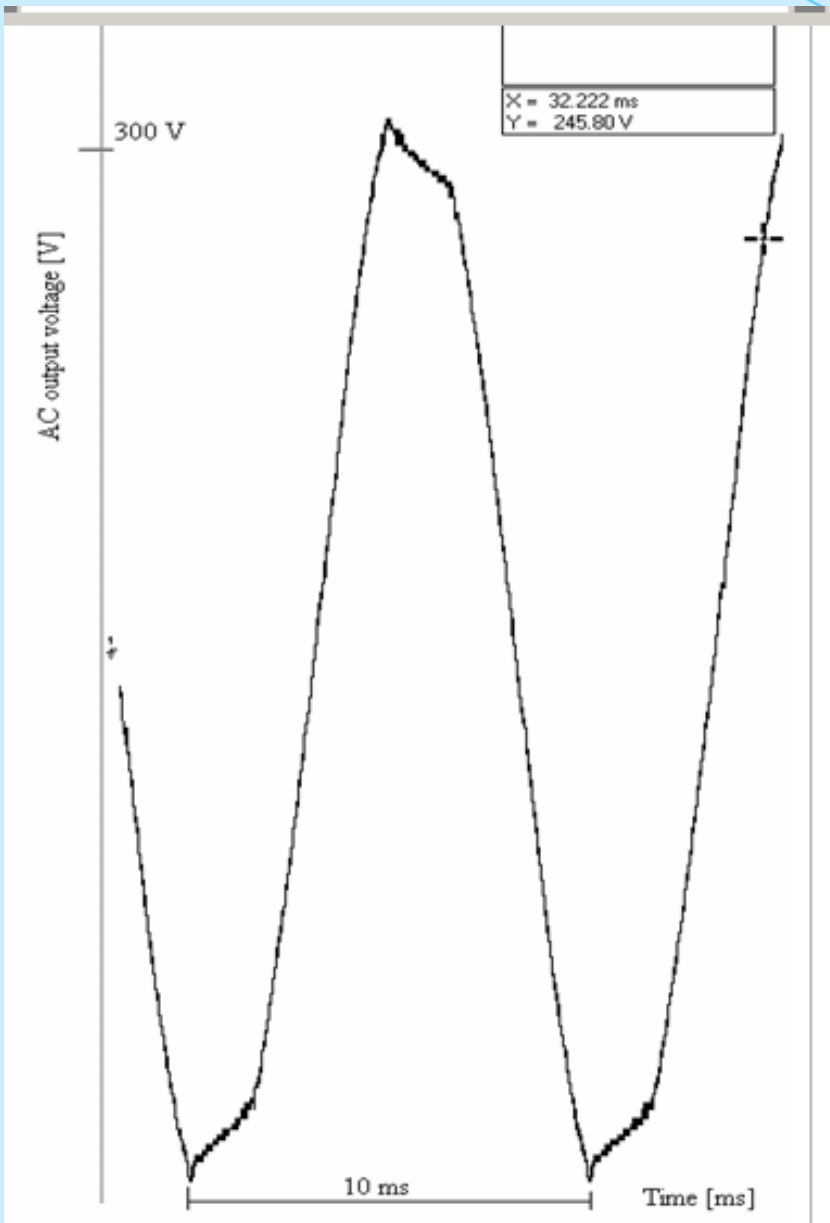

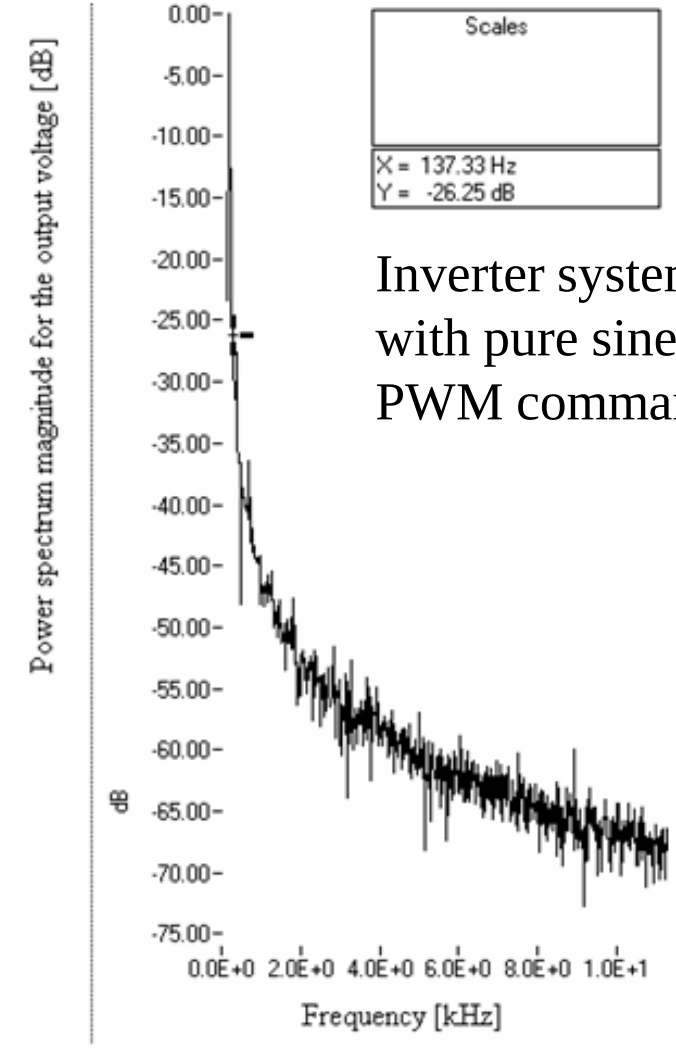

Inverter system with pure sine PWM command

RIPPLE EVALUATION ON FUEL CELL EGS

Use of the Low Pass Passive Filters - EXPERIMENTAL RESULTS

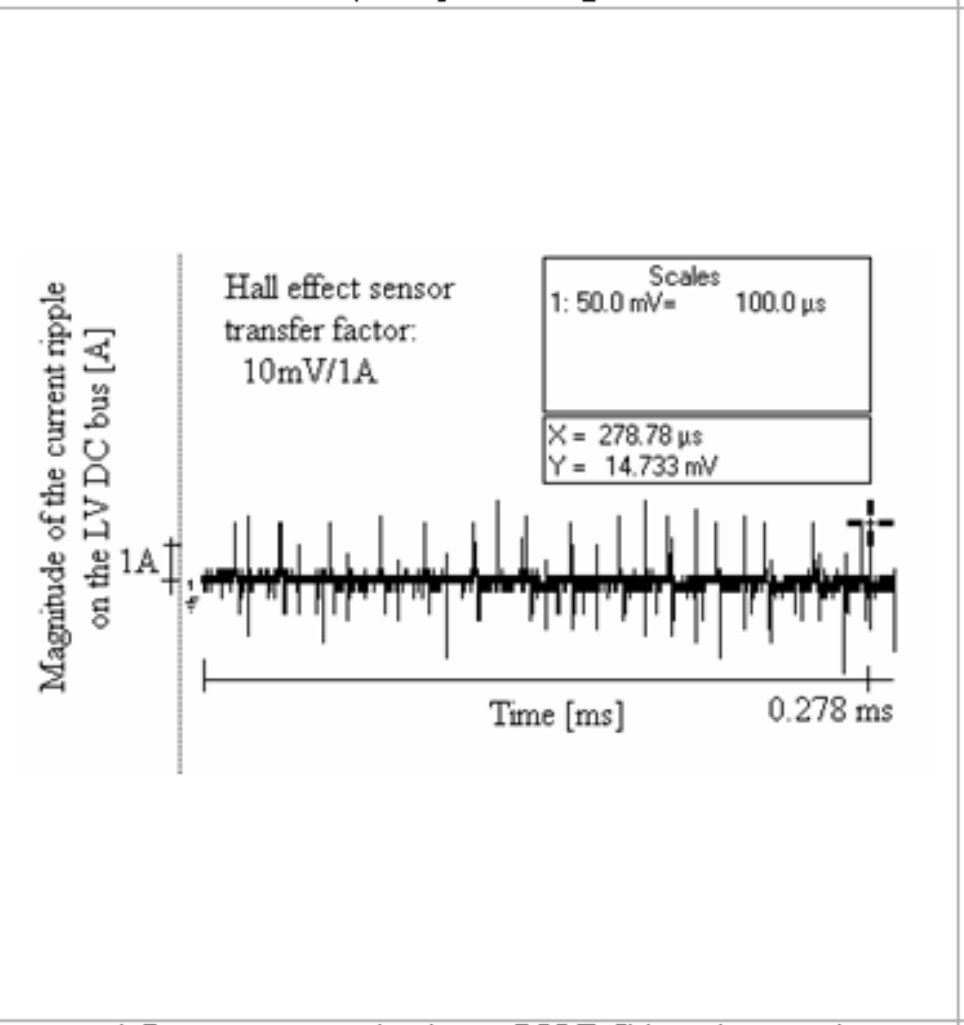

c) Input current ripple on LV DC bus (a zoom)

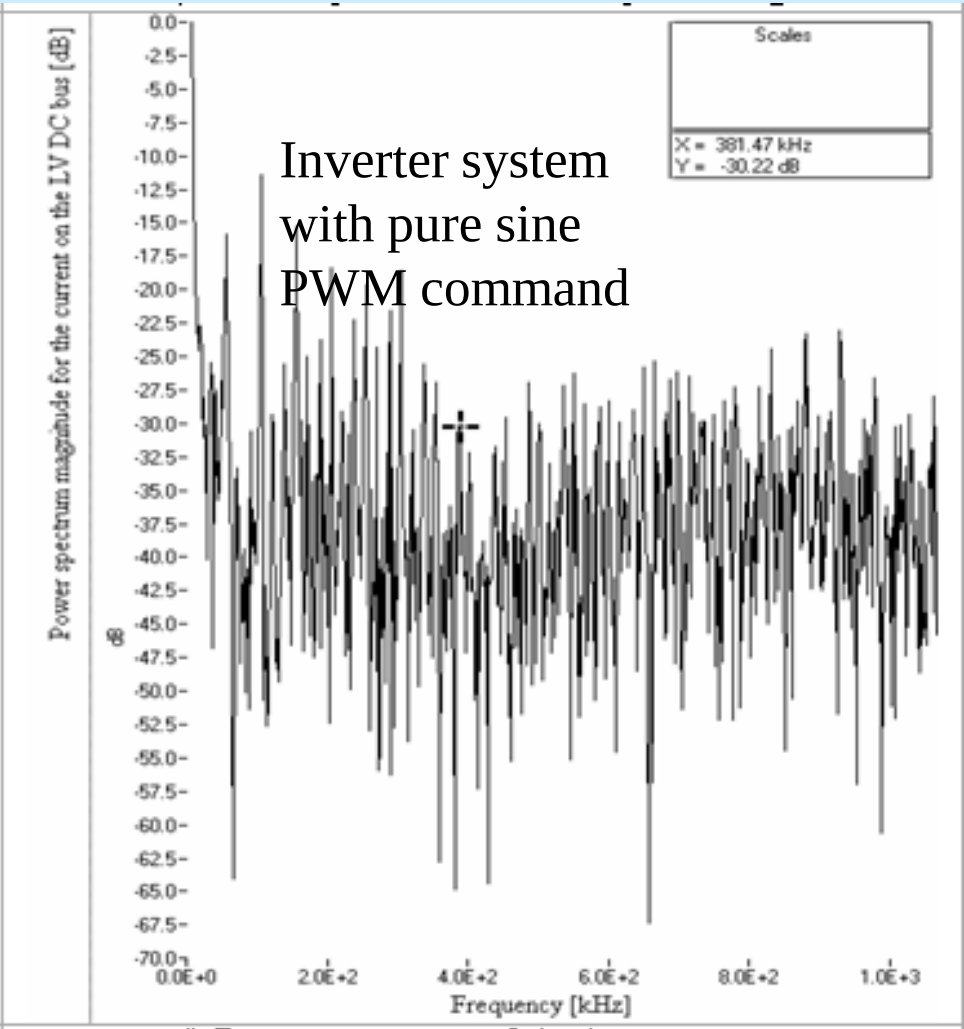

d) Power spectrum of the input current

Figure 51. Inverter system operation with pure sine PWM command

RIPPLE EVALUATION ON FUEL CELL EGS

Use of the Low Pass Passive Filters - EXPERIMENTAL RESULTS

Table 1. The LF harmonics magnitude for PEMFC current in case of C_{HVside} =0.22mF and different C_{LVside} values.

The harmonic amplitude of current [mA]					
C_{LVside} [mF]	Harmonics [Hz]				
	100	300	500	700	1500
0,1	364,295	110,601	64,678	47,84	21,598
0,6	363,188	104,259	55,618	36,18	10,915
1	358,665	94,721	45,693	27,855	7,2716
3	312,563	53,64	21,005	11,829	3,2614
6	232,428	30,772	12,196	7,1776	2,5022

Table 2. The LF harmonics magnitude for PEMFC current for different power values of load.

	LF harmonic magnitude value [mA]				
Load [W]	H_100 Hz	H_300 Hz	H_500 Hz	H_700 Hz	H_1500 Hz
0	38	18.4	14.6	1.39	0.49
100	223	26.1	25.9	3.30	2.22
200	282	16.0	38.1	1.69	1.96
300	384	31.1	33.7	2.42	2.61
400	396	49.4	47.9	3.79	2.2
500	774	31.2	31.9	6.16	5.21

RIPPLE EVALUATION ON FUEL CELL EGS

Use of the Low Pass Passive Filters - EXPERIMENTAL RESULTS

For all experiment the power of load is 100W and the ripple factor is around 6% (close enough to 5% value, which was estimated by simulation). The obtained results are shown in figure 52. Plot 52.a shows that the fundamental harmonic has in all cases the main contribution to the current ripple. Plot 52.b shows that the harmonics mitigation on LV DC bus is significant in all cases for C_{LVside} values higher than 1mF.

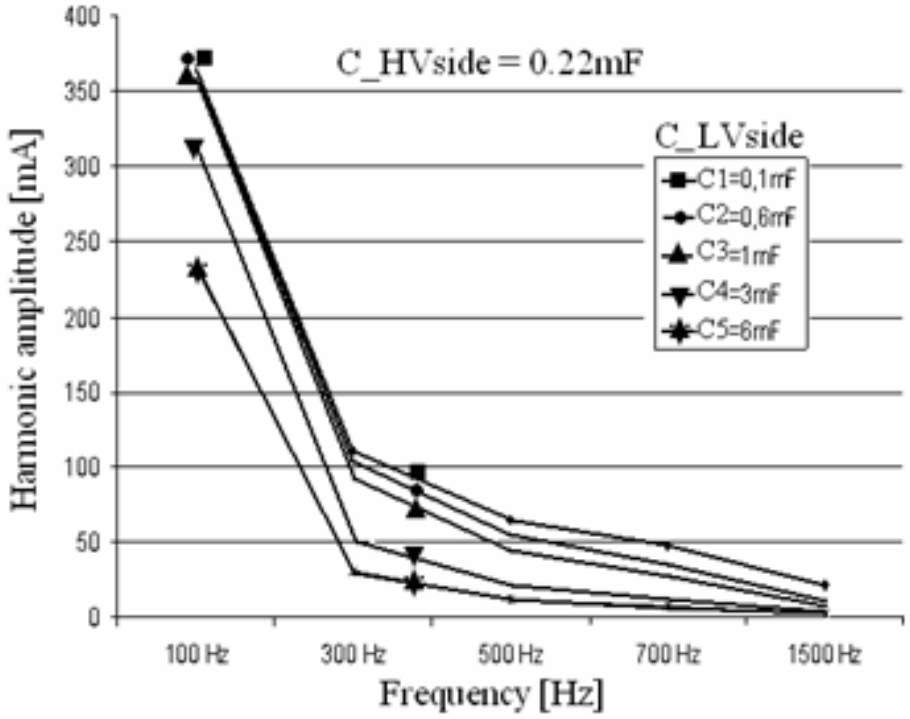

a) LF harmonic magnitude value [mA]

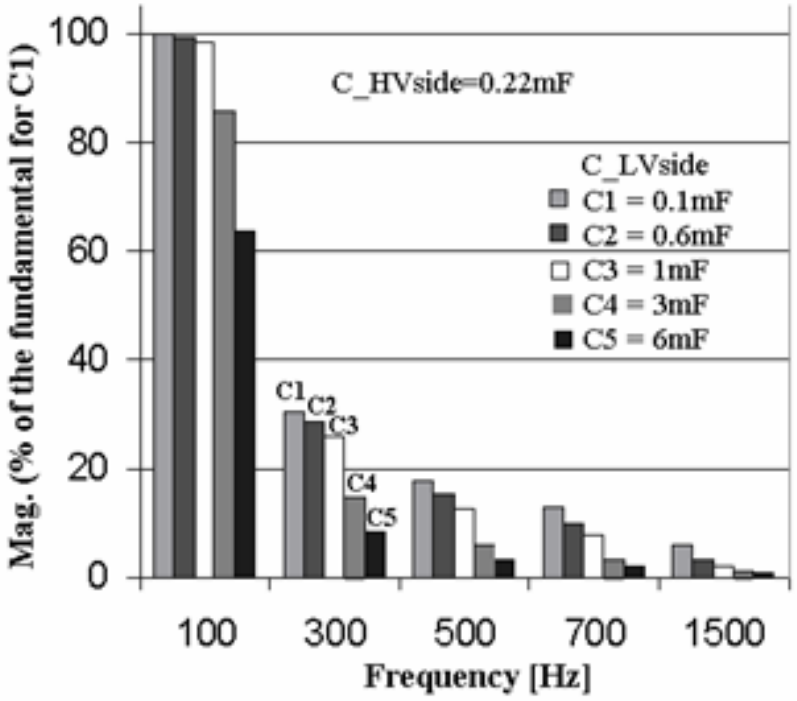

b) Normalized LF harmonic magnitude (% of the 100Hz harmonic for case C1=0.1mF)

Figure 52. The LF harmonic magnitude of PEMFC current for different C_{LVside} values (C_{HVside} =0.22mF)

RIPPLE EVALUATION ON FUEL CELL EGS

Use of the Low Pass Passive Filters - EXPERIMENTAL RESULTS

The measured LF harmonics magnitudes shown in table 2 are represented in figure 53. Plot 53.a shows that for different level of load power (excluding the case with no-load) the fundamental harmonic has the main contribution to the current ripple.
Plot 52.b shows that all harmonics starting from the seventh harmonic (H_700) are well mitigated by the passive filters.

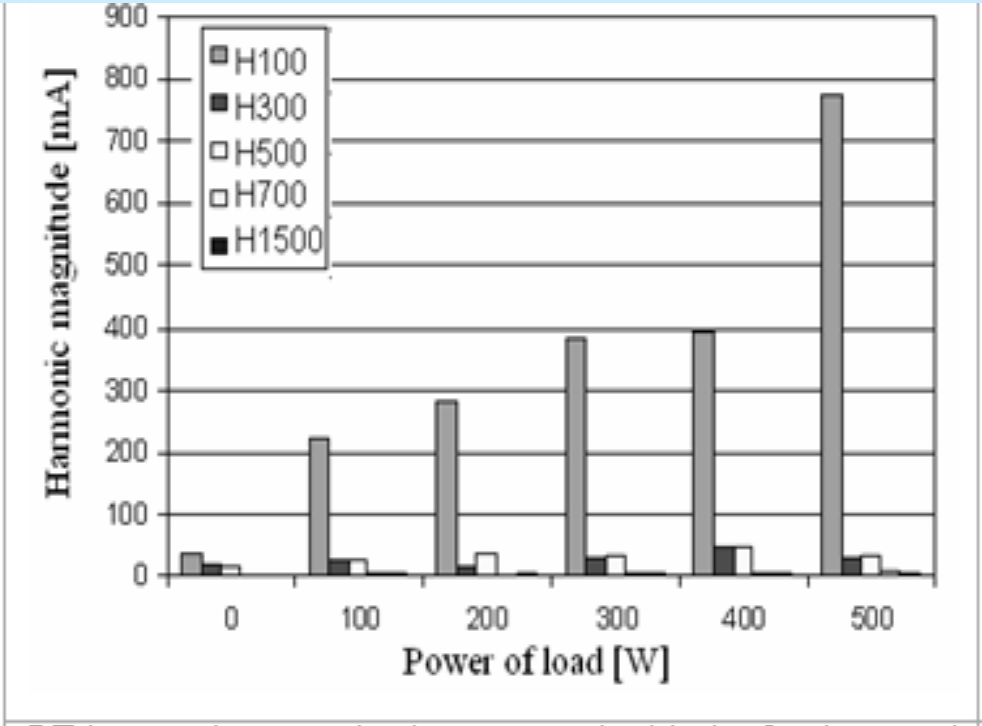

LF harmonics magnitude compared with the fundamental

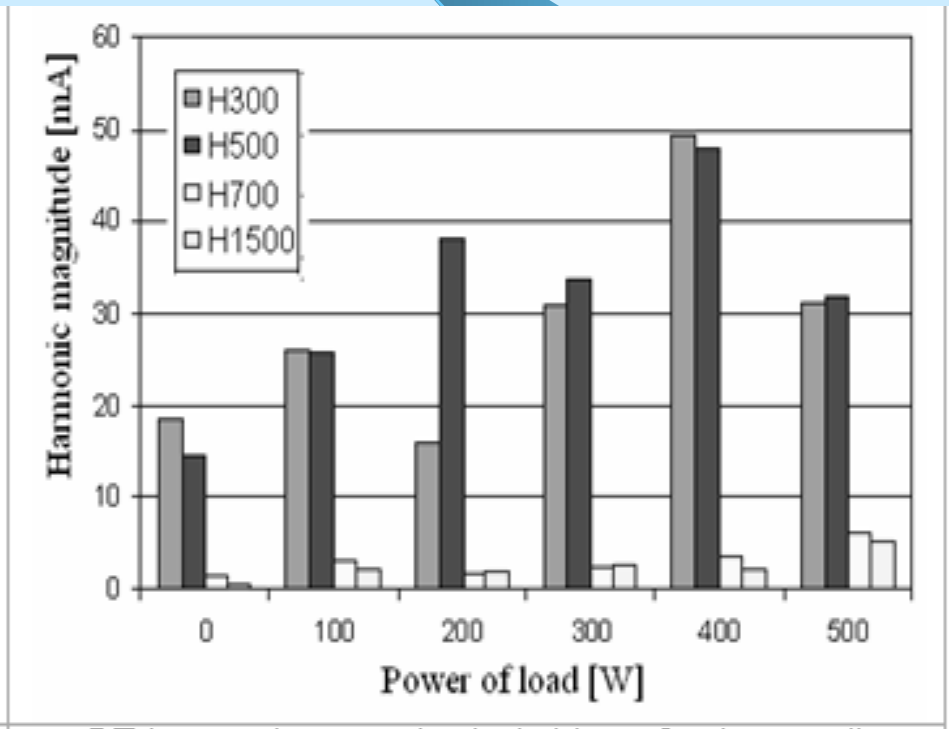

LF harmonics magnitude (without fundamental)

Figure 53. The LF harmonic magnitude of PEMFC current for different power of load

RIPPLE EVALUATION ON FUEL CELL EGS

Use of the Low Pass Passive Filters: 2 kW FC system - ICSI Rm.Valcea, Romania

RIPPLE EVALUATION ON FUEL CELL EGS

Use of the Low Pass Passive Filters: control of the 2 kW FC system

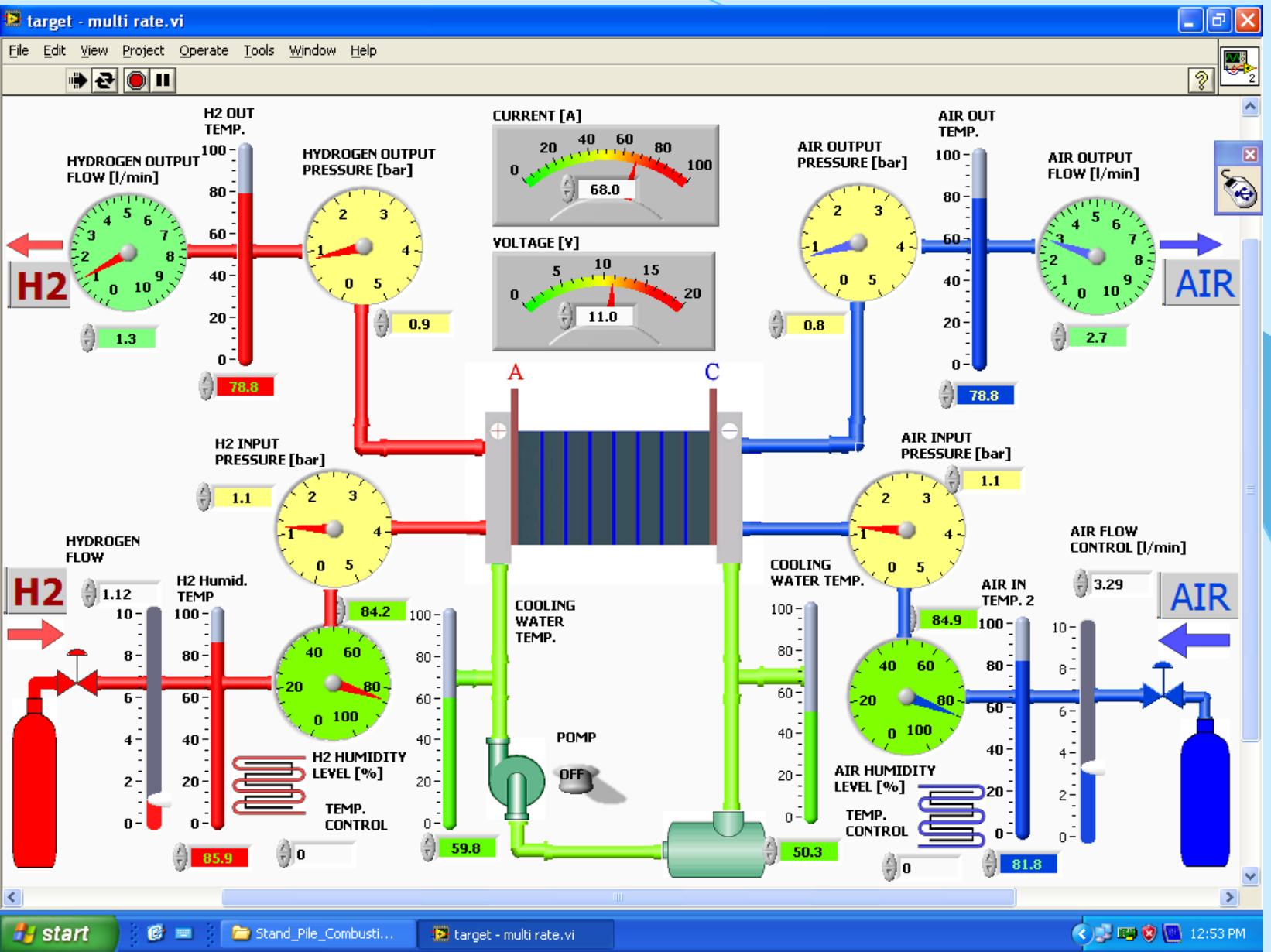

RIPPLE EVALUATION ON FUEL CELL EGS

Use of the Low Pass Passive Filters: FC system - ICSI Rm.Valcea, Romania

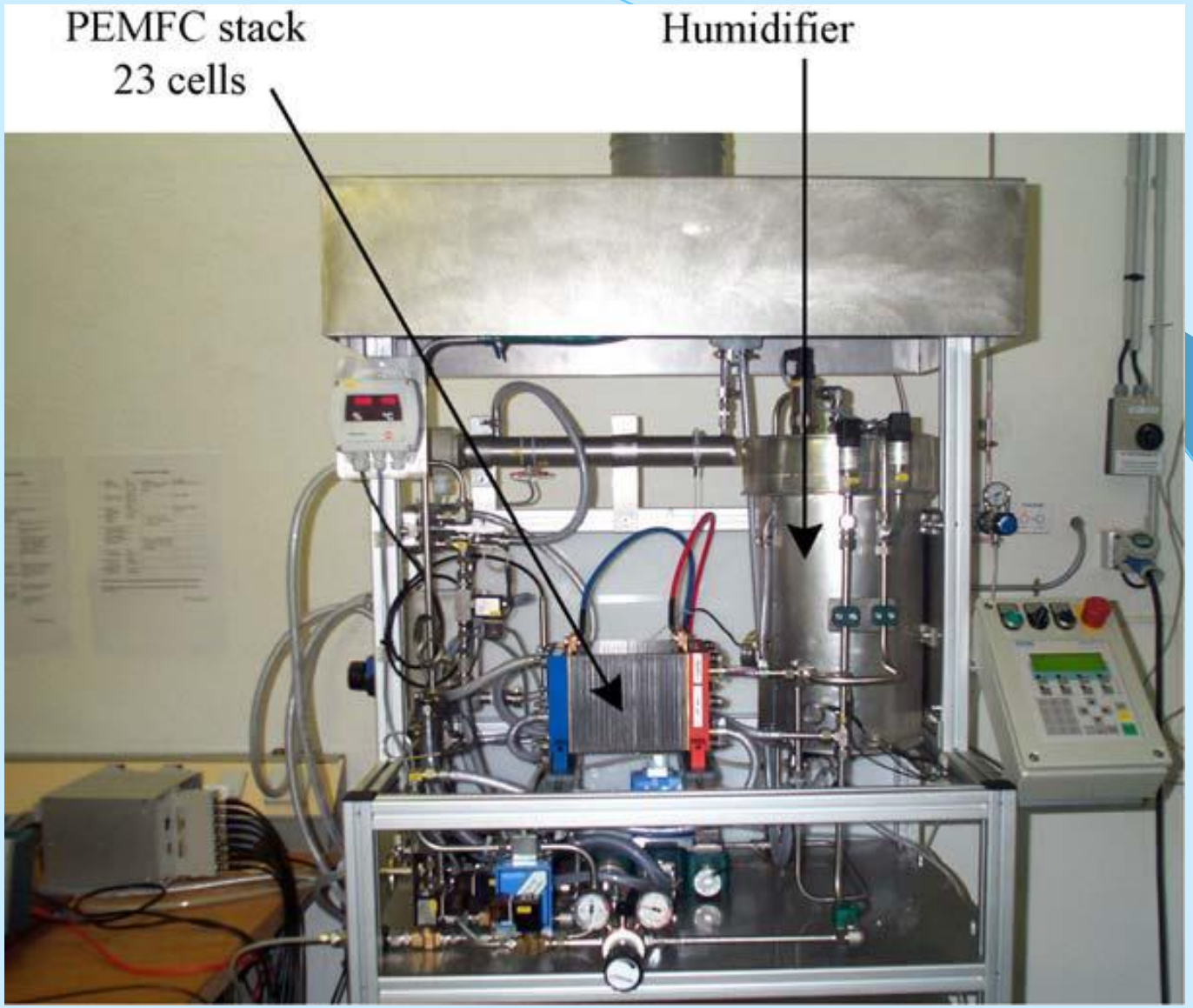

ZSW (Ulm, Germania) – 500 W PEMFC

RIPPLE EVALUATION ON FUEL CELL EGS

Use of the Low Pass Passive Filters - CONCLUSION

❖ FC ripple factor is recommended to be less than 5% for an efficient and safe operation, resulting bulky passive filters.

❖ Consequently, before the LV DC voltage bus, it is recommended to be used a boost power interface instead of a passive filter. In this case, it is obviously that a better filtering based on active control can be made, especially for the first LF harmonics, which mostly impose the value of the ripple factor. Note that all harmonics starting from the seventh harmonic are well mitigated by the passive filters.

❖ The filter on the HV DC bus must be redesigned to mitigate the current ripple under new imposed limit obtained, which are larger if the boost power interface is used. So, reasonable values could be now obtained for the passive components.

❖Advanced mitigation techniques for the FC current ripple will be presented in second part of this presentation.

Fuel Cell Hybrid Power Source: Part II

The second part of presentation is focused on:

- ✓**Techniques of active mitigation for the LF FC ripple;**
- ✓**Analysis of the appropriate FCHPS architectures for active mitigation control of the LF FC ripple;**
- ✓**Comparison of the results in active filtering by different control techniques: classical (peak current control (PCC) or hysteretic control), based on fuzzy rules, nonlinear, etc;**
- ✓**Evaluation of the FC current ripple in FCHPS with spread spectrum based on anti-control techniques;**
- ✓**Validation of the simulation results by measurements performed in different experiments.**

Active Mitigation of the Inverter Current Ripple

THE BOOST POWER INTERFACE

In this section the performances of ripple mitigation using a boost power interface is investigated. This DC-DC converter boost the voltage of the PEMFC stack to the requested voltage on the LV DC bus that supply the inverter system (see figure 54).

The main goals of the boost converter controller are to regulate the voltage on the LV DC bus and to mitigate the current ripple that are back-propagated to the PEMFC stack. Consequently, the voltage on LV DC bus and PEMFC current must to be both control variables of the appropriate controller.

Different control techniques may be used to optimize the control performances above mentioned. Two techniques of peak current control (PCC) are presented here to compare their ability to mitigate the current ripple (see figure 54).

The PCC laws are implemented using a fuzzy controller and a nonlinear controller (shown in figure 55.a and 55.b, respectively). Note that PC reference, $I_{pk(ref)}$, could be chosen close to the MPP current. Voltage on the LV DC bus will be boosted to the requested reference value, $V_{LV(ref)}$.

The ripple current is simply modelled by a rectified 50 Hz sine wave.

The load dynamic is modelled by a current controlled source.

Active Mitigation of the Inverter Current Ripple

THE BOOST POWER INTERFACE

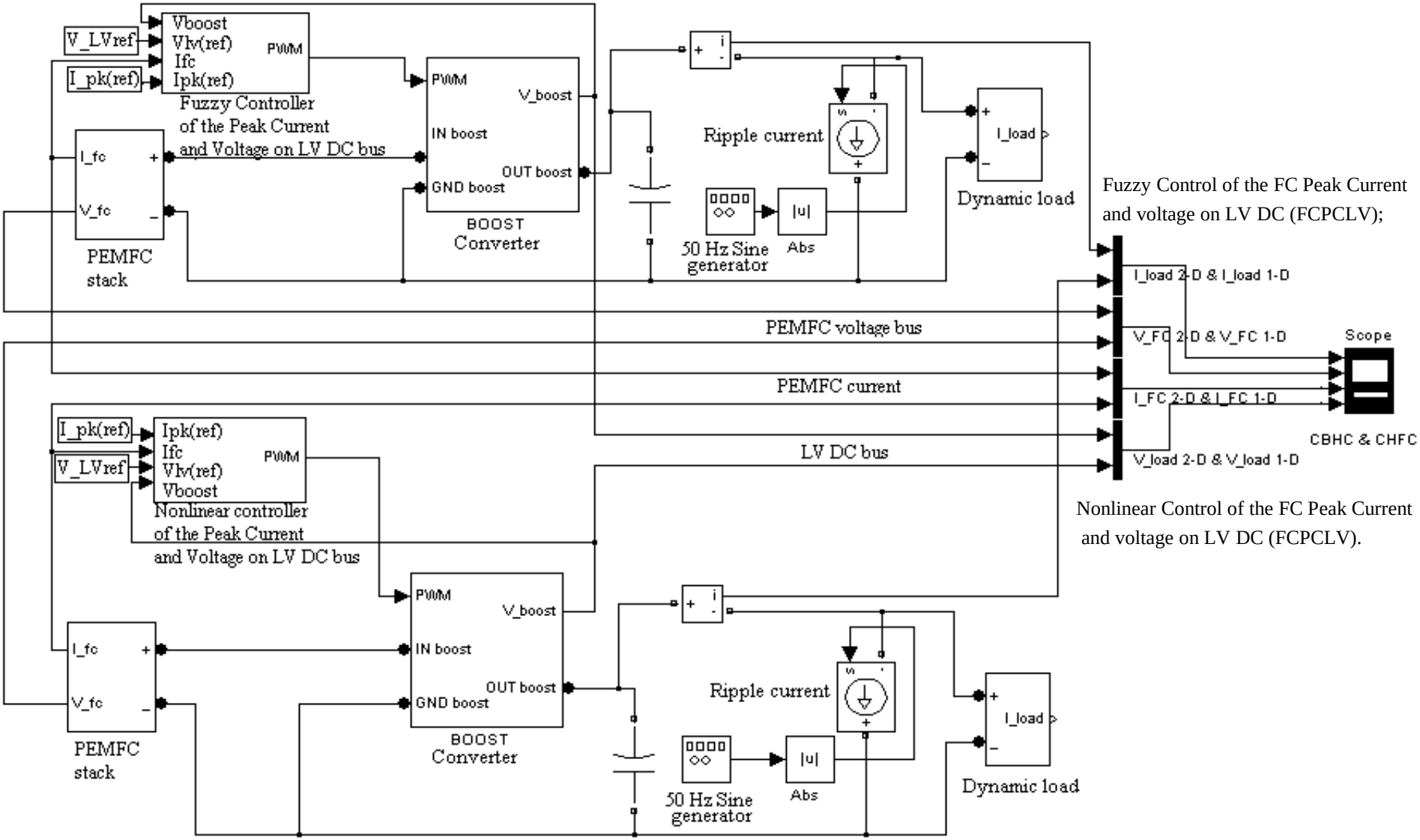

Figure 54. Boost interfaces with nonlinear and fuzzy control

Active Mitigation of the Inverter Current Ripple

THE BOOST POWER INTERFACE

a) Fuzzy Control of the PEMFC peak current and voltage on LV DC bus (FCPCLV)

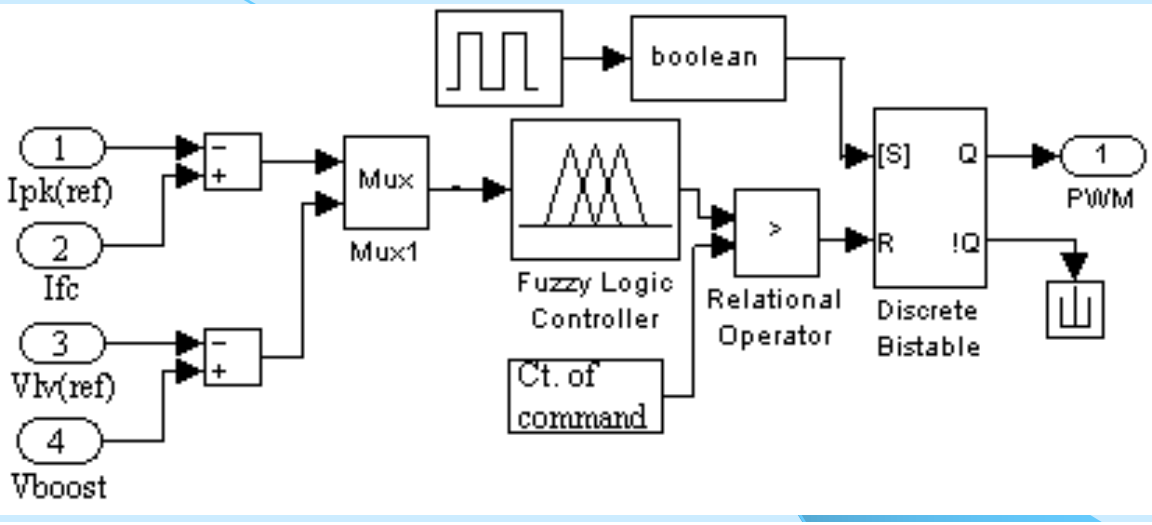

b) Nonlinear Control of the PEMFC peak current and voltage on LV DC bus (NCPCLV)

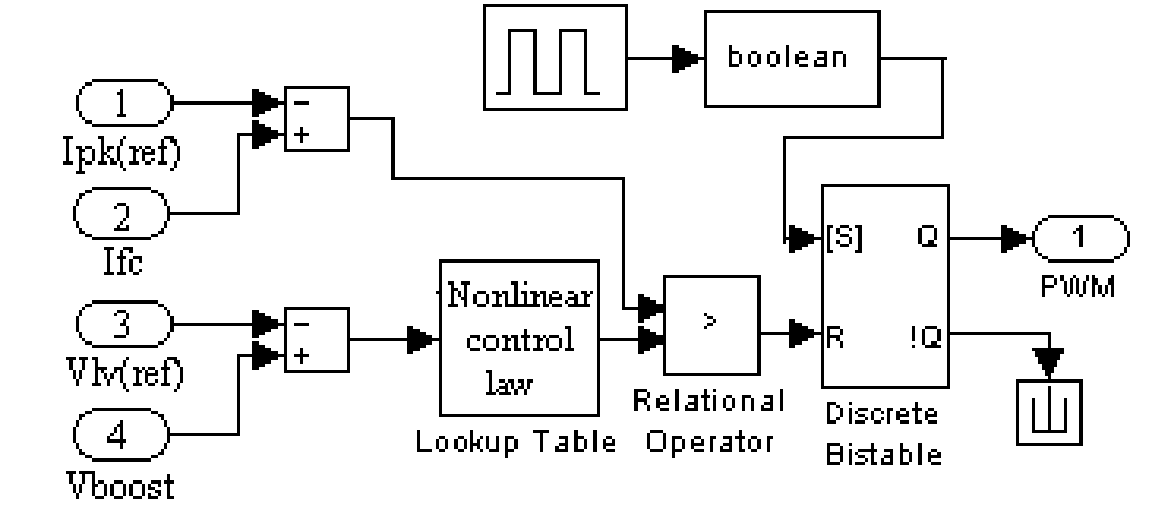

Figure 55. Control based on the PEMFC peak current and voltage on the LV DC bus

Active Mitigation of the Inverter Current Ripple

THE BOOST POWER INTERFACE

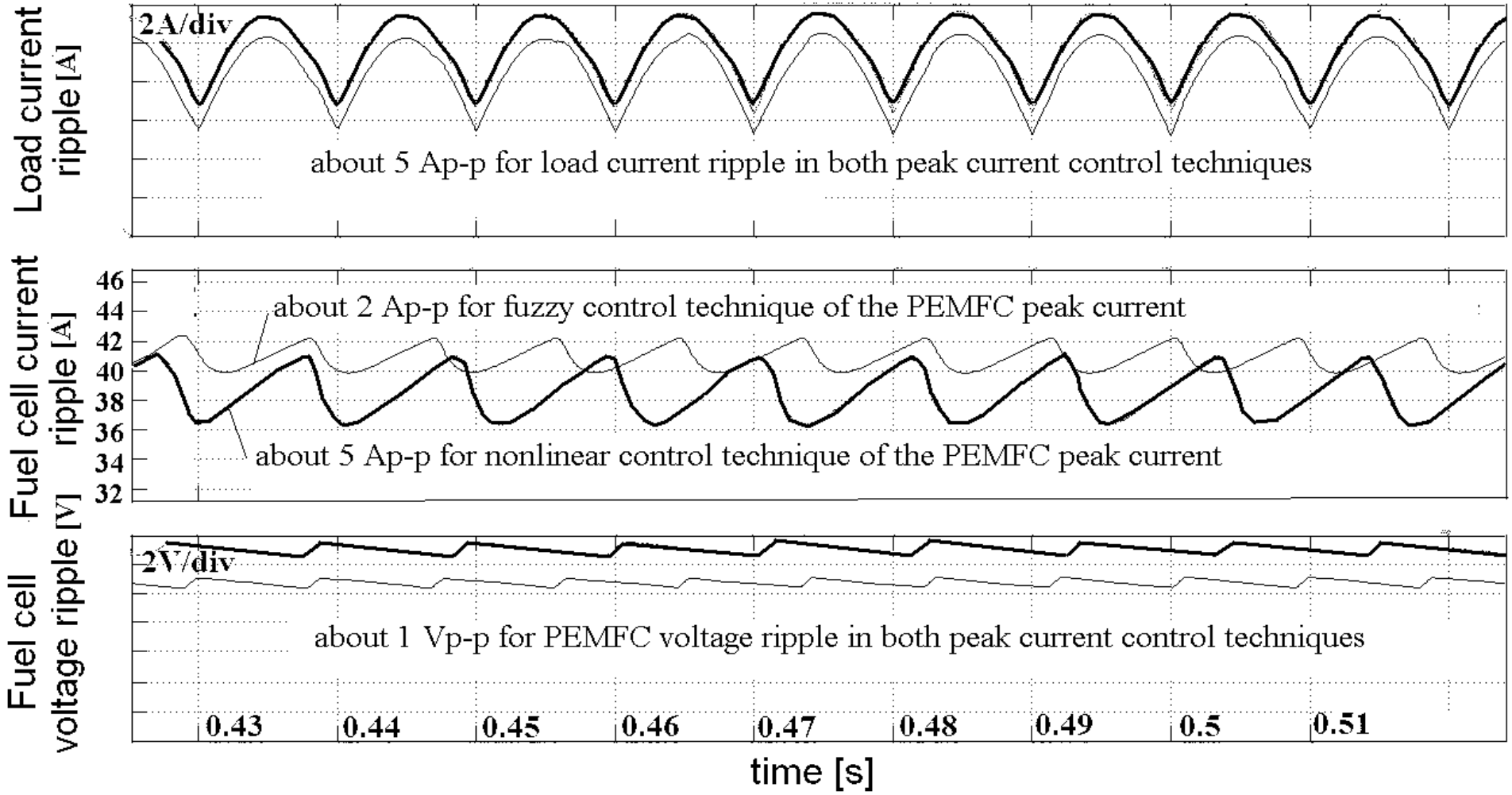

Figure 56. Fuel cell voltage ripple (bottom) and current ripple (middle) for the same load current ripple (top), using a boost power interface with peak current control of fuzzy (thin line) and nonlinear (thick line) type

Active Mitigation of the Inverter Current Ripple

THE BOOST POWER INTERFACE - conclusions

- The advantage of using a 2-D control surface for fuzzy controller is that the both control variables, fuel cell current and voltage on LV DC, can directly control the duty-cycle of the switching command.
- Instead of 2-D control surface, the NCPCLV controller uses a 1-D control surface to generate a current ripple reference. Control is less flexible and thus the performances of ripple mitigation are different, being lower in this case.
- The ripple factor is about 2A/40A=5% and 5A/40A=7.5% for case of using the fuzzy controller and nonlinear controller, respectively.
- Better performances to mitigate the LF ripple could be obtained if the DC-DC power interface is of multi-port type that use at least an auxiliary energy source to supply the Controlled Current Source (CCS), which generates the anti-ripple.

An efficient way to mitigate the HF current ripple is to use the interleaving switching technique. Some results are presented in next slides.

Active Mitigation of the Inverter Current Ripple

INTERLEAVED PWM COMMAND

Figure 57. Matlab diagram of the DC-DC converter

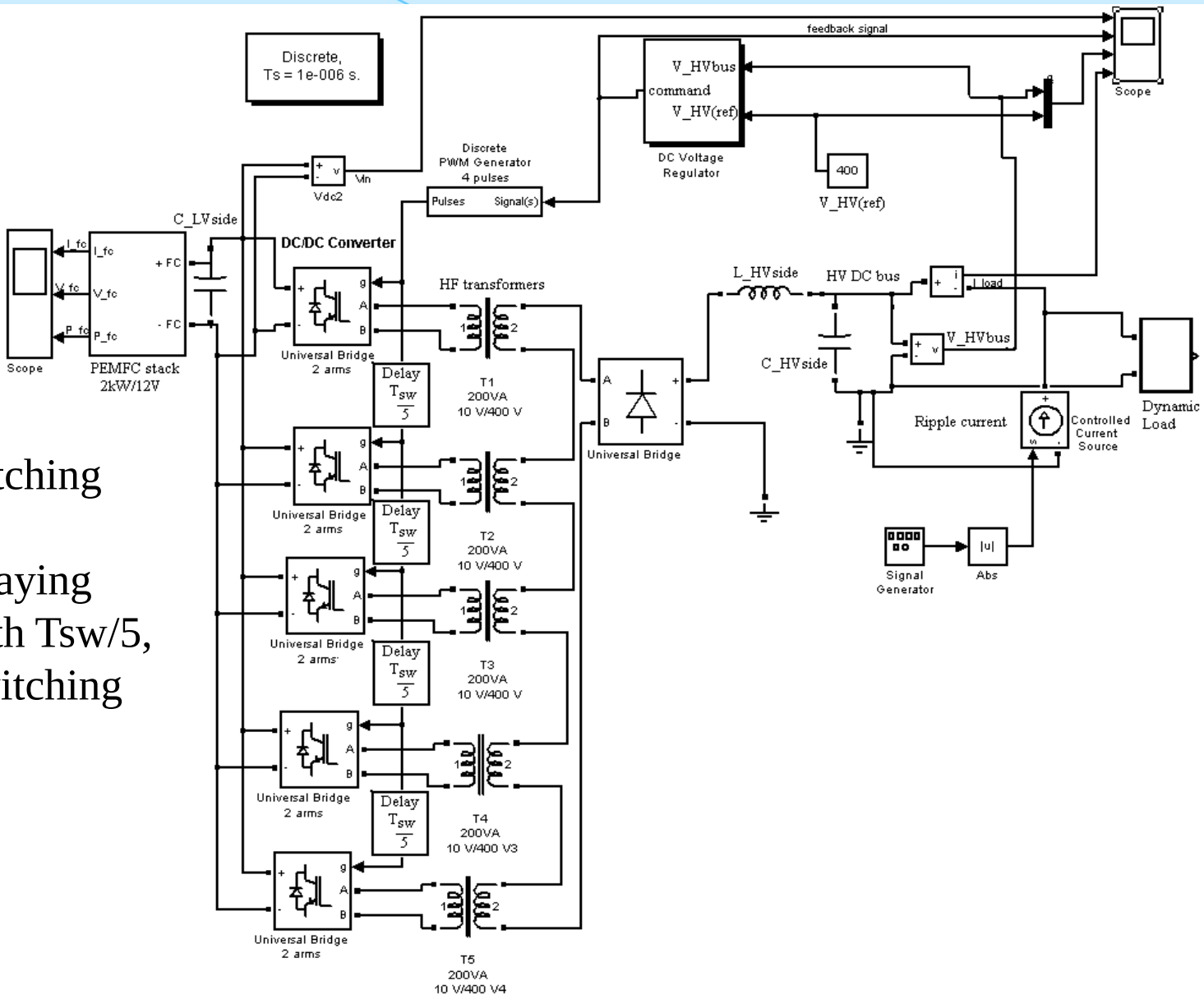

The interleaved switching technique is simply implemented by delaying the PWM pulses with Tsw/5, where Tsw is the switching period.

Active Mitigation of the Inverter Current Ripple

INTERLEAVED PWM COMMAND

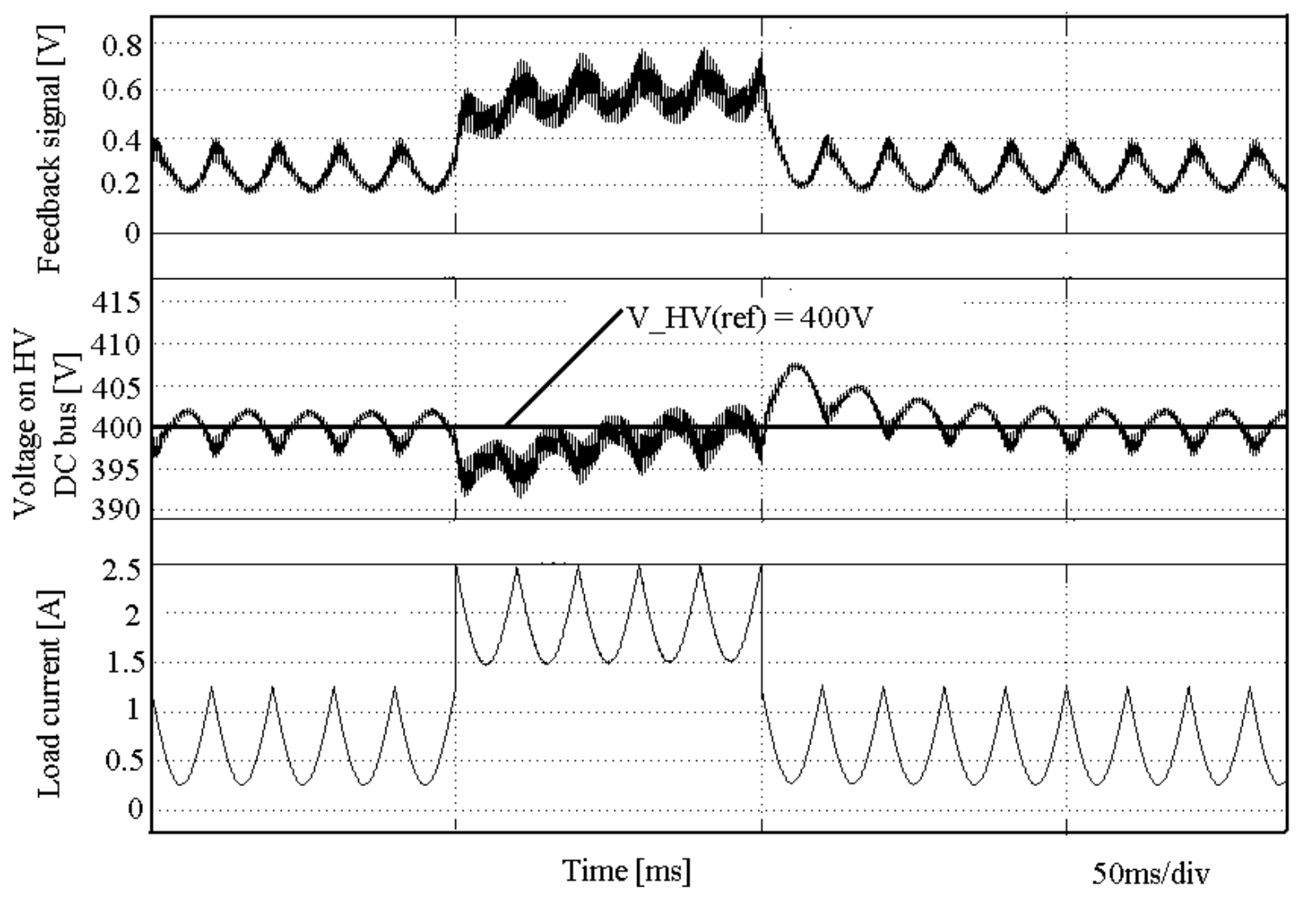

Figure 58. The DC-DC converter behaviour for a pulsed load

Active Mitigation of the Inverter Current Ripple

INTERLEAVED PWM COMMAND

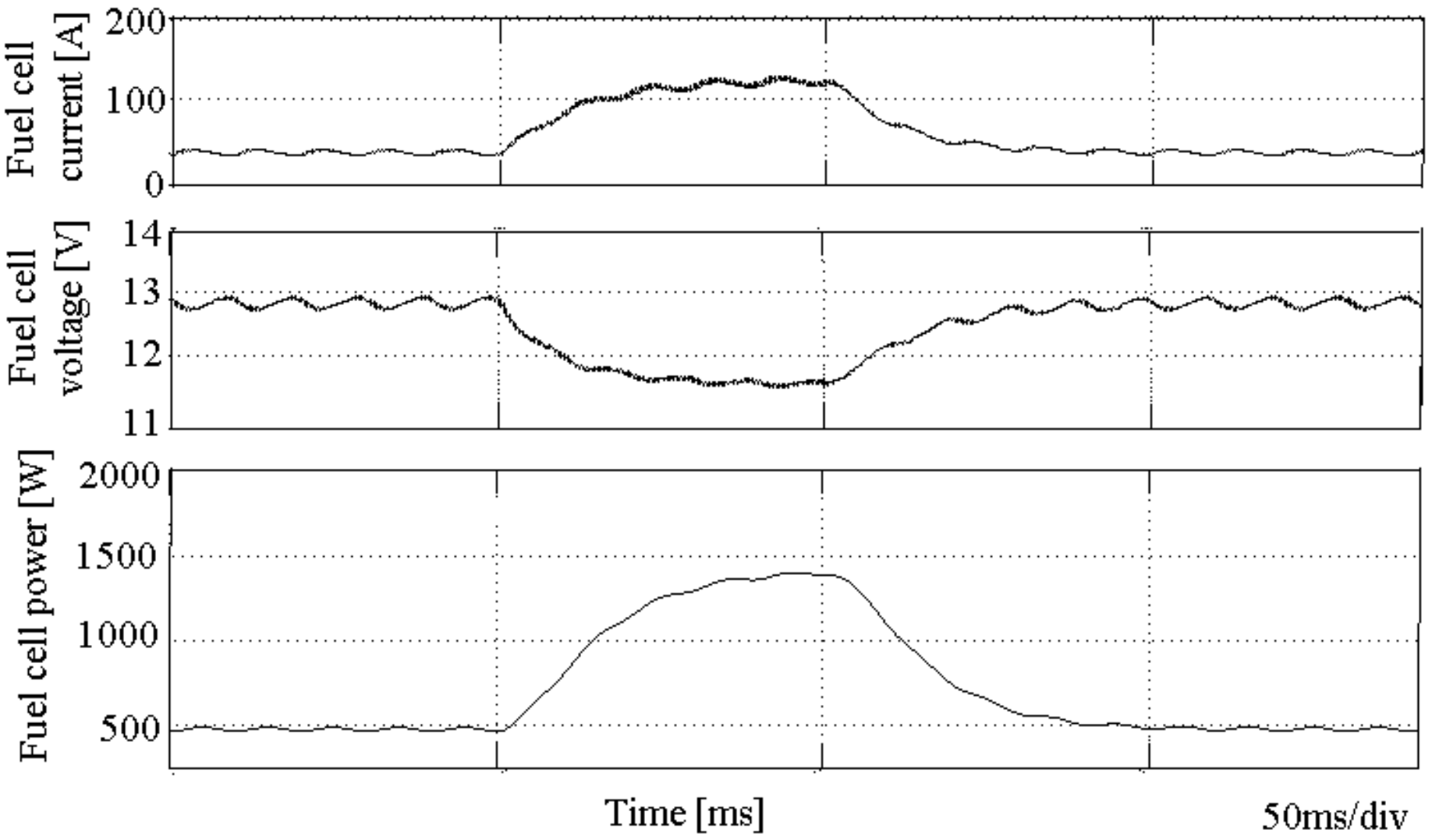

Figure 59. Fuel cell current (top), voltage (middle) and power (bottom) for pulse load

Active Mitigation of the Inverter Current Ripple

INTERLEAVED PWM COMMAND

Figure 60. Fuel cell current (top) and its power spectrum (bottom) for 0.5 kW load

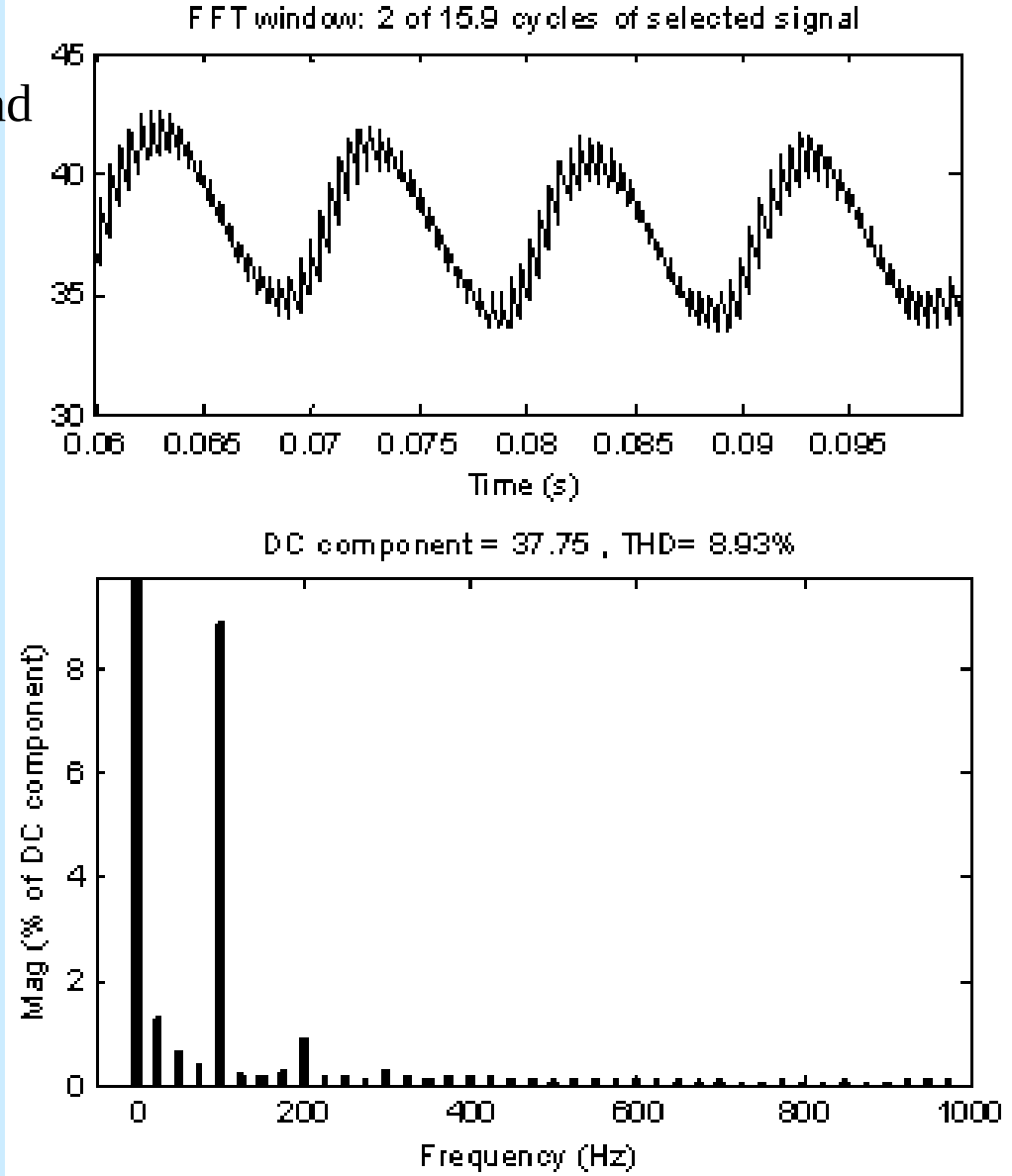

Passive filters' parameters:
L_{HVside}=0.5 mH, C_{HVside}=0.2 mF,
C_{LVside}=100 uF (a low value is set).

2kW/12V PEMFC stack

100 Hz ripple factor is of
10A/100A=10% (< 15%) and
7A/40A=17,5% (> 15%)
for 75% and 25% rated load, respectively.
RF for the HF current ripple is much lower: about 2A/40A=5%

Conclusion: RF is to high for the LF current ripple.

So, active mitigation based on bi-buck topology is necessary.

Active Mitigation of the Inverter Current Ripple

INTERLEAVED PWM COMMAND

Experimental results

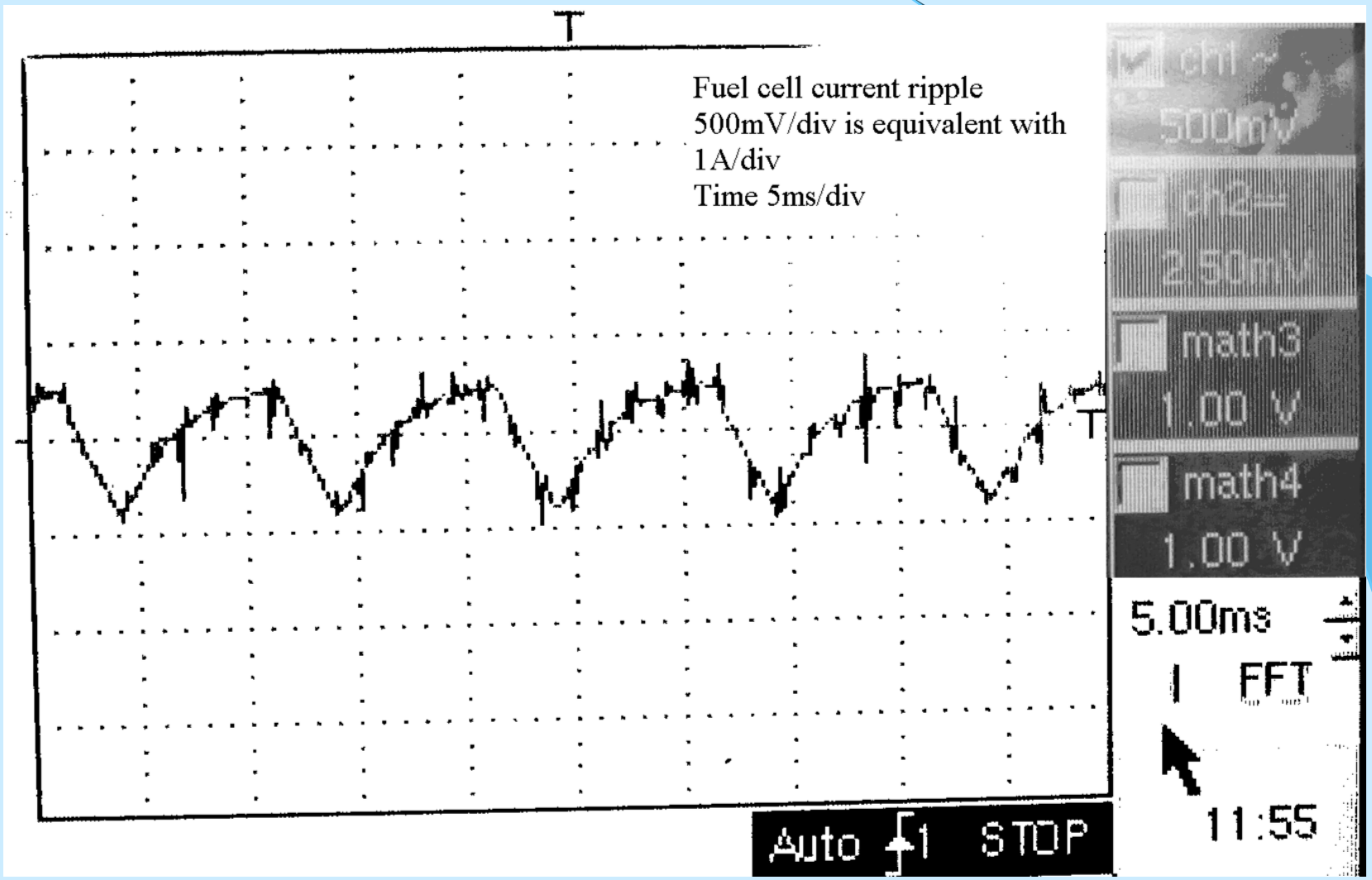

Active Mitigation of the Inverter Current Ripple

BI-BUCK TOPOLOGY

Figure 63. Bi-buck topology – Simulink diagram

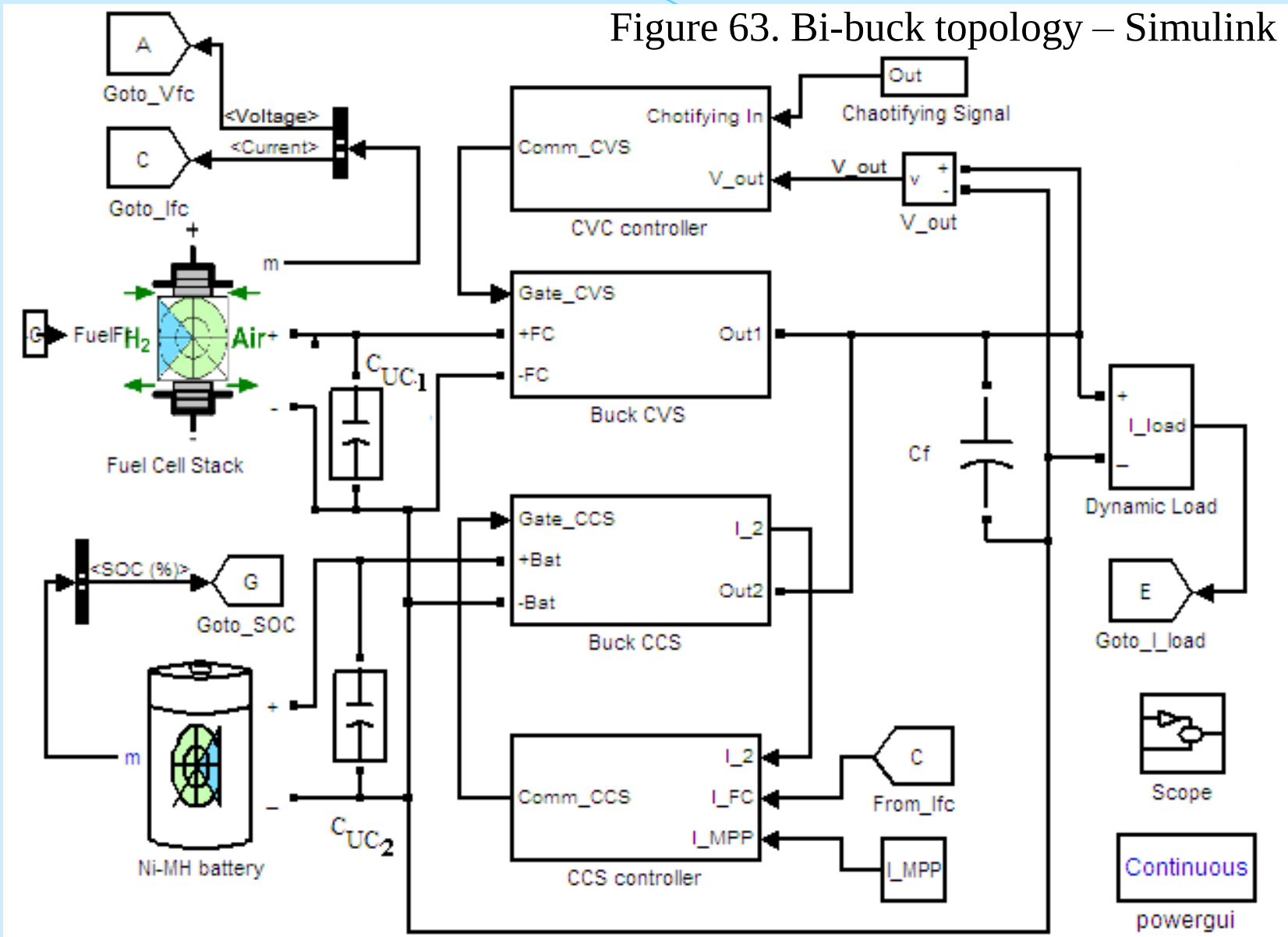

Active Mitigation of the Inverter Current Ripple

BI-BUCK TOPOLOGY

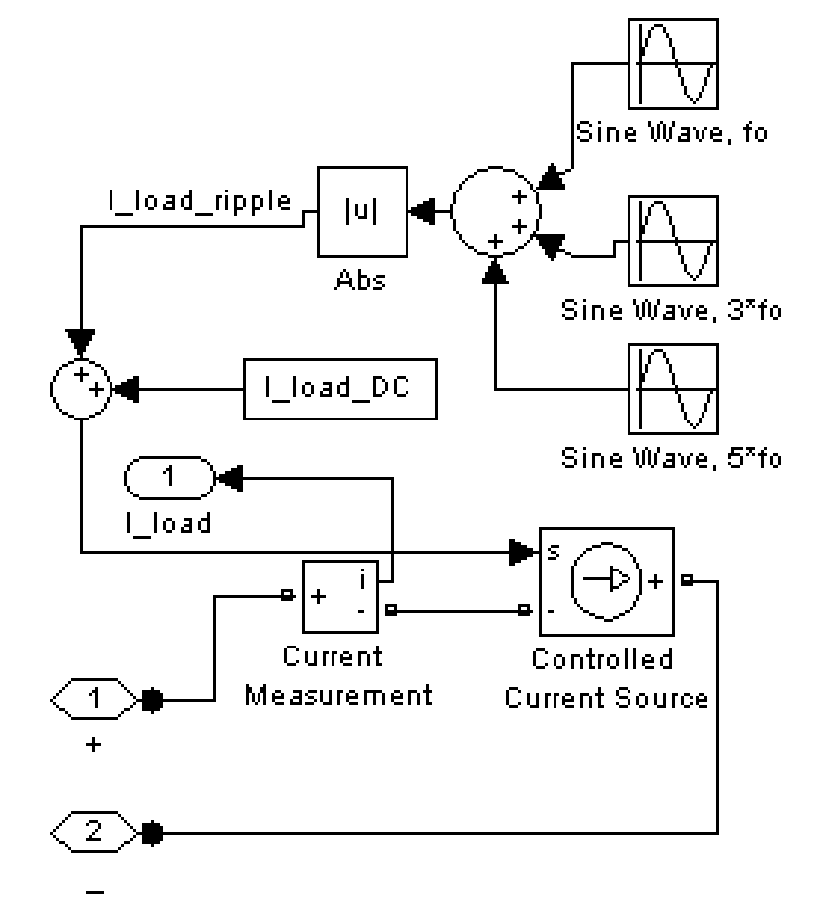

Figure 7. Model of the dynamical load

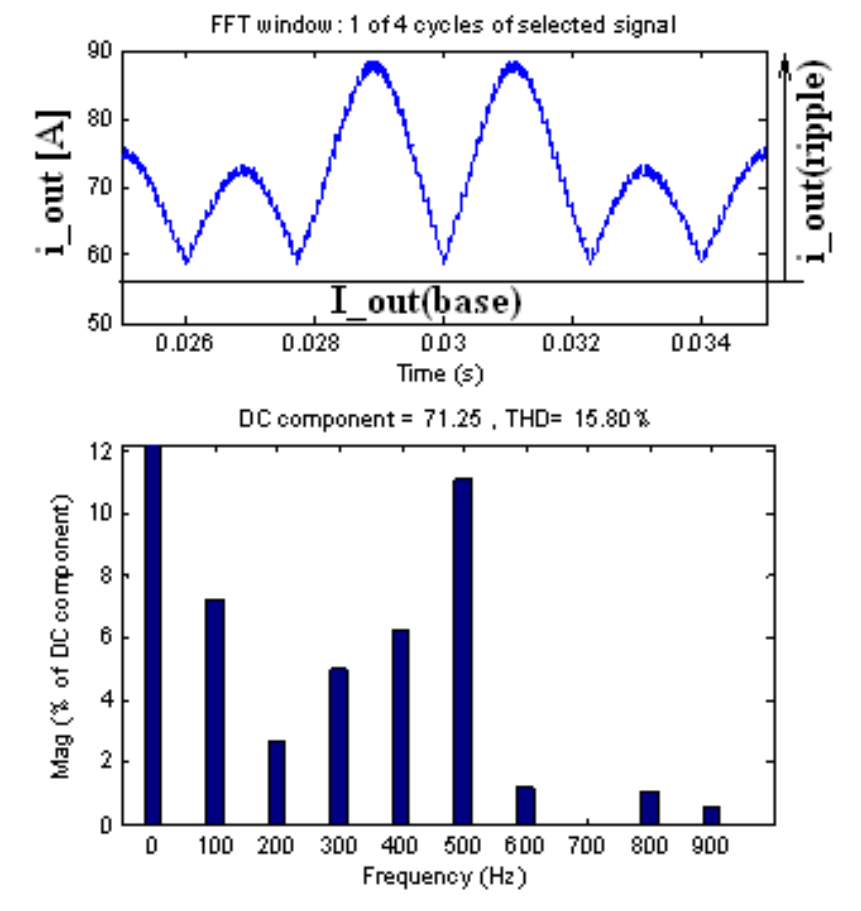

Figure 8. Load current in time (top) and its power spectrum (bottom)

Active Mitigation of the Inverter Current Ripple

BI-BUCK TOPOLOGY

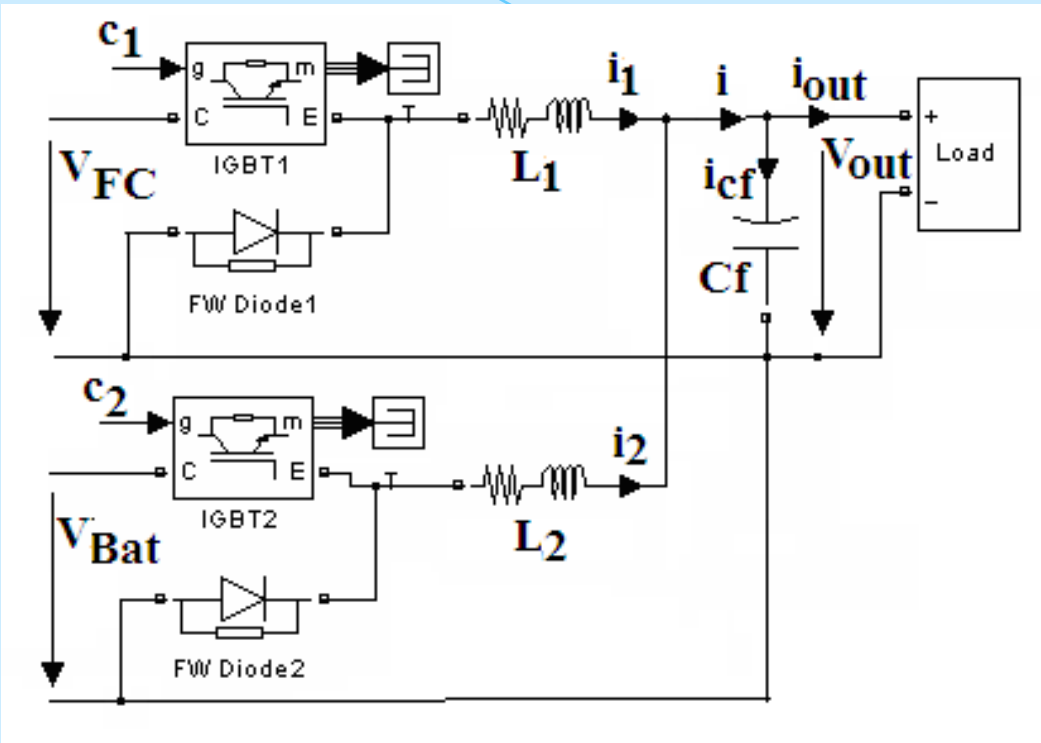

Figure 9. Bi-buck topology

Active Mitigation of the Inverter Current Ripple

BI-BUCK TOPOLOGY

Model of the bi-buck topology

$$c_1 v_{FC} = L_1 \frac{di_1}{dt} + v_{out}$$

$$c_2 v_{Bat} = L_2 \frac{di_2}{dt} + v_{out}$$

$$i_1 + i_2 = i_{out} + i_{Cf}$$

$$i_{Cf} = C_f \frac{dv_{out}}{dt} \qquad (8)$$

By simple manipulation of the equations above, a second-order differential equation is obtained:

$$\frac{L_1}{L_1 + L_2} c_1 v_{FC} + \frac{L_2}{L_1 + L_2} c_2 v_{Bat} = \frac{L_1 \cdot L_2}{L_1 + L_2} \frac{di_{out}}{dt} + v_{out} + C_f \cdot \frac{L_1 \cdot L_2}{L_1 + L_2} \frac{d^2 v_{out}}{dt^2} \qquad (9)$$

Considering identical inductors ($L_1 = L_2 = L$, with series resistance r_L), the second-order differential equation (9) is rewritten as:

$$\frac{1}{2}\left(c_1 V_{FC} + c_2 V_{Bat}\right) - \frac{r_L}{2} i_{out} - \frac{L}{2} \frac{di_{out}}{dt} = V_{out} + \frac{C_f r_L}{2} \frac{dv_{out}}{dt} + \frac{C_f L}{2} \frac{d^2 v_{out}}{dt^2} \qquad (10)$$

where the second-order system parameters, the natural frequency, ω_n [rad/s], and the dimensionless damping ratio, ξ, are respectively:

$$\omega_n = \sqrt{\frac{2}{C_f L}}, \quad \xi = \frac{C_f r_L}{4} \omega_n = \frac{r_L \sqrt{2}}{4} \sqrt{\frac{C_f}{L}} \qquad (11)$$

Active Mitigation of the Inverter Current Ripple
BI-BUCK TOPOLOGY – Controlled Voltage Source (CVS)

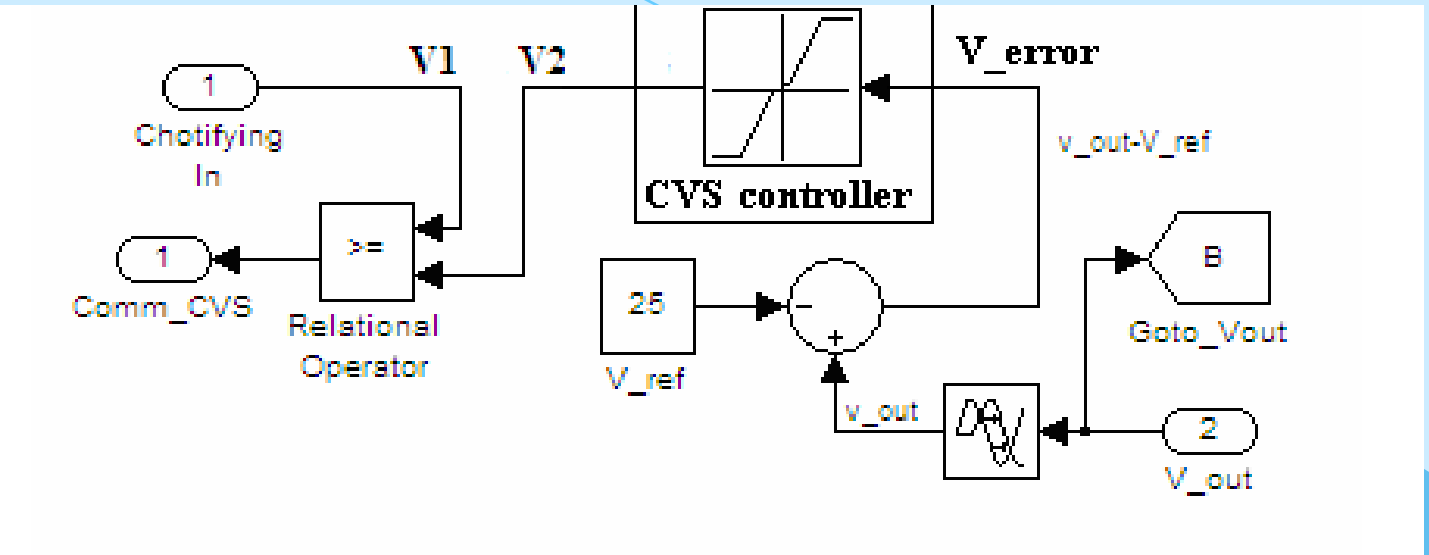

Figure 11. CVS controller that implement the voltage-mode nonlinear control

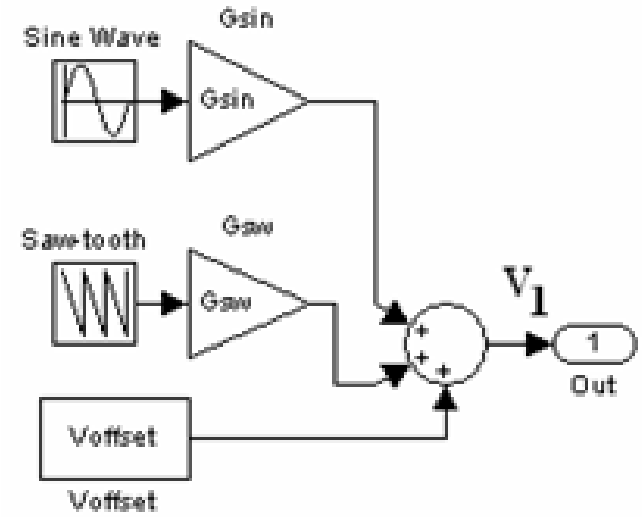

Figure 12. The chaotifying signal generator

Active Mitigation of the Inverter Current Ripple

BI-BUCK TOPOLOGY - CVS

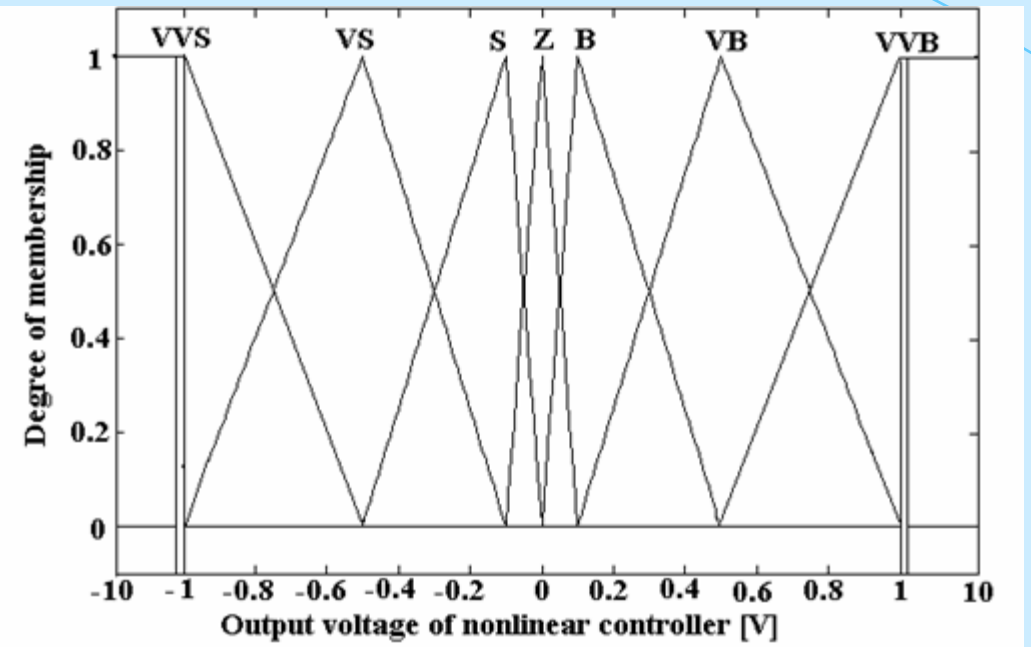

Figure 18. The membership functions for the output voltage of nonlinear voltage control

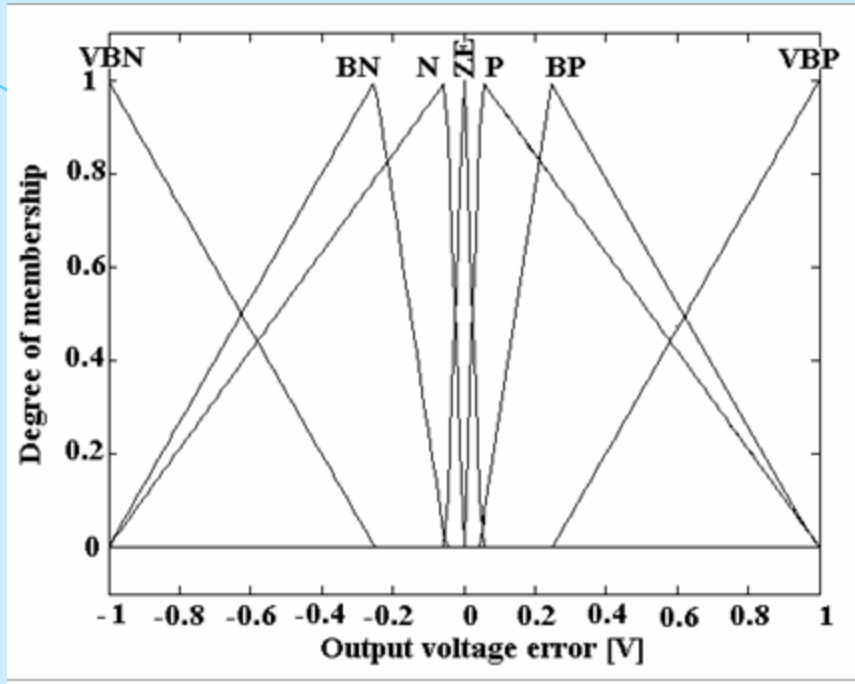

Figure 17. The membership functions for the output voltage error

Table 1
The rules base for CVS fuzzy controller

Rule	Output voltage error	Output voltage of the CVS controller
1	VBN	VVS
2	BN	VS
3	N	S
4	ZE	Z
5	P	B
6	VP	VB
7	VBP	VVB

Active Mitigation of the Inverter Current Ripple

BI-BUCK TOPOLOGY - CVS

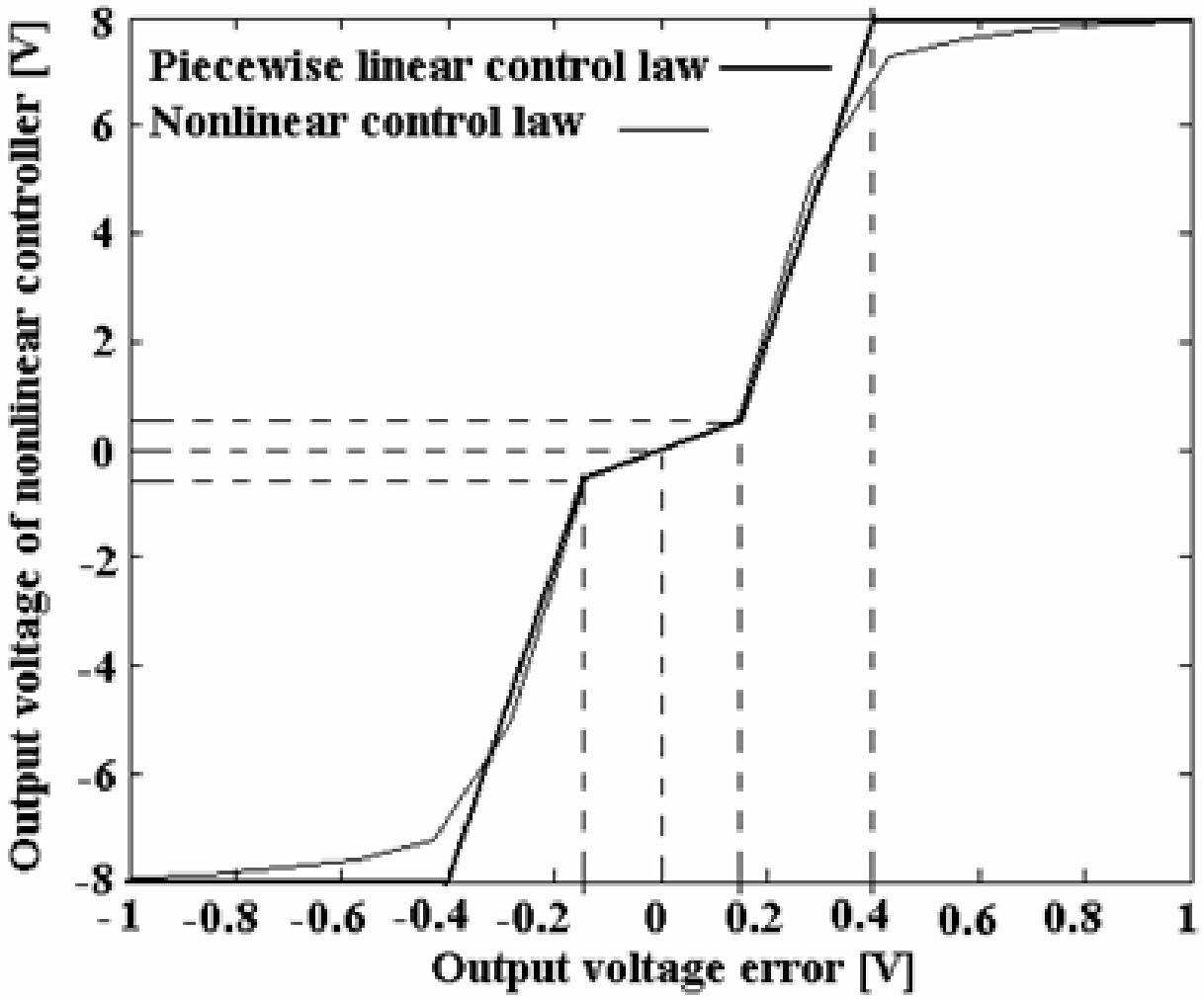

Figure 20. The nonlinear voltage control characteristic (thin line) and PWL voltage control characteristic (thick line) which is fitted on it.

PWL control characteristic:

- input vector:

[-1, -0.5,-0.15, 0.15, 0.5, 1];

- output vector:

[-10,-10,-0.4, 0.4, 10, 10].

Active Mitigation of the Inverter Current Ripple

BI-BUCK TOPOLOGY - CVS

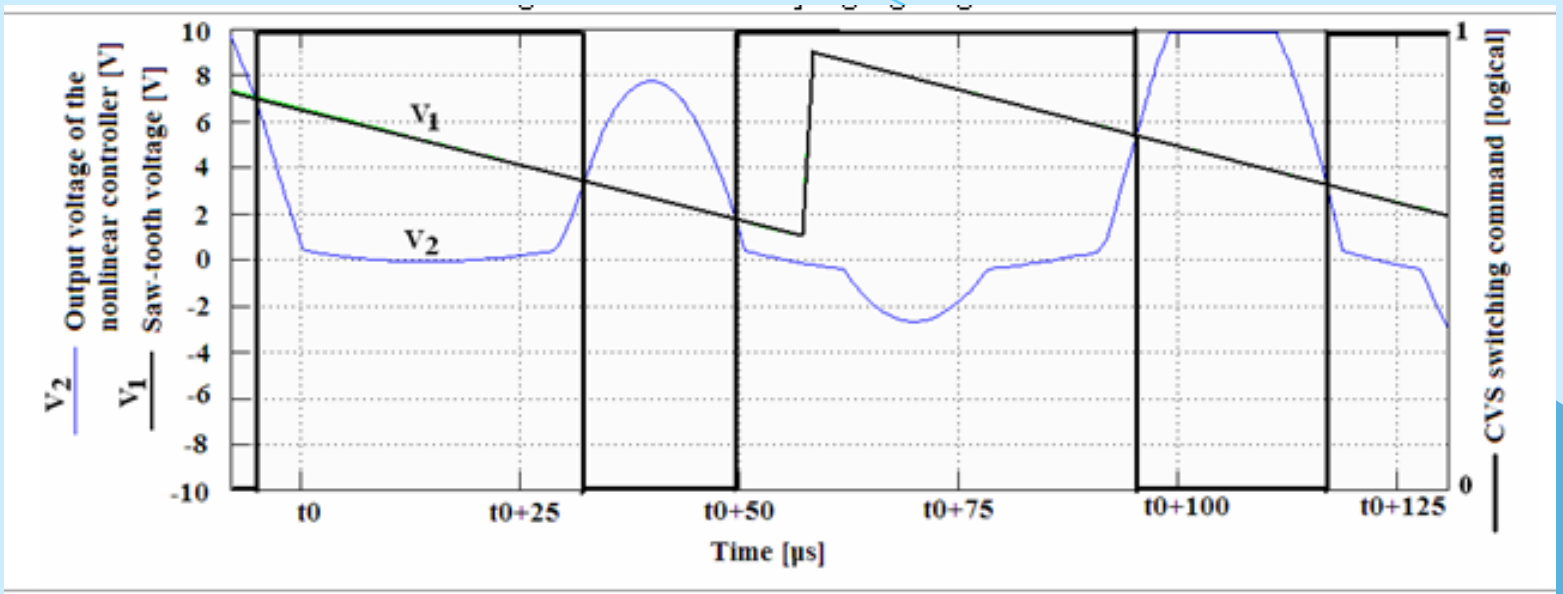

Figure 13. Signals related to CVS controller operation with saw-tooth as chotifying signal

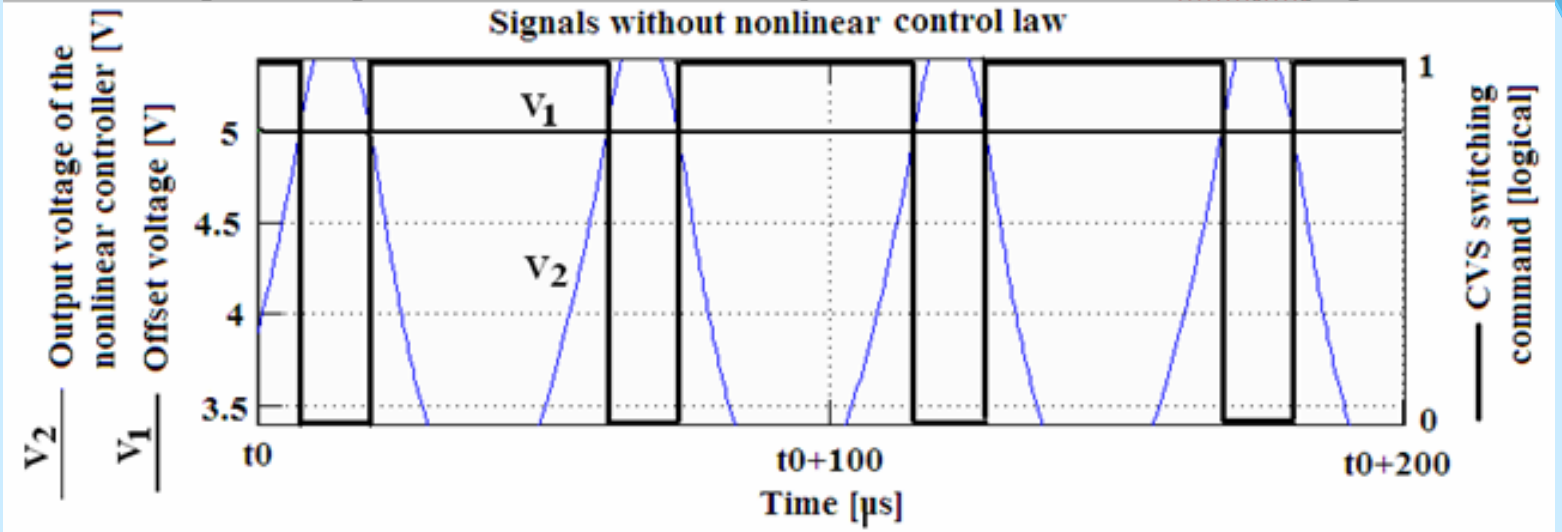

Figure 14. Signals related to CVS controller operation with only offset signal

Active Mitigation of the Inverter Current Ripple

BI-BUCK TOPOLOGY - CVS

Two performance indicators, PI_1 and PI_2, are used to quantify the spreading level of the output power:

$$PI_1 = \frac{\Delta f_{10\%}}{f_{COG}}, \quad PI_2 = \frac{S_{peak}}{THD} \tag{21}$$

where:

S_{peak} is the maximum spectral magnitude (as % of DC component), excluding the harmonics of the chaotifying signal that can possibly occur (see for example Fig. 16);

$\Delta f_{10\%Sp}$ - the frequencies band where the power spectral magnitude is over 10% of S_{peak};

f_{COG} - the center-of-gravity frequency of power spectrum;

THD - total harmonic distortion factor of output voltage.

Interpretation of performance indicators relating to quantification mode of the power spectrum spreading level is presented below:

- If PI_1 >50%, then $\Delta f_{10\%Sp} > f_{COG}/2$, and this means a large frequencies band where is situated the most part of the spread power spectrum;
- If PI_2 <50%, then S_{peak} <THD/2, and this means no high peak in the spread power spectrum.

The performance indicators are estimated for different load currents (see Fig. 21).

Table 2. The performance indicators for case study

I_{out} [A]	f_{RL} [kHz]	f_{RC} [kHz]	PI_1 [%]	PI_2 [%]	RF_{Vout}[%]
15	2.6526	2.0318	79	32	5.6
20	1.9894	2.7090	42	52	4
25	1.5915	3.3863	35	41	3.2
30	1.3263	4.0635	25	47	3.2
35	1.1368	4.7408	34	46	3.2
40	0.9947	5.4180	27	55	3.2

$$f_{RC} = \frac{1}{2\pi} \cdot \frac{1}{C_f R_{out}}, \quad f_{RL} = \frac{1}{2\pi} \cdot \frac{R_{out}}{L/2}, \quad f_{LC} = \frac{\omega_n}{2\pi}$$

Active Mitigation of the Inverter Current Ripple

BI-BUCK TOPOLOGY - CVS

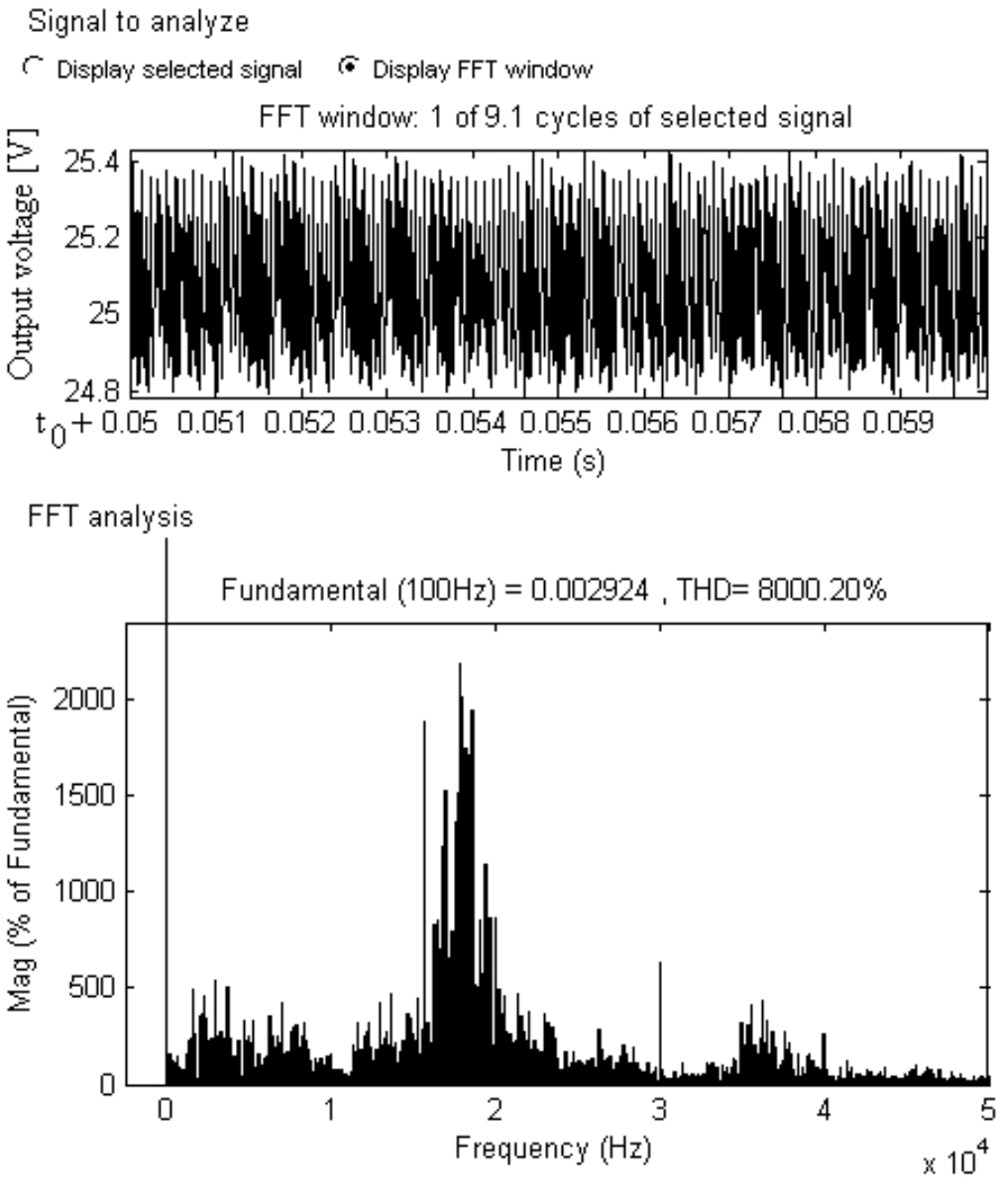

Figure 21. The output voltage (top) and its power spectrum (bottom) with simulation parameters: fsw=15 kHz, L=100 μH, C=47 μF, Rout=2/3 Ω

Active Mitigation of the Inverter Current Ripple

BI-BUCK TOPOLOGY - CVS

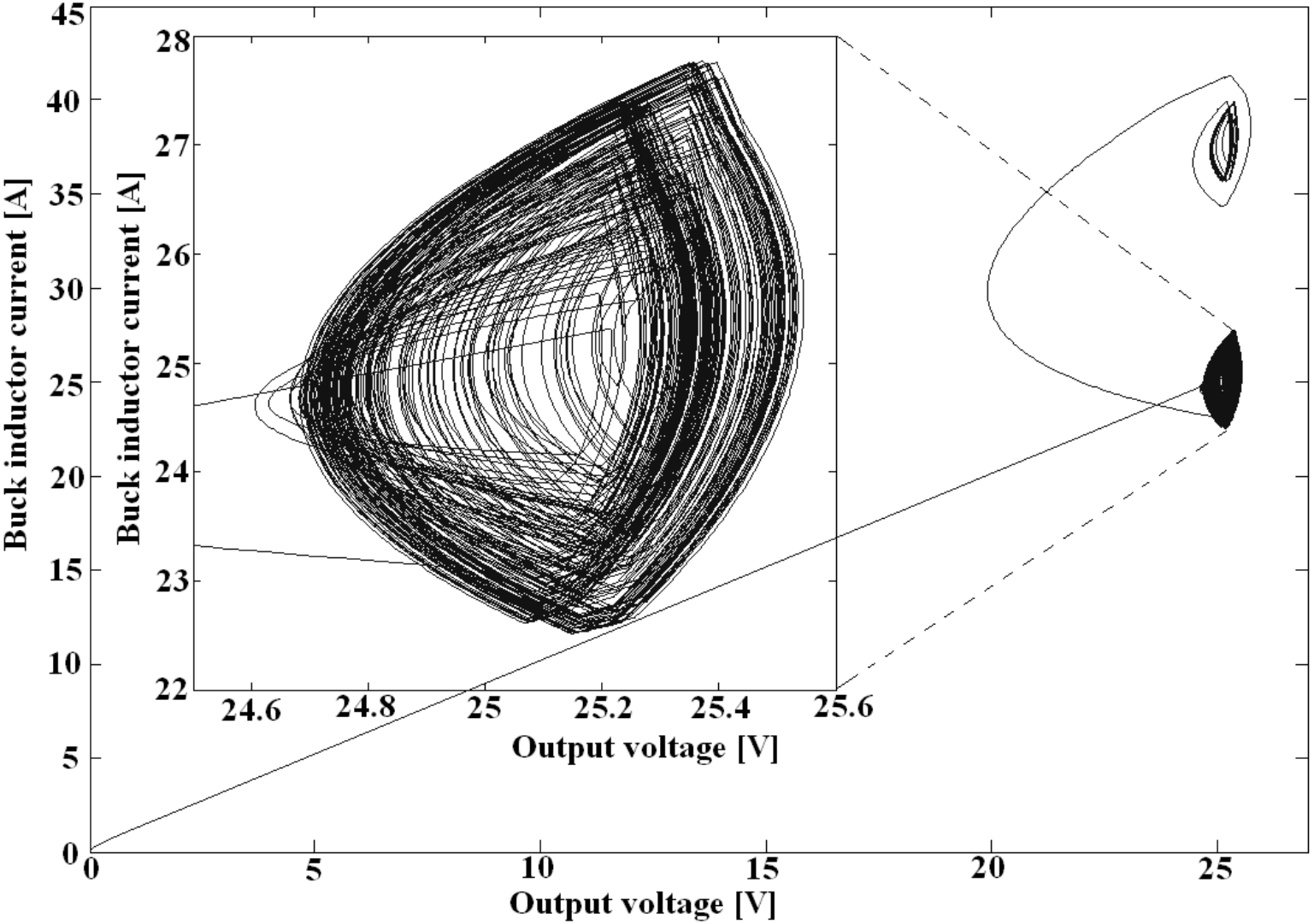

Figure 24. The CVS dynamic in phases plane using the simulation parameters: fsw=15 kHz, L=100 μH, C=47 μF, Rout=2/3 Ω

Active Mitigation of the Inverter Current Ripple

BI-BUCK TOPOLOGY – CVS: Conclusion

- The bi-buck HPS topology was proposed as solution to mitigate the LF current ripple on the HPS output node by injection of an anti-ripple current on this point, where are connected the nonlinear load, the CVS and the CCS. The injected current tracks the shape of LF inverter current ripple using an active control loop for the CCS controller, which will be shown in next slides.
- The proposed nonlinear CVS controller is designed to assure good performances in both frequency and time domain. The closed loop frequency value and voltage ripple could be tuned via the hysteresis level of the controller.
- All the reported results have been validated in several simulations. The nonlinear voltage CVS controller performs good performances:

- an output voltage ripple factor up to 4% for the load current in the rated range;
- a width of spread frequencies band in range of 3 kHz to 37 kHz, depending by load power level;
- the power peaks in the range of 30% to 55% from the THD value.

Active Mitigation of the Inverter Current Ripple

BI-BUCK TOPOLOG –Current Controlled Sources (CCS)

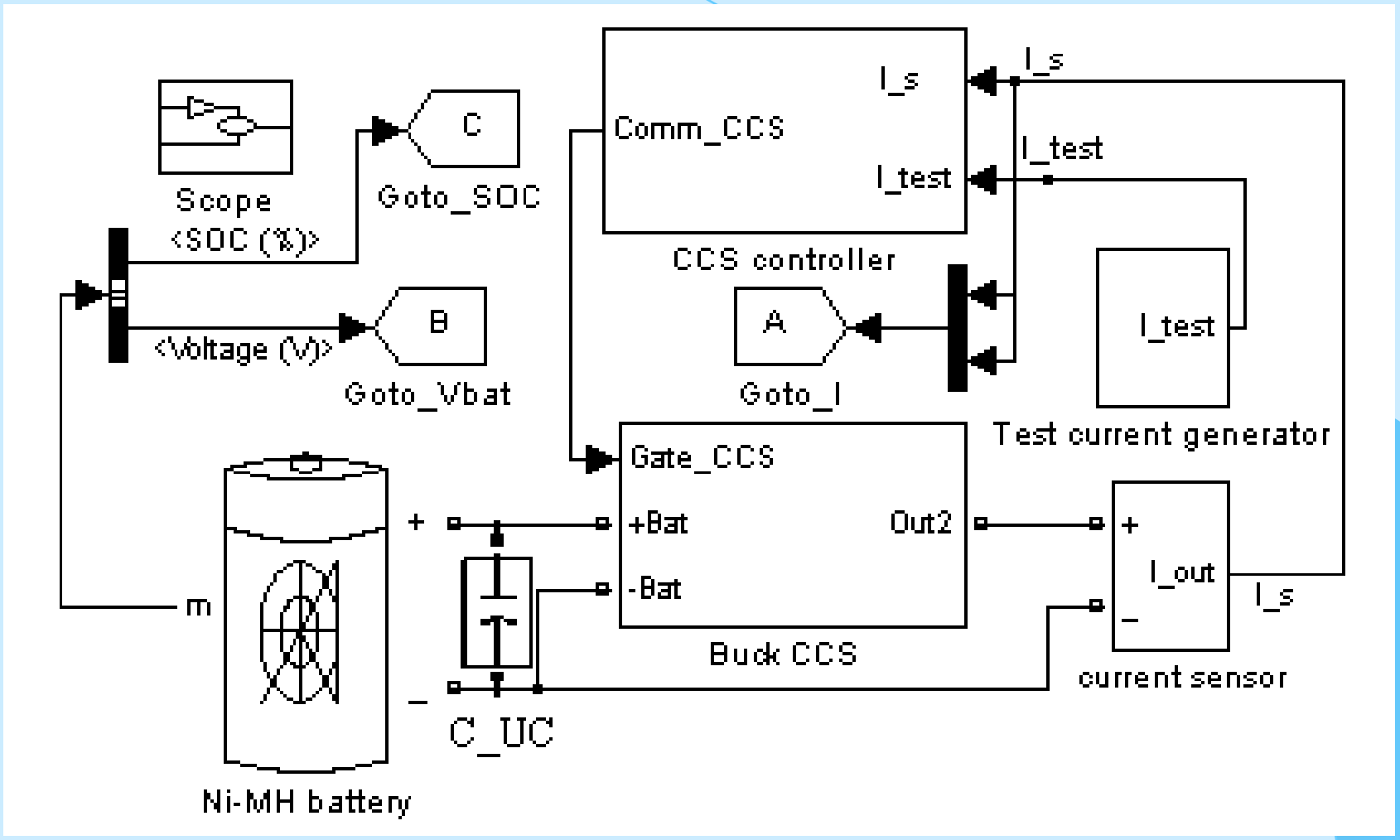

Figure 10. Buck CCS under test

Active Mitigation of the Inverter Current Ripple

BI-BUCK TOPOLOGY – CCS testing

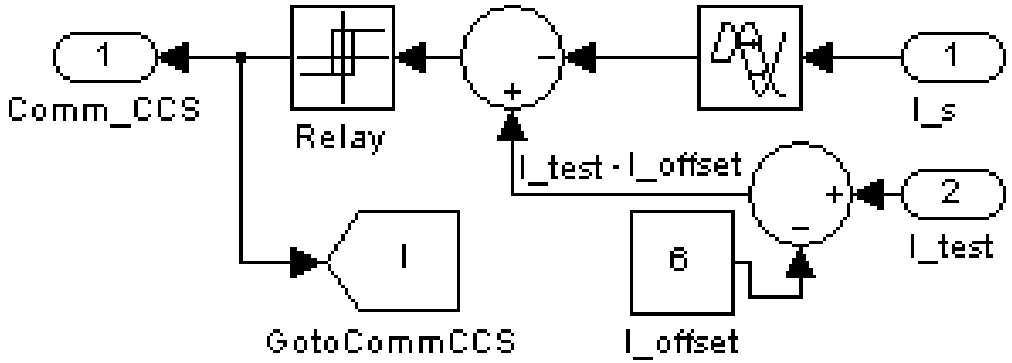

Figure 11. CCS hysteretic controller structure

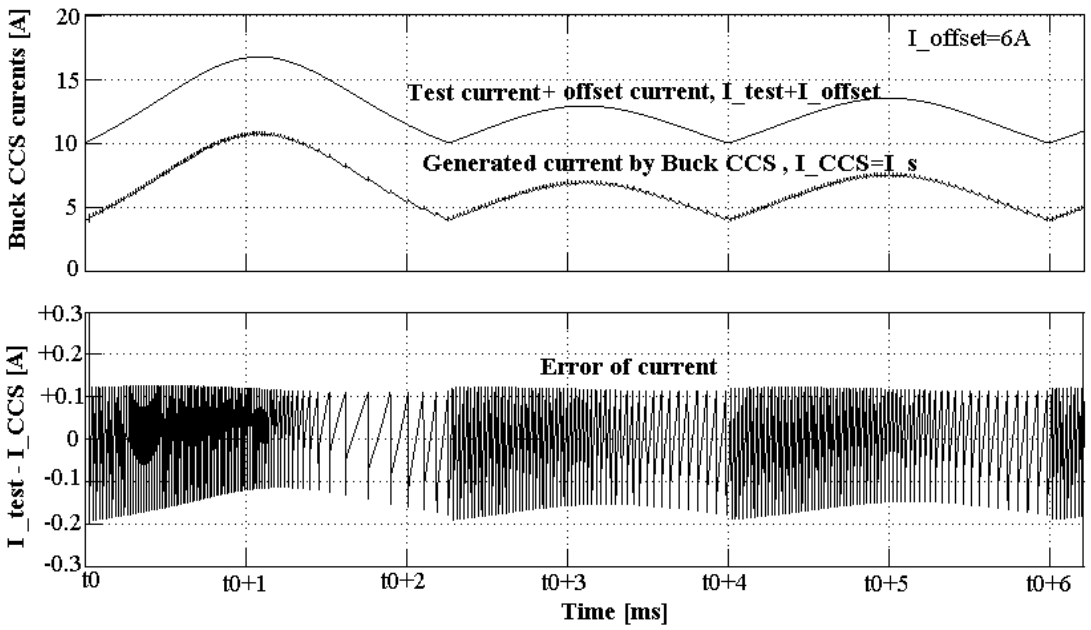

Figure 12. Simulation results for buck CCS

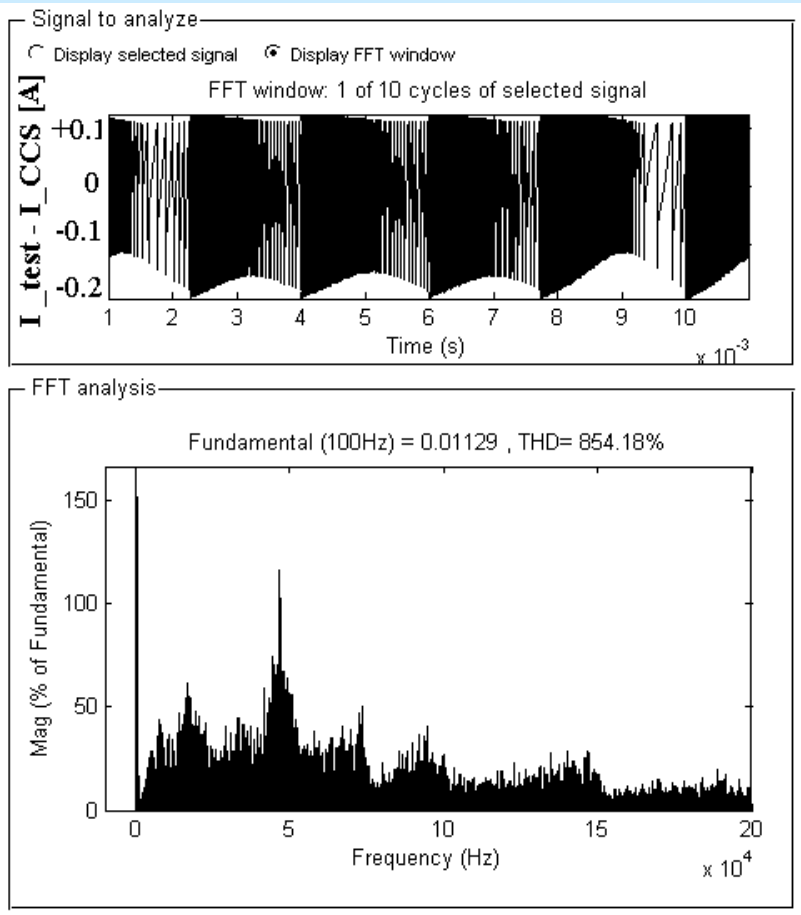

Figure 13. Error of current (top) and its power spectrum (bottom)

Active Mitigation of the Inverter Current Ripple

BI-BUCK TOPOLOGY – CCS

Hysteretic current-mode control

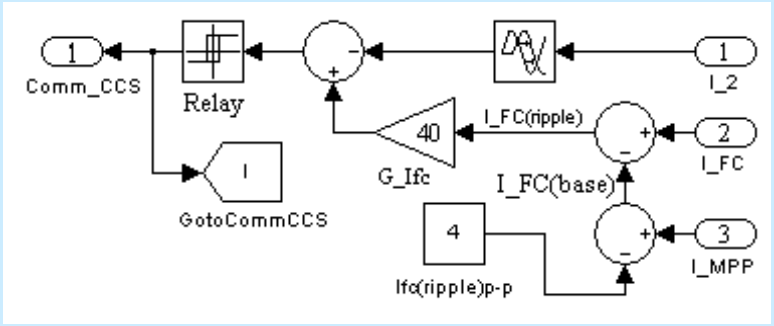

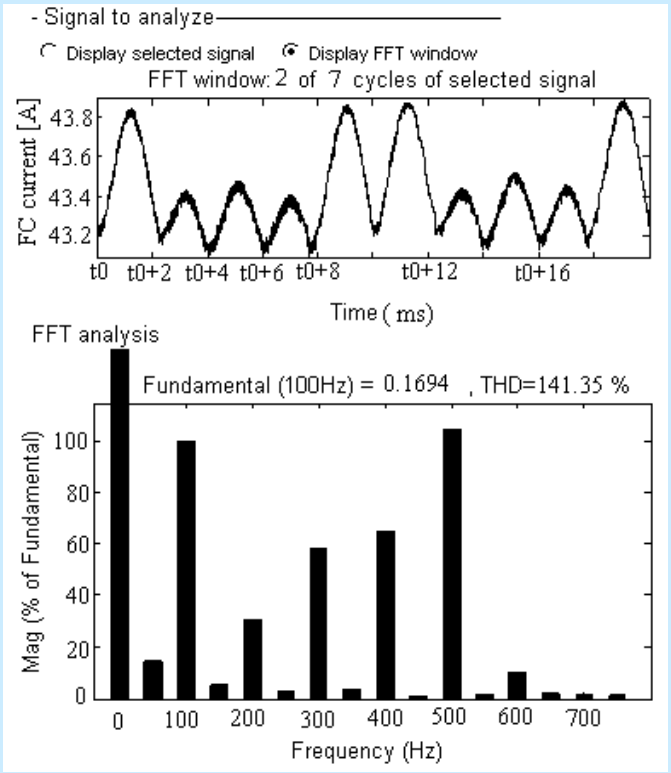

Peak current-mode control (PCC)

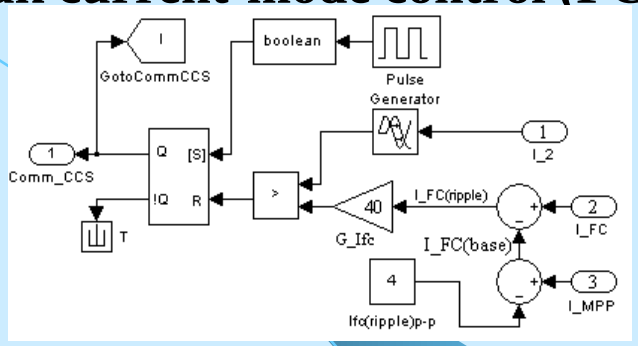

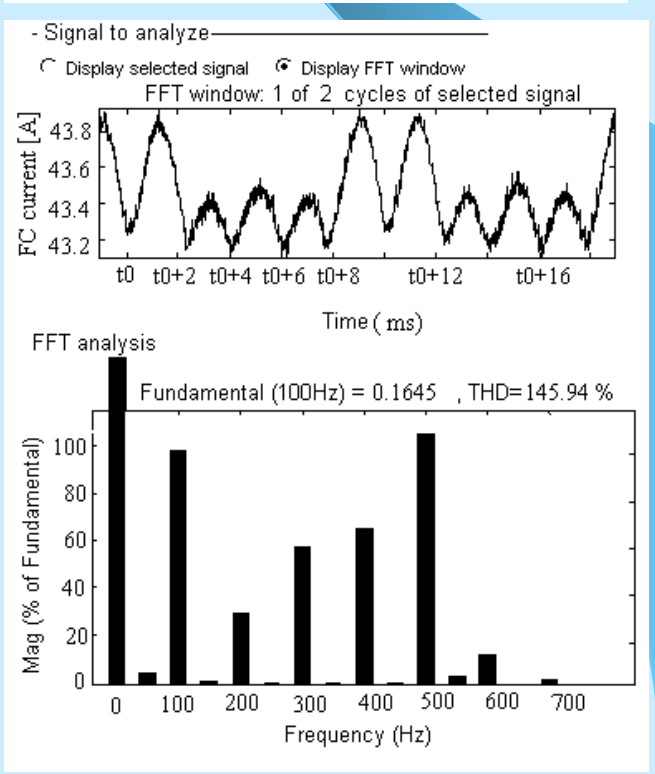

FC current (top) and its power spectrum (bottom): 1.26 kW HPS, GIfc=80

Active Mitigation of the Inverter Current Ripple

BI-BUCK TOPOLOGY – CCS: nonlinear control law

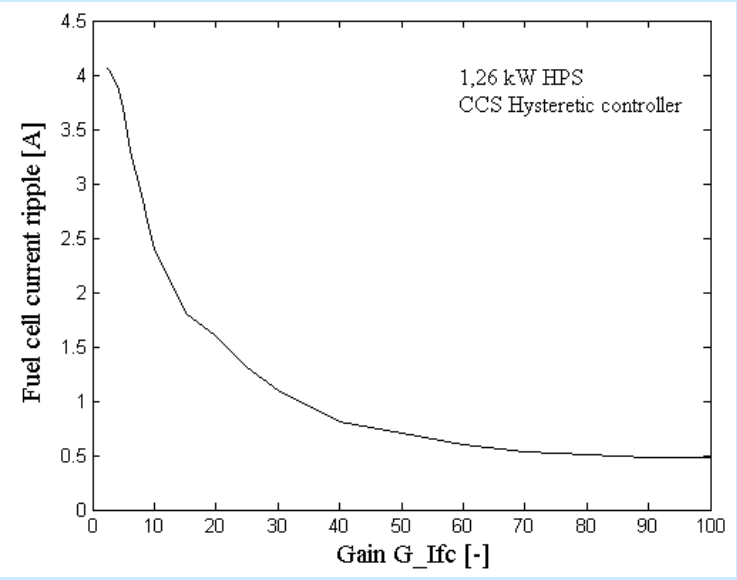

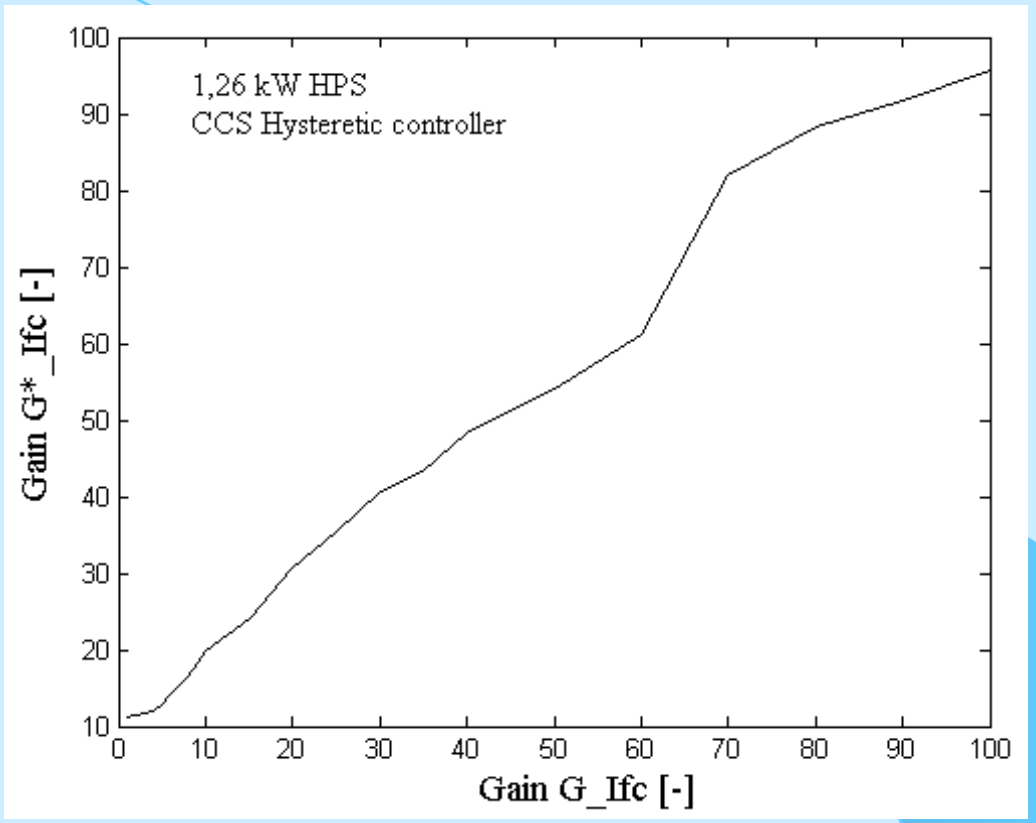

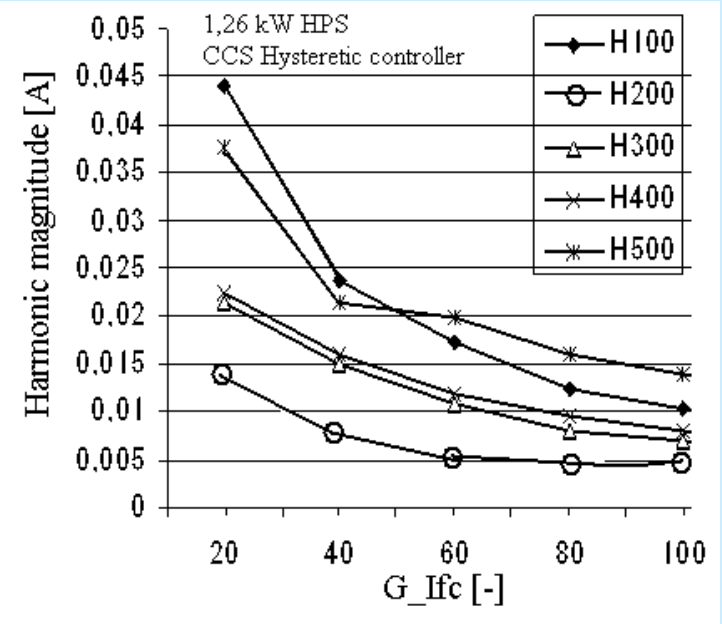

Computed gain G^*_{Ifc} vs. set value of the G_{Ifc} gain

$$G^*_{Ifc} = \frac{\Delta I_{CCS(ripple)}}{\Delta I_{FC(ripple)}} \cong \frac{\Delta I_{out(ripple)}}{\Delta I_{FC(ripple)}} \cong \frac{RF_{out}}{RF_{FC}} \cdot \frac{\eta_1 V_{FC(base)}}{V_{out}} \Rightarrow$$

$$G^*_{Ifc} \cong \frac{RF_{out}}{RF_{FC}} \cdot G_{1(base)}$$

Active Mitigation of the Inverter Current Ripple

BI-BUCK TOPOLOGY – CCS: designing of FLC

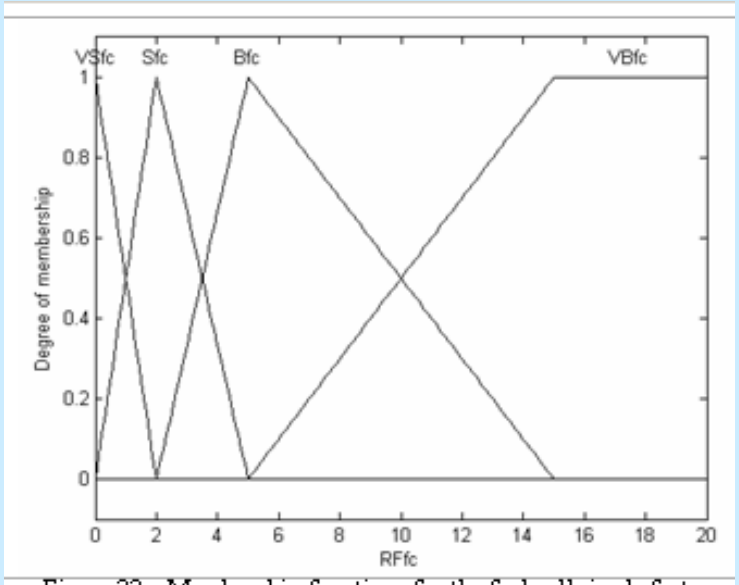

Figure 22a. Membership functions for the fuel cell ripple factor

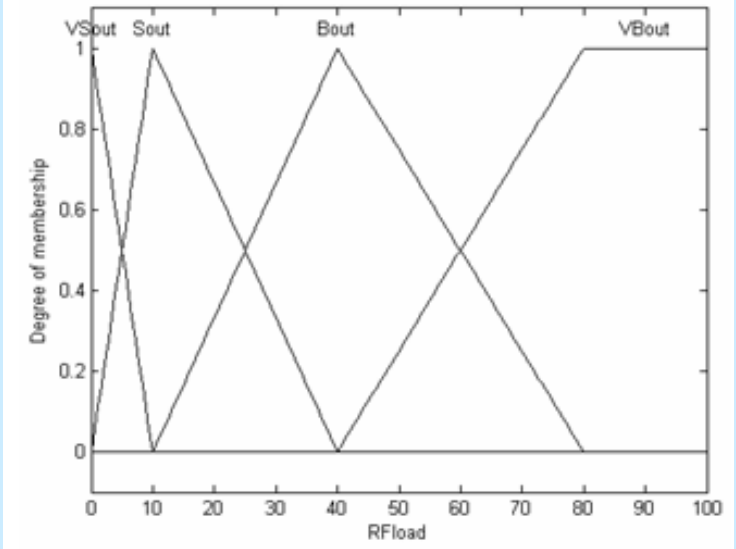

Figure 22b. Membership functions for the load ripple factor

Command signal		RFfc			
		VSfc	Sfc	Bfc	VBfc
RFload	VSrm	Mcom	Scom	VScom	VScom
	Srm	Bcom	Mcom	VScom	VScom
	Brm	VBcom	VBcom	Mcom	Scom
	VBrm	VBcom	VBcom	Bcom	Mcom

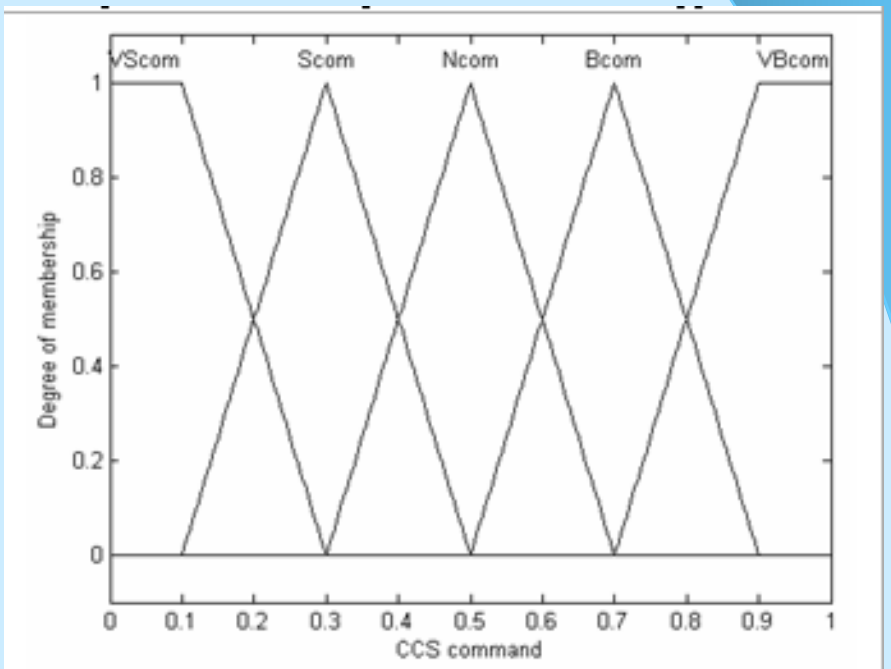

Figure 22c. Membership functions for the command signal

Active Mitigation of the Inverter Current Ripple

BI-BUCK TOPOLOGY – CCS: FLC

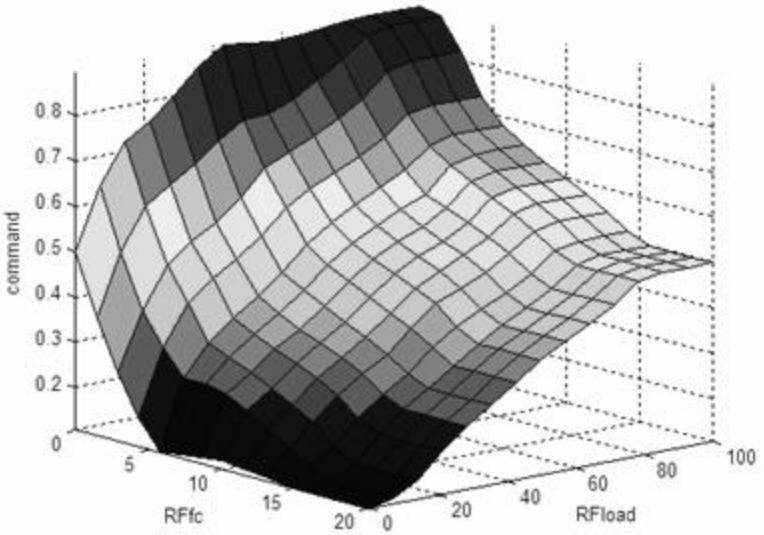

Figure 23. The FLC control surface

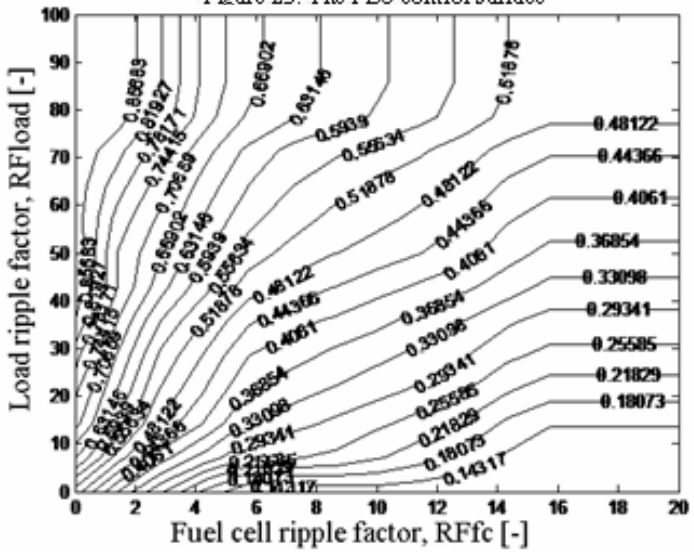

Figure 24. The projected contours for the FLC control surface

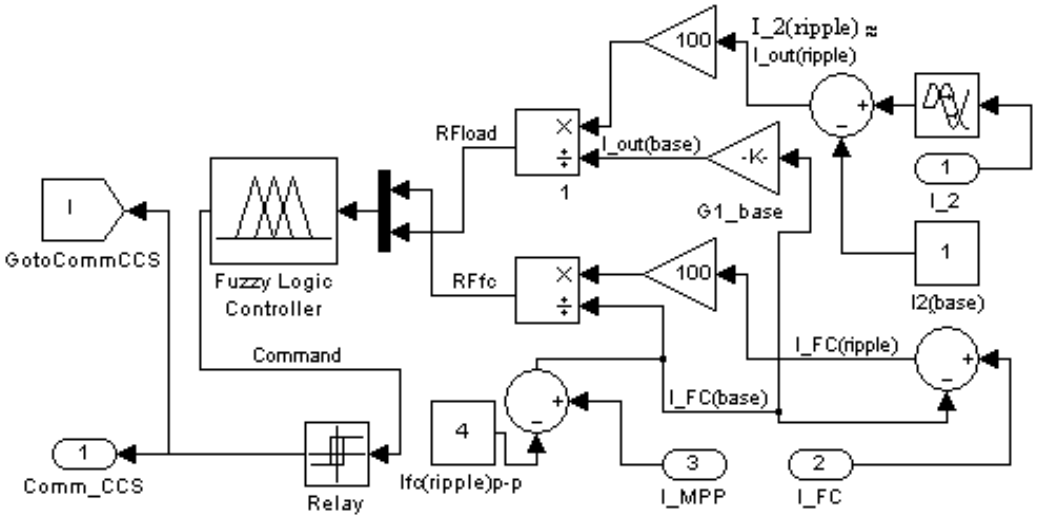

Active Mitigation of the Inverter Current Ripple
BI-BUCK TOPOLOGY – CCS: nonlinear controller

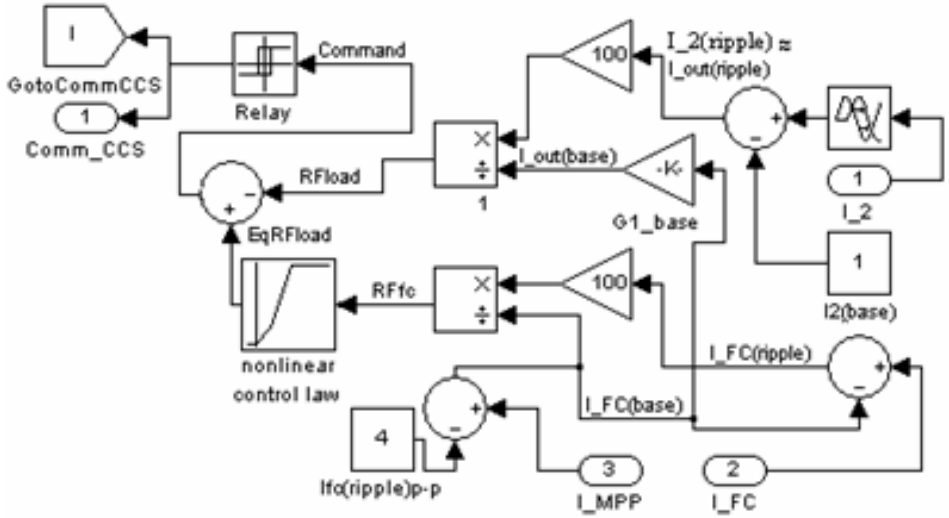

Figure 26. The structure of CCS nonlinear controller

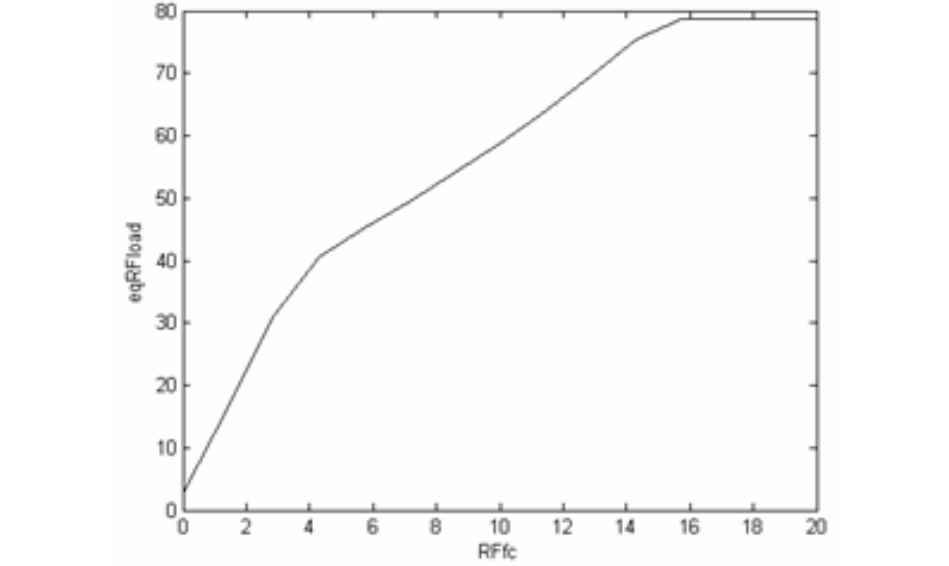

Figure 27. The nonlinear control law of EqRFload vs. RFfc

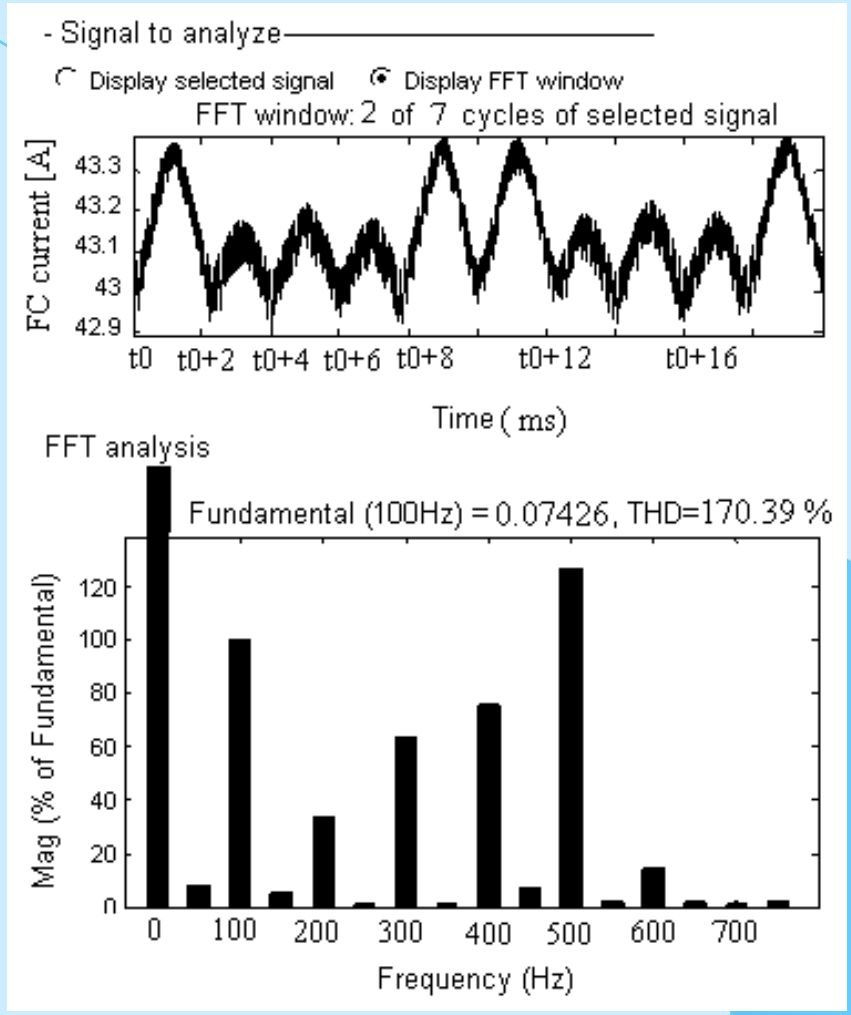

Active Mitigation of the Inverter Current Ripple
BI-BUCK TOPOLOGY: simulation results

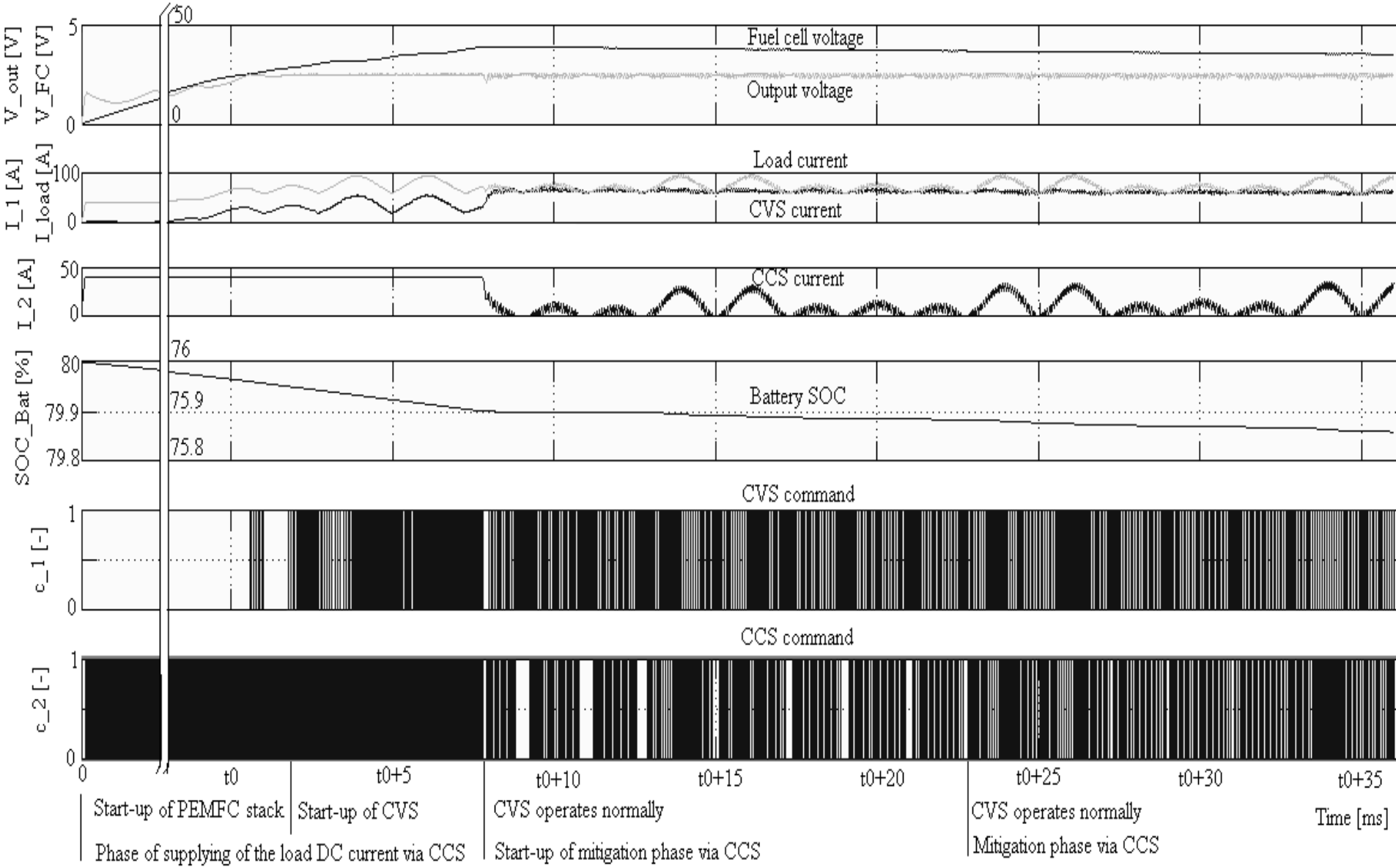

Active Mitigation of the Inverter Current Ripple
BI-BUCK TOPOLOGY: simulation results

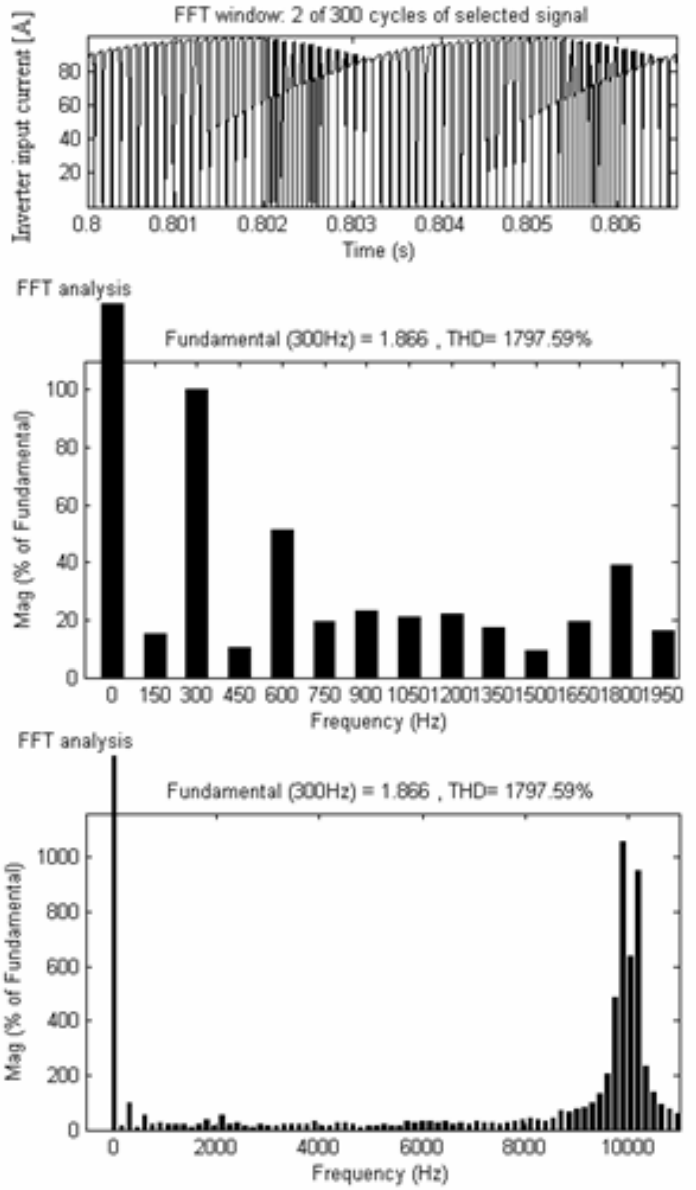

Figure 37. Input current of the three-phase inverter system

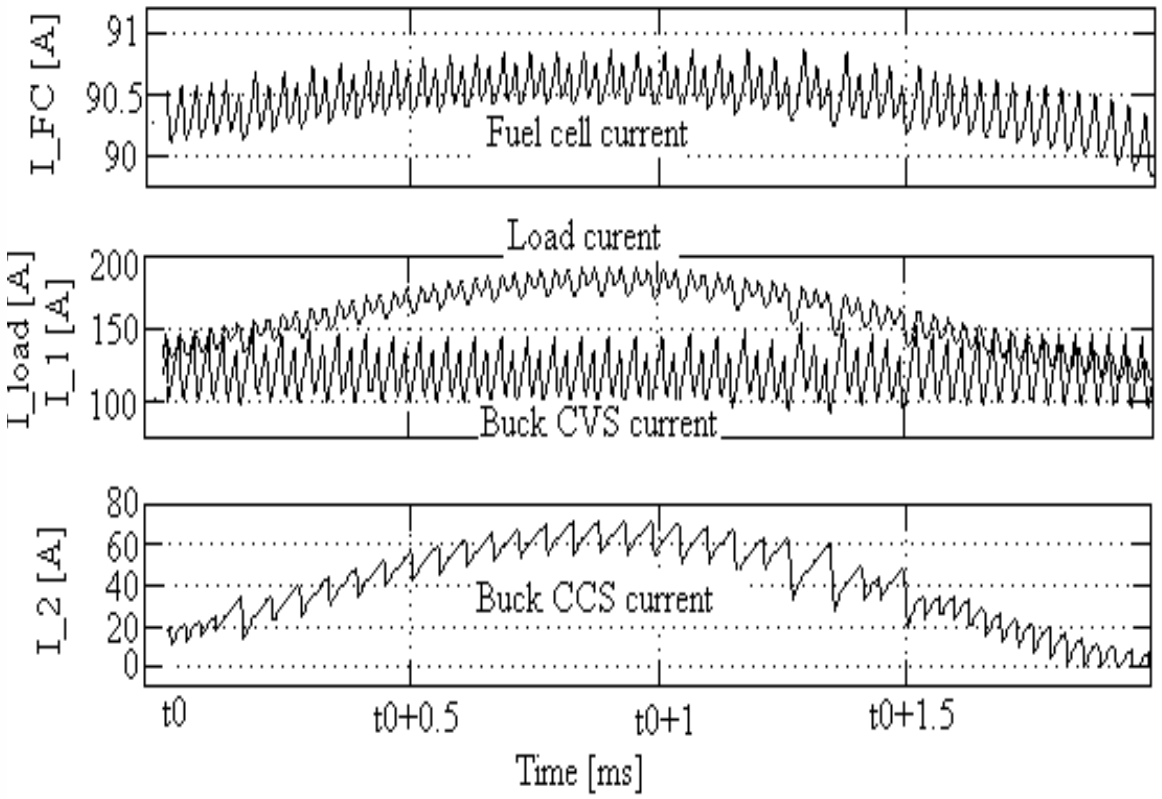

Active Mitigation of the Inverter Current Ripple

BI-BUCK TOPOLOGY: Conclusion

- The LF current ripple normally appears in operation of the fuel cell inverter system and this is back propagated on the HPS voltage bus, and finally to the PEMFC stack.
- The design goal of the CCS controller is to mitigate this LF current ripple based on an anti-ripple current generated by the buck CCS.
- The input current of the inverter system has big HF harmonics close to the carrier frequency. So, a low-pass filter is needed to extract its LF shape of this signal.
- This filter introduces a variable phase-shift on the processed signal, thus a delayed anti-ripple current is generated. Consequently, the desired mitigation performance (RF up to 3%) can't be obtained.
- To avoid this problem, the anti-ripple current is generated using a mitigation control loop for the CCS current that will track the FC current amplified by the G_{Ifc} gain.
- The design methodology for the GIfc gain was presented here in detail.
- Note that the CCS current will indirectly track the LF shape of the input current of the inverter system based on proposed active control.
- Consequently, the proposed bi-buck topology can effectively depress current RF to be up to 3%, maintaining the voltage ripple factor up to 4% (or lower).
- In simulation, the obtained current ripple factor is about 1%.

Part III: ESC schemes

- In this part of the presentation, the architecture of the Hybrid Power Source based on Maximum Power Point tracking controller to harvest the energy available from used Renewable Energy Sources is presented. Usually, the energy harvesting is based on Extremum Seeking Control (ESC) loop.
- Two ESC schemes are proposed and analyzed in relation with the classical ESC schemes: (1) the modified ESC scheme (named mESC scheme because is based on band-pass filter BPF use, instead of series connection of the high-pass and low-pass filters such as used in higher order ESC scheme) and (2) its equivalent representation (named EQmESC because is based on modified higher order ESC scheme).
- The cut-off frequency of low-pass filter is chosen larger than in higher order ESC schemes in both ESC schemes proposed. This improves the dither persistence on the proposed ESC schemes, so the search speed of the extremum increases accordingly.

Introduction

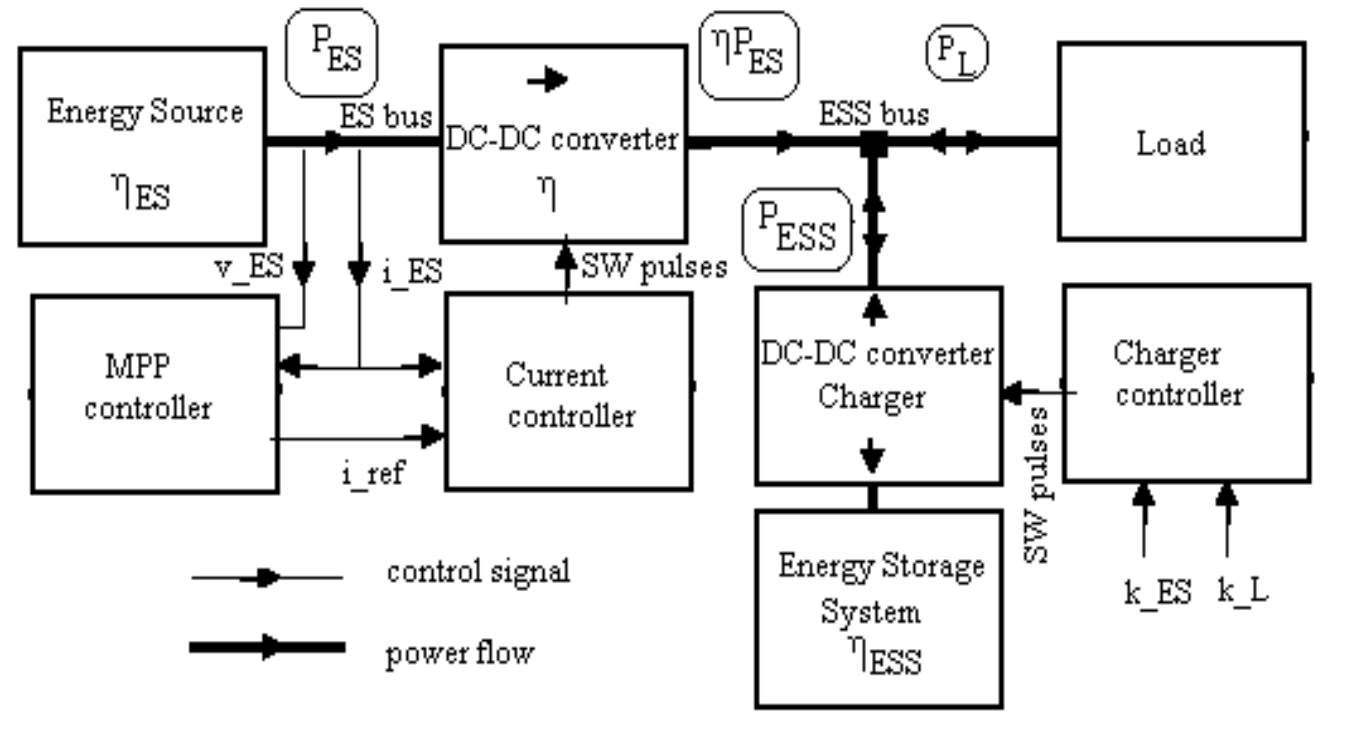

Architecture of the Hybrid Power Source

- **The power flow balance for the HPS**

$$p_L = \eta \cdot p_{FC} + p_{ESS}$$

- **The ESS power is**

$$p_{ESS} = p_L - \eta \cdot p_{FC}$$

Introduction

- Different Energy Management Strategies (EMSs) were proposed for the HPS used as distributed generation units in the smart grids or that supply the power-train units in the hybrid vehicles.
- If a load-following control loop is used, then the Energy Storage System (ESS) will operate on Charge-Sustaining (CS) mode, dynamically compensating the load changes.
- If the load-following control loop is not used, then the ESS will operate in one of the above mentioned mode by controlling the ESS charger based on two available parameters, the charging ESS factor, k_{ES}, and the regenerative load factor, $k_{L.}$
- The charger is a bidirectional DC-DC converter controlled by the EMS unit.
- This part is organized as follows. Section 2 briefly presents some topologies of the MPP tracking controller based on classical and proposed ESC schemes. Analysis of the ESC schemes on the frequency domain is performed in Section 3. Last section concludes the first part of this presentation.

MPP tracking controller

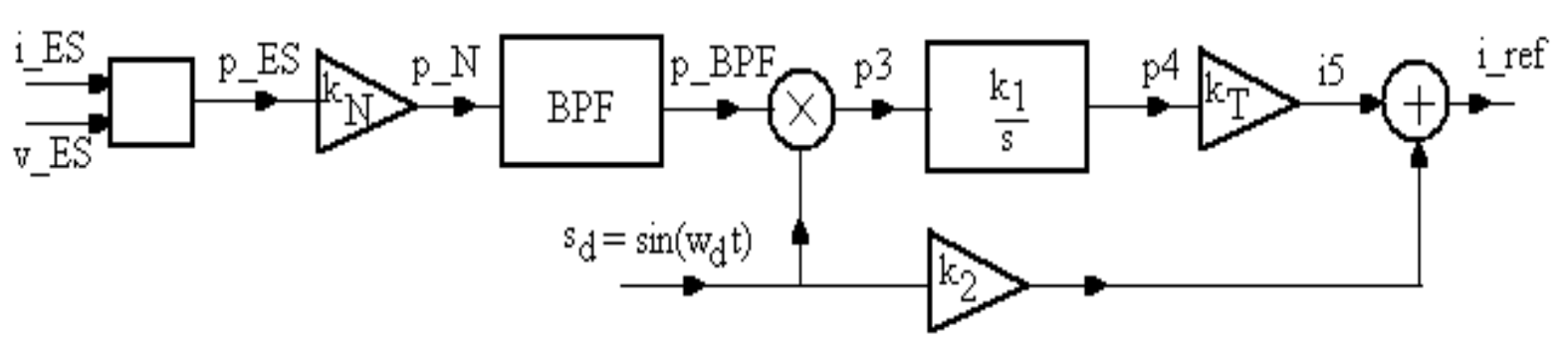

- Figure 2 MPP tracking controller based on BPF

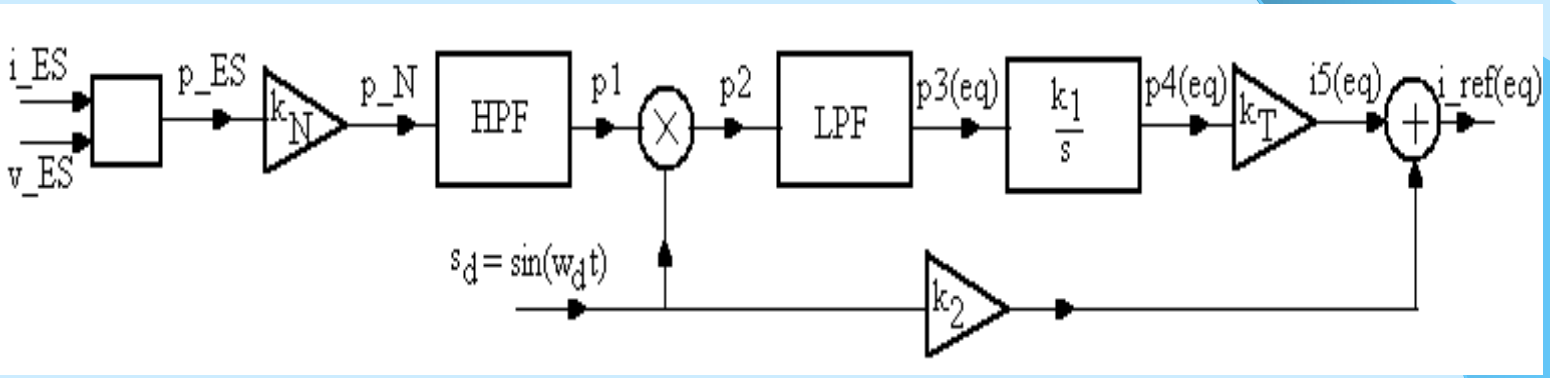

- Figure 3 MPP tracking controller based on series connection of two filters (HPF+LPF)

MPP tracking controller

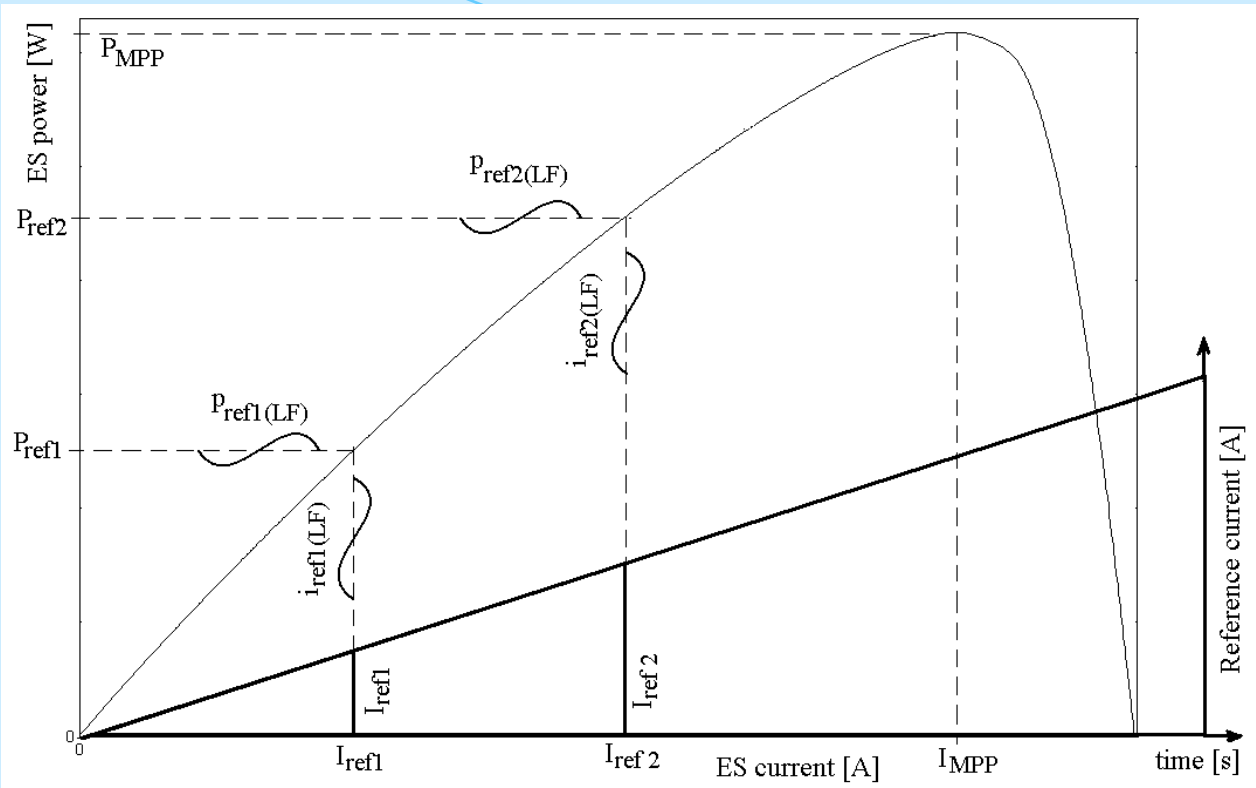

- **Searching of the MPP on the P-I characteristic with one extremum**

- **The ESC is an adaptive closed-loop control used for searching of unknown extremum on a static input-output characteristic based on dither signal.**

- **The MPP tracking accuracy is defined as:** $100 \cdot (P_{ES(AV)} / P_{MPP})\,[\%]$

MPP tracking controller

- *The higher order ESC schemes*
- The higher order extremum seeking control (hoESC) schemes are based on classical ESC scheme, which is augmented with LPF and/or HPF as in Figure 3.
- In this presentation, the cut-off frequency of LPF, ω_l, is chosen larger ($\omega_l=\alpha_l\omega_d$, $3<\alpha_l$) than in hoES schemes proposed in the literature, where $\omega_l=\alpha_l\omega_d$, $0<\alpha_l<1$, and ω_d is the dither frequency. Thus, at least three harmonics of the ES power are processed into the ESC control loop to improve the searching speed gain, G_{SS}, based on increased level of the dither persistence.
- For example, the second harmonic of the reference current results through the demodulation of first and third harmonics.
- In this presentation, other approximate relationships of the magnitudes for the first low frequency (LF) harmonics' are shown in first and second part, demonstrating the improved dither persistence on the reference current.

MPP tracking controller

- *The proposed ESC scheme*
- In this section the modified ESC scheme, Figure 2 and its equivalent representation (named EQmESC because is based on series connection of the HP and LP filters; see Figure 3) are analyzed.
- It may be noted that EQmESC scheme has the same topology with the hoES control scheme, except the LPF cut-off frequencies that are larger ($\alpha_{l(EQmES)}=\alpha_{l(mES)}>3>1>\alpha_{l(hoES)}$).

- The current-mode controller operates the DC-DC converter such as:

$$i_{ref\,(eq)} \cong i_{ES}$$

- Thus:

$$i_{ref\,(eq)} \to I_{MPP} \Rightarrow i_{ES} \to I_{MPP}$$

Analysis of the ESC schemes on the frequency domain

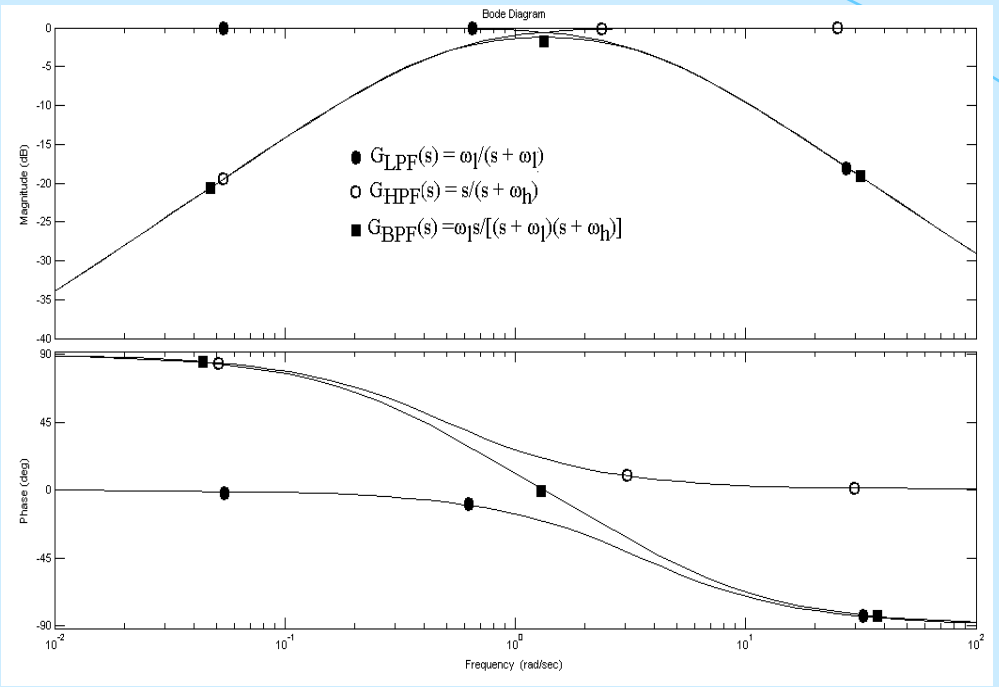

$$\left|G_{HPF}(\omega)\right| = 1/\sqrt{1+\left(\omega_h/\omega\right)^2},$$

$$\phi_{HPF}(\omega) = \arg(G_{HPF}) = \arctan\left(\omega_h/\omega\right)$$

$$\left|G_{LPF}(\omega)\right| = 1/\sqrt{\left(\omega/\omega_l\right)^2+1},$$

$$\phi_{LPF}(\omega) = \arg(G_{LPF}) = -\arctan\left(\omega/\omega_l\right)$$

$$\left|G_{BPF}(\omega)\right| = \left|G_{HPF}(\omega)\right|\left|G_{LPF}(\omega)\right|,$$

$$\phi_{BPF}(\omega) = \arg(G_{BPF}) = \phi_{HPF}(\omega)+\phi_{LPF}(\omega)$$

- The frequency characteristics of the HP, LP, and BP filters used are given by the relationships , considering $G_{BPF}(s) = G_{HPF}(s)\cdot G_{LPF}(s) = \omega_l\cdot s/[(s+\omega_l)\cdot(s+\omega_h)]$, and shown in Figure 5 for $\alpha_h=0.5$ and $\alpha_l=3.5$

Analysis of the ESC schemes on the frequency domain

- Because the BPF topology can be represented as an equivalent series combination of the HP and LP filters, then both mESC and EQmES schemes operate equivalently based on the following signal processing relationships on the ESC loop.

$$p_{3(eq)}(t) = \left[\left(p_{1(LF)}(t) + p_{1(HF)}(t)\right) \cdot A\sin(\omega_d t)\right] * L^{-1}\left\{G_{LPF}(s)\right\} \cong \left[p_{1(LF)}(t) \cdot A\sin(\omega_d t)\right] * L^{-1}\left\{G_{LPF}(s)\right\} \cong p_{3(eq)(LF)} \Rightarrow$$

$$\Rightarrow p_{3(eq)(LF)}(t) \cong \left\{\left[p_{N(LF)}(t) * L^{-1}\left\{G_{HPF}(s)\right\}\right] \cdot A\sin(\omega_d t)\right\} * L^{-1}\left\{G_{LPF}(s)\right\} \cong\cong \left[p_{N(LF)}(t) * L^{-1}\left\{G_{HPF}(s) \cdot G_{LPF}(s)\right\}\right] \cdot A\sin(\omega_d t) =$$

$$= \left[p_{N(LF)}(t) * L^{-1}\left\{G_{BPF}(s)\right\}\right] \cdot A\sin(\omega_d t) \cong p_{BPF(LF)}(t) \cdot A\sin(\omega_d t) \cong p_{3(LF)}(t)$$

- Thus, p_3 and $p_{3(eq)}$ signals, and, obviously, the next signals on the ESC loops have almost the same LF power spectrum:

$$p_{3(eq)(LF)}(t) \cong p_{3(LF)}(t) \Rightarrow i_{ref\,(eq)(LF)}(t) \cong i_{ref\,(LF)}(t)$$

Analysis of the ESC schemes on the frequency domain

- if only first harmonic of p_1 signal is considered, having the $P_{1(1)}$ magnitude, then the p_2 signal is:

$$p_2(t) = \left(P_{1(1)} \cdot \sin(\omega_d t)\right) \cdot \left(A \cdot \sin(\omega_d t)\right) = P_{1(1)} A \cdot \sin^2(\omega_d t) = P_{2(AV)} - P_{2(2)} \cos(2\omega_d t)$$

- Thus, the $p_{3(eq)}$ signal has the same average component and the second harmonic magnitude is mitigated by the LPF:

$$p_{3(eq)}(t) = \left[P_{2(AV)} - P_{2(2)} \cos(2\omega_d t)\right] * L^{-1}\left\{G_{LPF}(s)\right\} = P_{2(AV)} - G_{LPF(2)} P_{2(2)} \cos(2\omega_d t) = P_{3(AV)} - P_{3(2)} \cos(2\omega_d t + \phi_{LPF(2)})$$

- So, after the integration block, the $p_{3(eq)}$ signal will have an average component that is time dependent and of course the second harmonic, having the magnitude gained by k_1:

$$p_{4(eq)}(t) = \int p_{3(eq)}(t)dt = k_1 P_{3eq(AV)} t - (k_1 P_{3eq(2)} / 2) \sin(2\omega_d t + \phi_{LPF(2)}) =$$
$$= P_{1(1)} k_1 A t / 2 - P_{4eq(2)} \cos(2\omega_d t + \phi_{LPF(2)})$$

Analysis of the ESC schemes on the frequency domain

- Consequently, the time dependent component of the $i_{ref(eq)}$ signal is proportional with the ESC loop gain (k_1), the dither amplitude (A) and the magnitude of first harmonic of the ES power which is gained by $k_{aux} = (k_N \cdot k_T) / 2$.

$$i_{ref\,(eq)}(t) = k_{aux} P_{ES(1)} k_1 A t + i_{ref\,(LF)}(t) \Rightarrow G_{SS} = k_{aux} P_{ES(1)} k_1 A$$

- The LF components are obtained in same manner shown above. If only first three harmonics will be considered, then $i_{ref(LF)}$ signal could be represented for both MPP controllers' structures as:

$$i_{ref\,(LF)}(t) = \sum_{k=1}^{3} I_{ref\,(k)} \sin(k\omega_d t + \phi_k)$$

CONCLUSION

The advantages of proposed MPP tracking technique based on mES control are the following:

(1) a rate of search speed higher that classical ES control schemes,

(2) a search speed that could be set how high is required by choosing the k_1 ESC loop gain appropriately,

(3) an almost unitary value for the MPP tracking accuracy by choosing a smaller value for the k_2 dither gain, which will assures ;

(4) a negligible power ripple after the MPP is caught.

Part IV. Dither persistence on the ESC loop

- In this part, the dither persistence on the Extremum Seeking Control (ESC) loop is analyzed.
- The ESC scheme is usually used on Maximum Power Point (MPP) tracking controller to harvest the energy available from used renewable or green Energy Sources (ES). Two ESC schemes are analyzed in relation with dither persistence on output reference current:
  (1) the modified ESC scheme (named mESC scheme because is based on band-pass filter BPF use, instead of series connection of the high-pass and low-pass filters such as used in higher order ESC scheme);
  (2) its equivalent representation (named EQmESC because is based on modified higher order ESC scheme).
- The pass band (the cut-off frequency of low-pass filter) is chosen larger than in higher order ESC schemes in both ESC schemes proposed. Thus, dither persistence on the proposed ESC loop is improved. Consequently, the search speed of the extremum increases accordingly.
- These are shown by mathematical modeling and simulation.

Harmonics' persistence on the reference current

- If only first three harmonics will be considered, then $i_{ref(LF)}$ signal could be represented for both MPP controllers' structures as:

$$i_{ref\,(LF)} = \sum_{k=1}^{3} I_{ref\,(k)} \sin(k\omega_d t + \phi_k)$$

- The dither persistence on the ESC loop based on LF harmonics of the reference current will be analyzed using the following simplifying assumptions, without losing the generality of the problem:
  - ideal HP and LP filters;
  - unitary value for each of k_N and k_T gains;
  - initial value for the ϕ_k is set to zero;
  - $\omega_d >> \omega_{h(ES)}$, where $\omega_{h(ES)}$ is the cut-off frequency of the ES transfer function.

Harmonics' persistence on the reference current

- **The dither harmonics not interact with ES dynamic and ES power signal will result from superposition of the LF dither harmonics via the ES static characteristic.**
- **The time-dependent gradient component will assure the searching of the MPP. Usually, the ES static characteristic has a single MPP that dynamically moves in the P-I plane.**
- **Also, it is known that high power ES can be obtained by series/parallel connections of multiple ESs. In this case the ES static characteristic could have multiple MPPs and the global MPP is little bit more difficult to be caught and then to be tracked.**
- **The reference current, i_{ref}, which is used as probing signal to investigate the power response via the ES power characteristic, will be given by the following relationship:**

$$i_{ref}(t) = I_{ref} + i_{ref\,(LF)}(t) \cong I_{ref} + a_1 \cdot \sin(\omega_d t) + a_2 \cdot \sin(2\omega_d t) + a_3 \cdot \sin(3\omega_d t)$$

Harmonics' persistence on the reference current

- **The harmonics of the $i_{5(LF)}$ signal are:**

$$I_{5(1)} = \sqrt{b_1^2 + c_1^2},$$

$$I_{5(2)} = \sqrt{b_2^2 + c_2^2} = b_2,$$

$$I_{5(1)} = \sqrt{b_3^2 + c_3^2}$$

$$b_1 = k_1 \cdot \frac{1}{\omega_d} \cdot \left[\frac{\dot{p}_{ES} \cdot a_2}{2} + \frac{\dddot{p}_{ES} \cdot a_2^3}{16} \right],$$

$$c_1 = k_1 \cdot \frac{1}{\omega_d} \cdot \left[\frac{\ddot{p}_{ES} \cdot a_1^2}{8} \right],$$

$$b_2 = k_1 \cdot \frac{1}{2 \cdot \omega_d} \cdot \left[\frac{\dot{p}_{ES} \cdot (a_3 - a_1)}{2} + \frac{\dddot{p}_{ES} \cdot \left(3 \cdot a_3^3 - 4 \cdot a_1^3\right)}{48} \right],$$

$$c_2 = 0,$$

$$b_3 = k_1 \cdot \frac{1}{3 \cdot \omega_d} \cdot \frac{\left[8 \cdot \dot{p}_{ES} \cdot a_2 + \dddot{p}_{ES} \cdot a_2^3\right]}{16},$$

$$c_3 = k_1 \cdot \frac{1}{3 \cdot \omega_d} \cdot \left[\frac{\ddot{p}_{ES} \cdot \left(a_2^2 - a_1^2\right)}{8} \right]$$

- **The $i_{ref(eq)}$ signal has at least three harmonics beside the time-dependent gradient component and gained dither:**

$$i_{ref\,(eq)} = G_{SS(m)} \cdot t + \sum_{k=1}^{3} I_{5(k)} \cdot \sin(k\omega_d t + \phi_{5(k)}) + k_2 \cdot A \sin(\omega_d t)$$

Testing the dither persistence

- The dither persistence will be testing using a fuel cell (FC) stack as ES. A preset 6 kW / 45 V model from the SimPower® toolbox of the Matlab-Simulink®, version 2009b, is used. The FC stack has the parameters and characteristics shown in next figures. If the fuel flow rate is set to nominal value (50 lpm), then the P-I characteristic is shown in Figure 5.

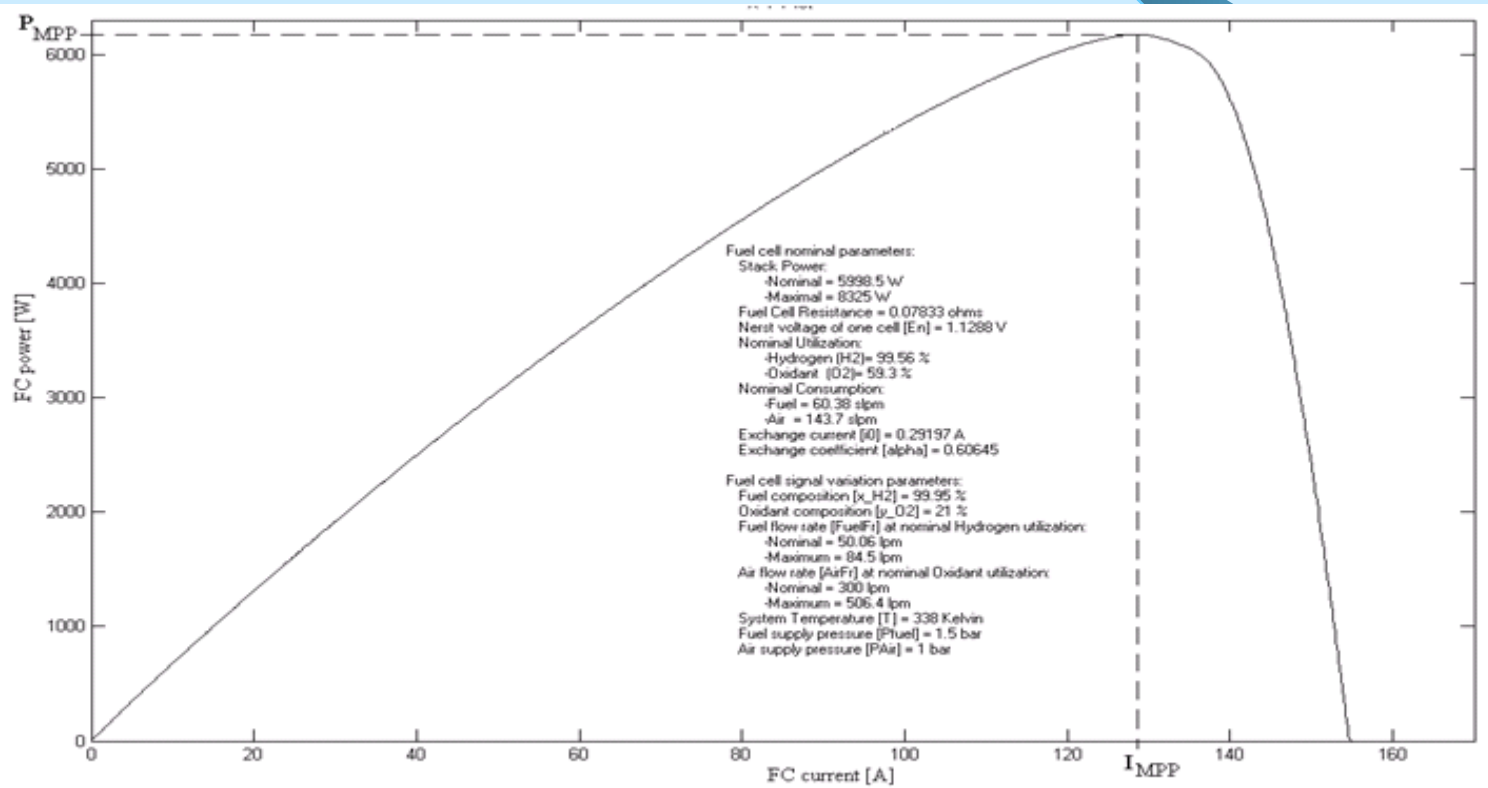

Figure 5 P-I characteristic of the FC stack on nominal fueling conditions

Testing the dither persistence

- The controlled current source is controlled by the reference current, i_{ref}, given by relationship (5), where a_1=0.3, a_2=0.2, a_3=0.1, and I_{ref} value is varied on the admissible range (up to I_{MPP}=133 A) using linear variable generator. The harmonics of the power response ($p_{fc}=v_{fv} \cdot i_{fc}$) and next signals on the signal processing ESC loop are computed and displayed.

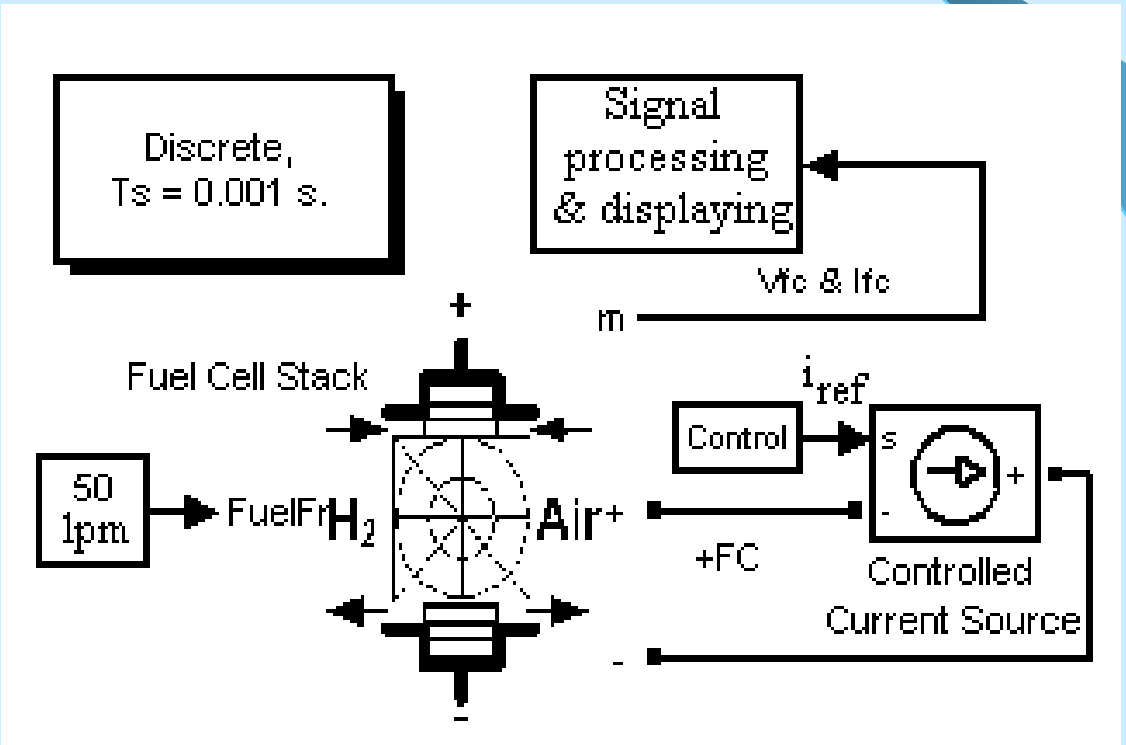

- Figure 6 Testing diagram using the reference current as load

Testing the dither persistence

- It is important to know if the harmonics of the $i_{5(LF)}$ signal have the same value as the $i_{5(LF)}$ harmonics computed based on signal processing related to ESC loop. So, the testing diagram that is shown in Figure 7 implements the above mentioned relationships. The reference current, I_{ref}, is varied on the admissible range (up to I_{MPP}=133 A) using a linear variable generator.
- The $i_{5(LF)}$ harmonics using the power derivatives computed for a given I_{ref} value.

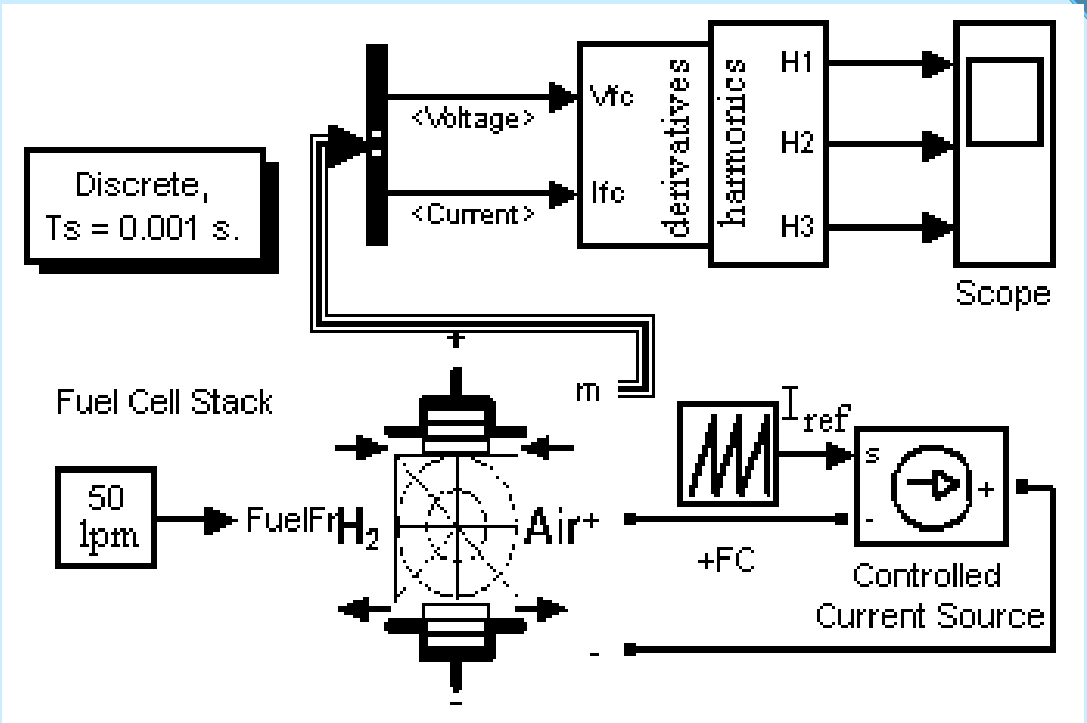

Figure 7 Testing diagram using the power derivatives to compute the signals' harmonics

RESULTS

- The FC characteristics using the testing diagram shown in Figure 7 (a linear variable generator for the i_{fc} current is used) are shown in Figure 8. First derivatives of the p_{fc} signal are shown in Figure 9 using a signal processing block to compute these derivatives.

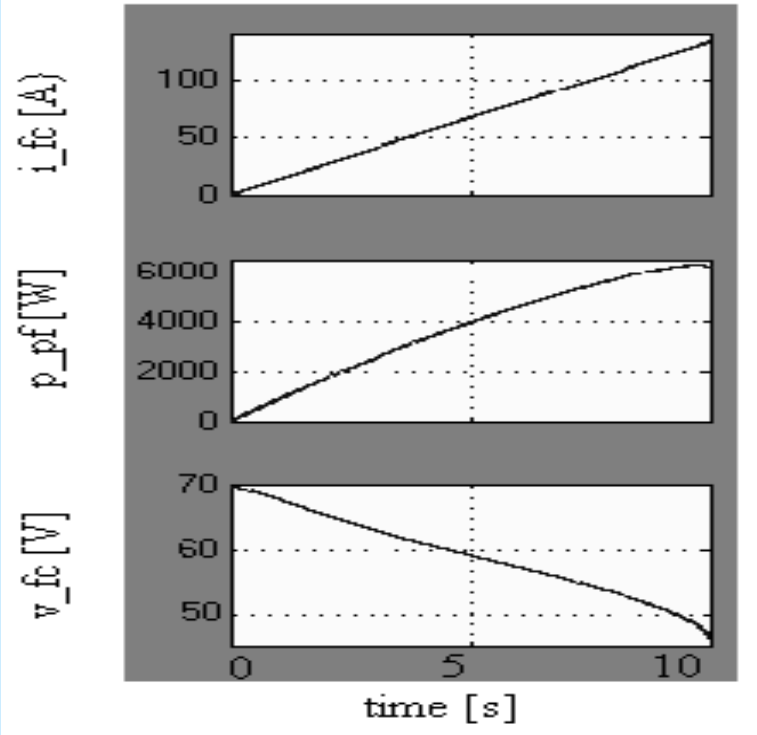

Figure 8 FC characteristics using a linear variable generator as load

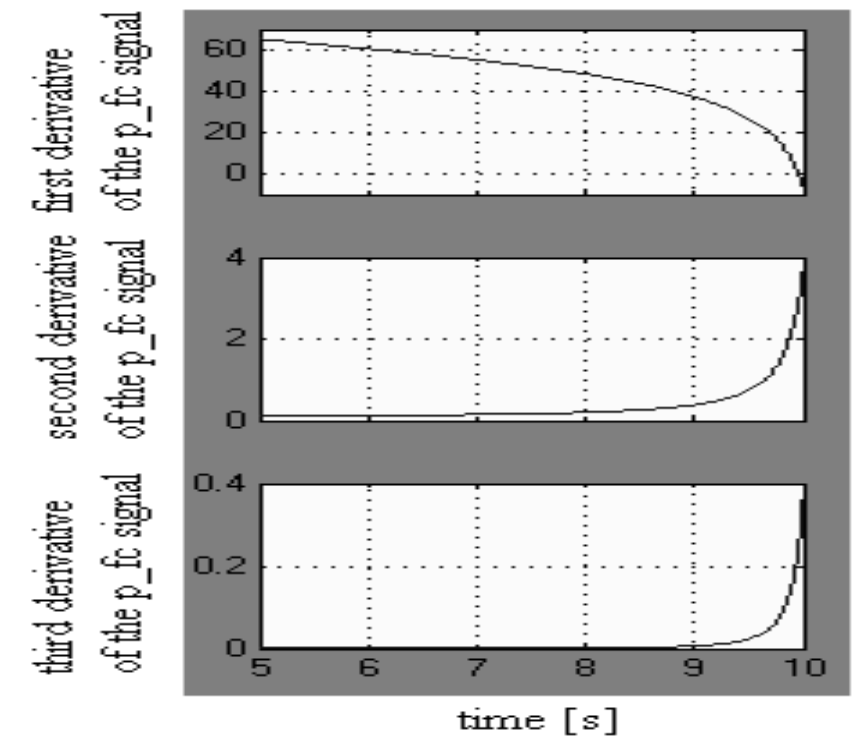

Figure 9 Derivatives of the p_fc signal

RESULTS

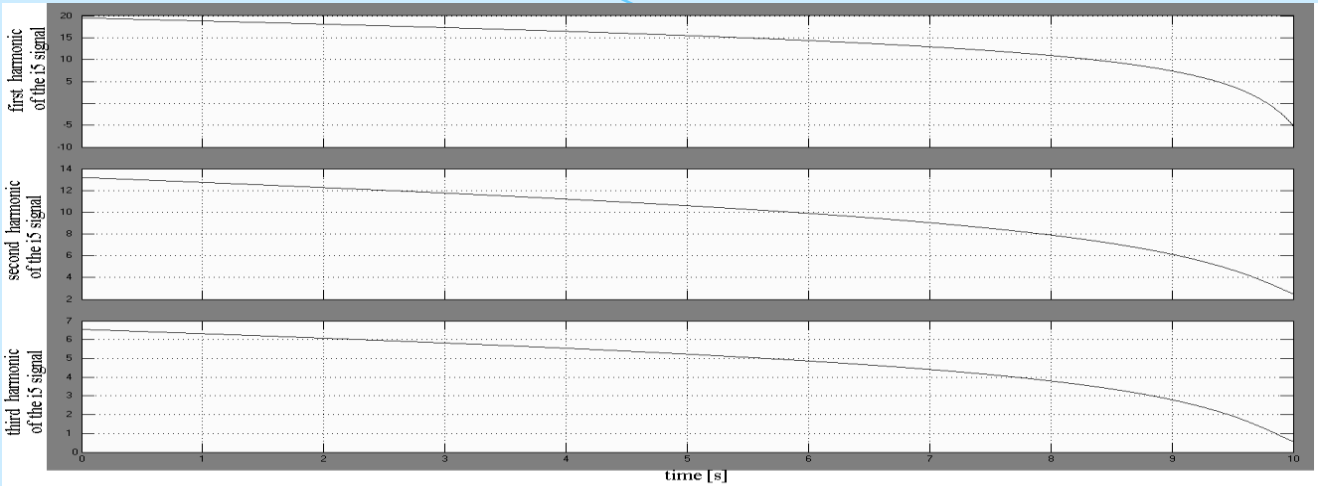

- Figure 10 Harmonics of the i5 signal computed based on the power derivatives

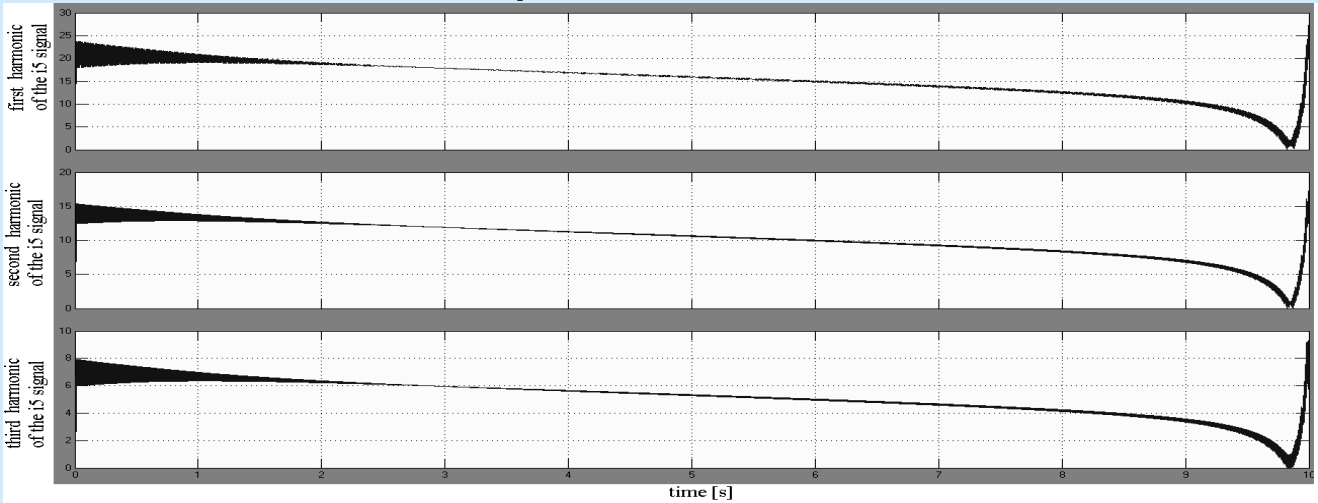

- Figure 11 Harmonics of the i5 signal computed based on the signal processing in the ESC loop

CONCLUSION

In this presentation, an approximation for the harmonics' magnitudes of the reference current is obtained based on first components of the Taylor series of the p_{ES} power response.

The relationships between the harmonics' magnitudes of the reference current and the derivatives of the p_{ES} power response are validated by simulation.

Besides the above mentioned computation, the harmonics' magnitudes of the reference current are computed based on signal processing related to the ESC loop.

The harmonics of the $i_{5(LF)}$ signal can be approximated during the searching and tracking phase considering the derivatives of the p_{ES} power response shown in Figure 9.

It is easy to shown that during of searching and tracking phase the magnitude of the first, second and third harmonics of the reference current is mainly proportional with the absolute value of the first and third derivatives, and with the second derivative of the ES power signal, respectively.

The searching speed is proportional with a linear combination of the first and third derivatives of the p_{ES} power response, besides the ESC loop gain (k_1) and the dither amplitude (A).

Consequently, the searching speed and dither persistence is dependent to the pass band set for the BPF (set values for the cut-off frequencies related to dither frequency).

Part V. Global Maximum Power Point Tracking algorithms for Photovoltaic arrays under Partially Shaded Conditions

1. Global Maximum Power Point Tracking (GMPPT) algorithms - a brief review
2. The performance of the GMPP algorithms based on the Extremum Seeking Control (ESC) schemes

- **The main objective of these presentations is to present an Introduction in the Global Maximum Power Point (GMPP) algorithms applied on power generated by the Photovoltaic (PV) arrays.**
- **Besides this survey on the GMPP algorithms proposed in last decade, the Perturbed-based Extremum Seeking Control (PESC) methods and their applications in PV arrays under Partially Shaded Conditions (PSCs) are investigated as well.**
- **The PESC schemes proposed to seek and track the GMPP of the PV power will be analyzed as performance obtained for the following indicators:**
- **the searching resolution,**
- **tracking accuracy,**
- **tracking efficiency,**
- **tracking speed,**
- **and percent of the hit count.**

Global Maximum Power Point Tracking algorithms

The searching resolution (R_S) is defined by:

$$R_S = \frac{\min_i \left| y_{GMPP} - y_{LMPPi} \right|}{y_{GMPP}} \cdot 100[\%]$$

The tracking accuracy (T_{acc}) is defined by:

$$T_{acc} = \frac{y_{PV}}{y_{GMPP}} \cdot 100[\%]$$

where y_{PV} is the PV power that is theoretically available and y_{GMPP} is the power extracted by the GMPP algorithm.

The number of iterations to locate the GMPP is a measure of the tracking speed. An iteration for the PESC-based GMPPT algorithms means a dither period (which is a step of scanning). Iteration can be defined for all GMPPT algorithms and it refers to the number of times the specific function of the algorithm is calculated, and this is related only to the method

Global Maximum Power Point Tracking algorithms

The tracking efficiency (T_{eff}) is given by:

$$T_{eff} = \frac{\int_0^t y_{PV}\,dt}{\int_0^t y_{GMPP}\,dt} \cdot 100[\%]$$

The percent of the hit count (PHC) is defined by:

$$PHC = \frac{\text{number of positive results in finding the GMPP}}{\text{number of tests performed}} \cdot 100[\%]$$

The results obtained will be shown and commented as well. The performance of the PESC-based GMPPT algorithms will be compared with that of other GMPP algorithms proposed in the literature. Different PV and nonlinear multimodal patterns will be used to test the PESC-based GMPPT schemes. The results obtained under different PSCs simulated have shown a very good performance related to search speed and tracking accuracy of the PESC-based GMPPT algorithms.

- **The first Asymptotic Perturbed Extremum Seeking Control (aPESC) scheme was proposed in [41] for GMPP search based on Scalar PESC (PESCs) scheme [42]. The PESCs scheme and its Asymptotic variant (aPESCs) are shown in Figure 1 for switch in position (1) and (2).**

- [41] Tan Y, Nešic D, Mareels I, Astolfi A. On global extremum seeking in the presence of local extrema. Automatica 2009;45(1):245–51.

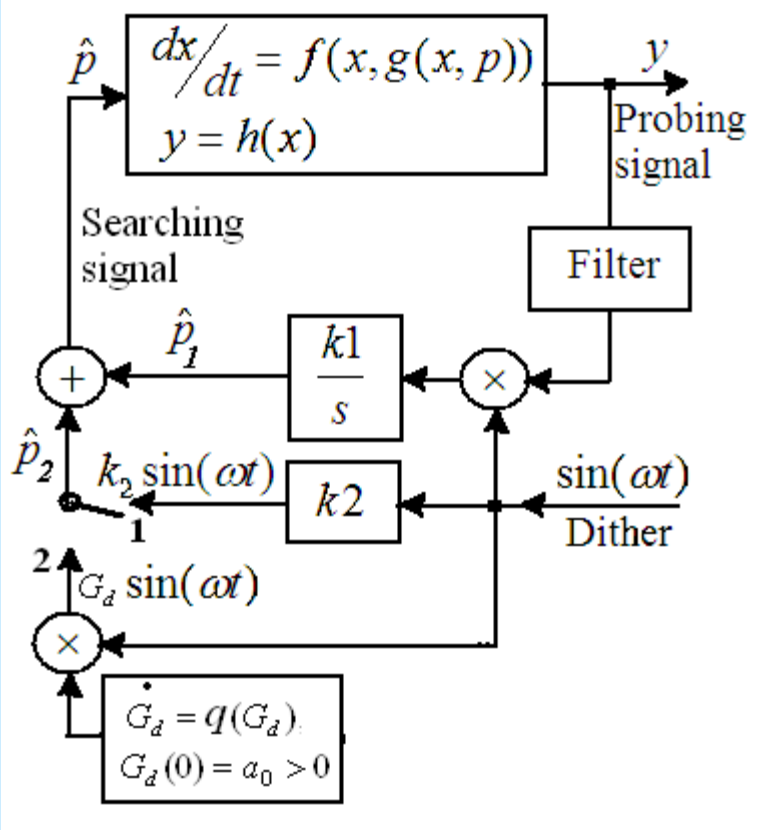

Figure 1. The scalar PESC (PESCs) scheme and its asymptotic variant (aPESCs)

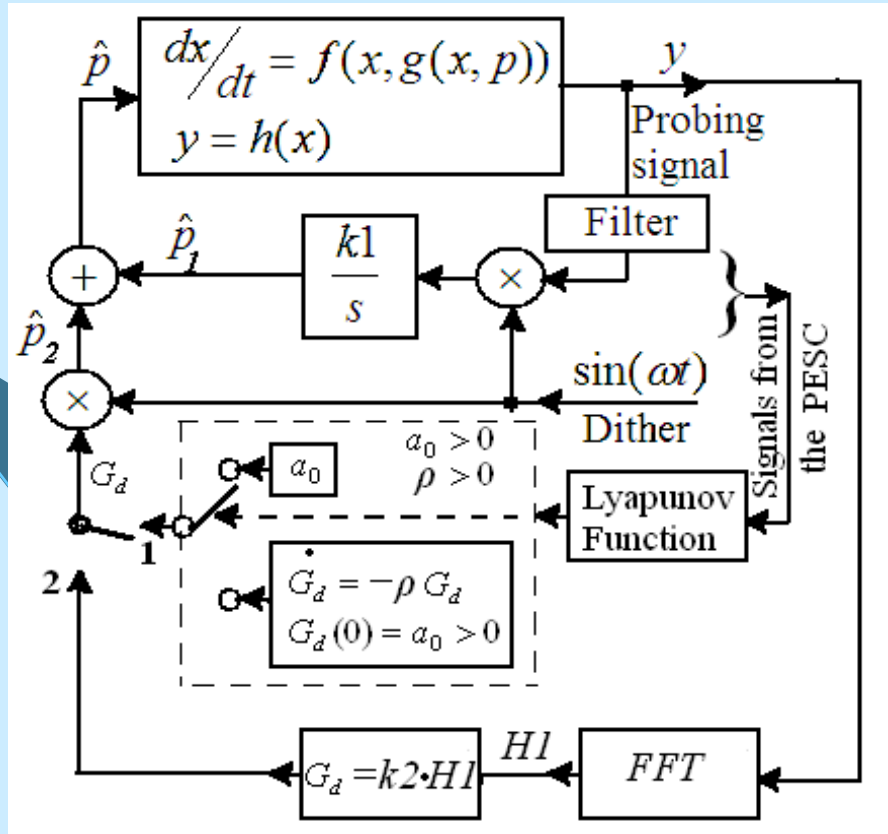

Figure 2. The aPESC schemes based on (1) the Lyapunov function (aPESCLy) and (2) the H1 harmonic (aPESCH1)

- **The tracking loop is the same for all aPESC schemes proposed in the literature and contains the following signal processing blocks of the process output ($y=y_{CC}+y_{AC}$): the filtering (of the CC value, y_{CC}), demodulation (product of the AC value, y_{AC}, with the dither signal), integration (of the demodulated signal), and amplification (with k_1). The filter can be of High-Pass Filter (HPF) type or Band-Pass Filter (BPF) type [34]. The average value of the gradient for the tracking signal is given by:**

$$\frac{d\overline{p}_1}{dt} = \frac{A^2 \cdot k_1}{2} \cdot \frac{dy}{dx} \overset{A=1}{\Rightarrow} \frac{d\overline{p}_1}{dt} = \frac{k_1}{2} \cdot \frac{dy}{dx}$$

- **The sweeping signal (p2) can have different expressions depending on the asymptotic function chosen to modulate the dither:**
- **- The asymptotic function is based on an exponential implementation [41];**
- **- The asymptotic function is obtained through commutation between constant and exponential amplitude of dither based on the Lyapunov switching function [44];**
- **- The asymptotic function is based on the magnitude of first harmonic (H1) of the process output, which is obtained with Fast Fourier Transform (FFT)**

- **[44] Moura SJ, Chang YA. Lyapunov-based switched extremum seeking for photovoltaic power maximization. Control Eng Pract 2013;21(7):971–80.**

The H1 magnitude of the process output can be approximated by a using a BPF2 centered on the first harmonic, a derivative operator, or the BPF1 (see Figure 3). Thus the following variants of the aPESCH1 scheme can be obtained in order to be tested for GMPP search:

- **(1) the GaPESC scheme based on the BPF1,**
- **(2) the GaPESCbpf scheme based on the BPF2,**
- **(3) the GaPESCH1 scheme based on the H1 magnitude computed with the FFT, and**
- **(4) the GaPESCd scheme based on the derivative operator.**

- **If the BPF2 is designed to approximate the H1 magnitude, then the behavior of both GaPESCbpf and GaPESCH1 schemes are almost the same. So, only GaPESCH1 scheme will be considered below.**

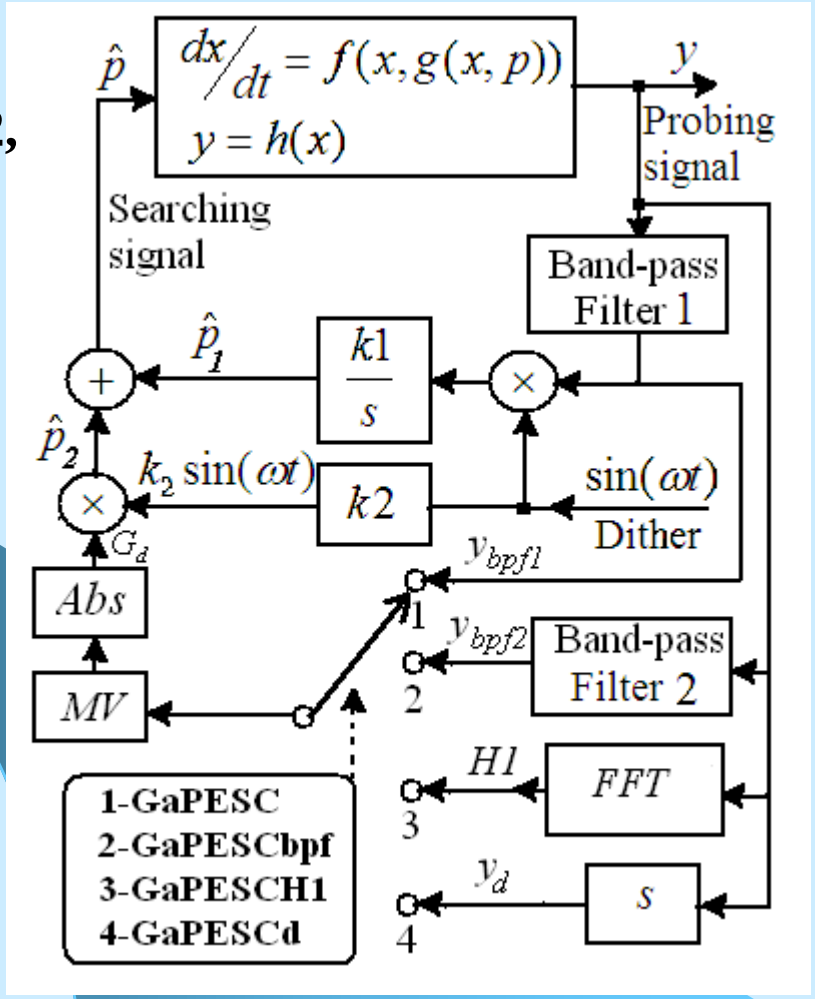

Figure 3. The aPESC schemes

Figure 4. The diagram of the GaPESC scheme

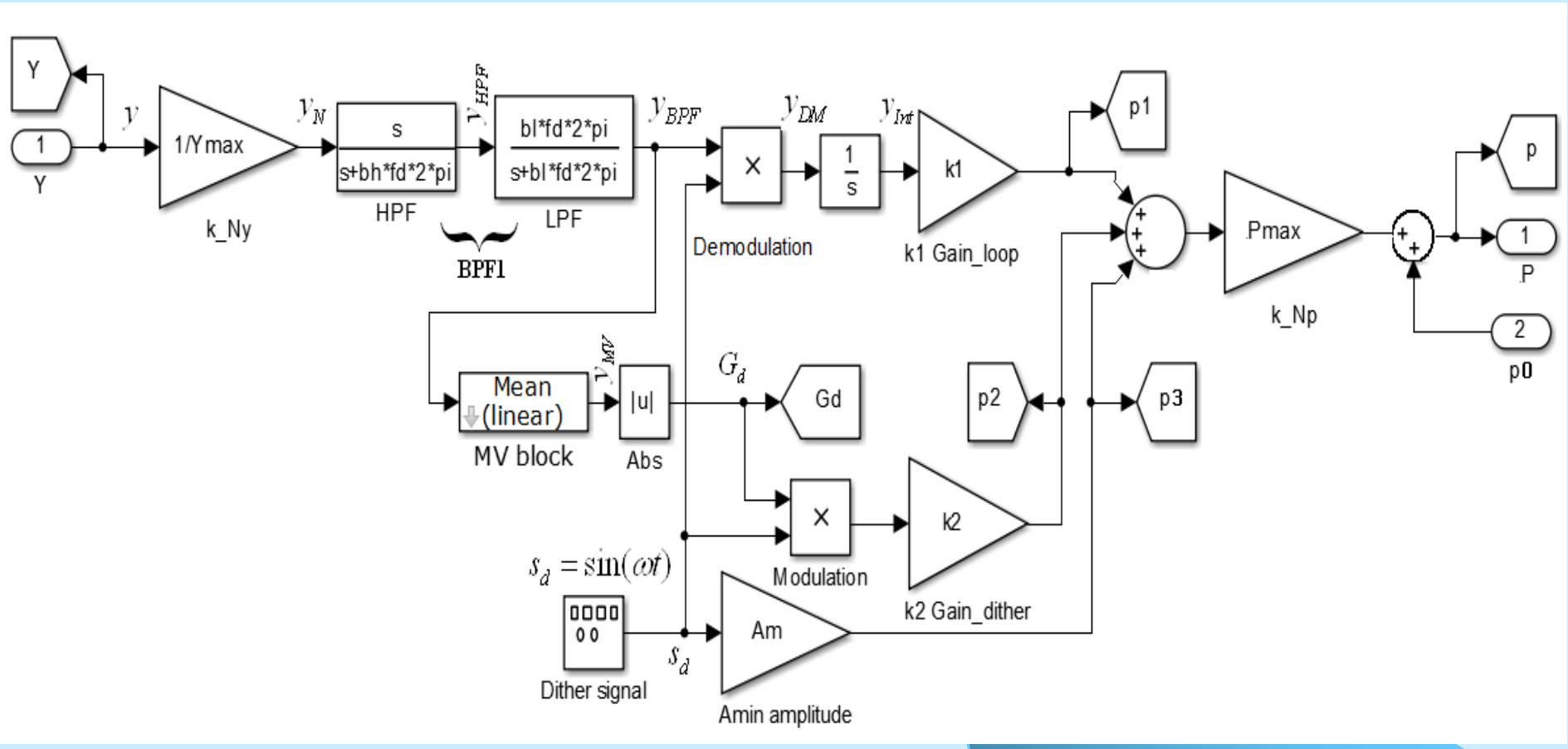

The parameters used in simulation are the following:

- the dither frequency is $f_d=1/T_d=\omega/2\pi=100$ Hz;
- the dither amplitude is set to 1;
- the cut-off frequency of the HPF1, $f_{h1}=\beta_{h1}\cdot f_d$, where $\beta_{h1}=0.1$;
- the cut-off frequency of the LPF1, $f_{l1}=\beta_{l1}\cdot f_d$, where $\beta_{l1}=1.9$ in order to approximate the H1 amplitude [40];
- the cut-off frequency of the HPF2, $f_{h2}=\beta_{h2}\cdot f_d$, where $\beta_{h2}=0.5$;
- the cut-off frequency of the LPF2, $f_{l2}=\beta_{l2}\cdot f_d$, where $\beta_{l2}=5.5$ in order to increase the dither persistence on the control loop [46];
- the minimum amplitude of dither, A_m, is set to 0.001, but can be smaller that this value in order to obtain a very low ripple on the probing signal during the stationary phases;
- the normalization gains, $k_{Ny}\cong 1/y_N$ and $k_{Np}\cong p_N$, where the p_N value sets the initial amplitude of the dither and the y_N value is chosen in the range of maximum and maximum values estimated for the GMPP on the nonlinear map, $y=h(p)$; $k_{Ny}=k_{Np}=1$ for the nonlinear map (6); note that '$\cong$' means in a large range around the mentioned value;
- the gain of the dither amplitude, $k_2\cong\Delta p$, where $\Delta p=|p_{GMPP}-p_0|$, and p_0 is the initial value for starting the search of the p_{GMPP}; $k_2=3$ for the nonlinear map (6);
- the loop gain, $k_1=\gamma_{sd}\cdot\omega$, where $\gamma_{sd}=1.5$ was set based on the dynamic performance analysis shown below.

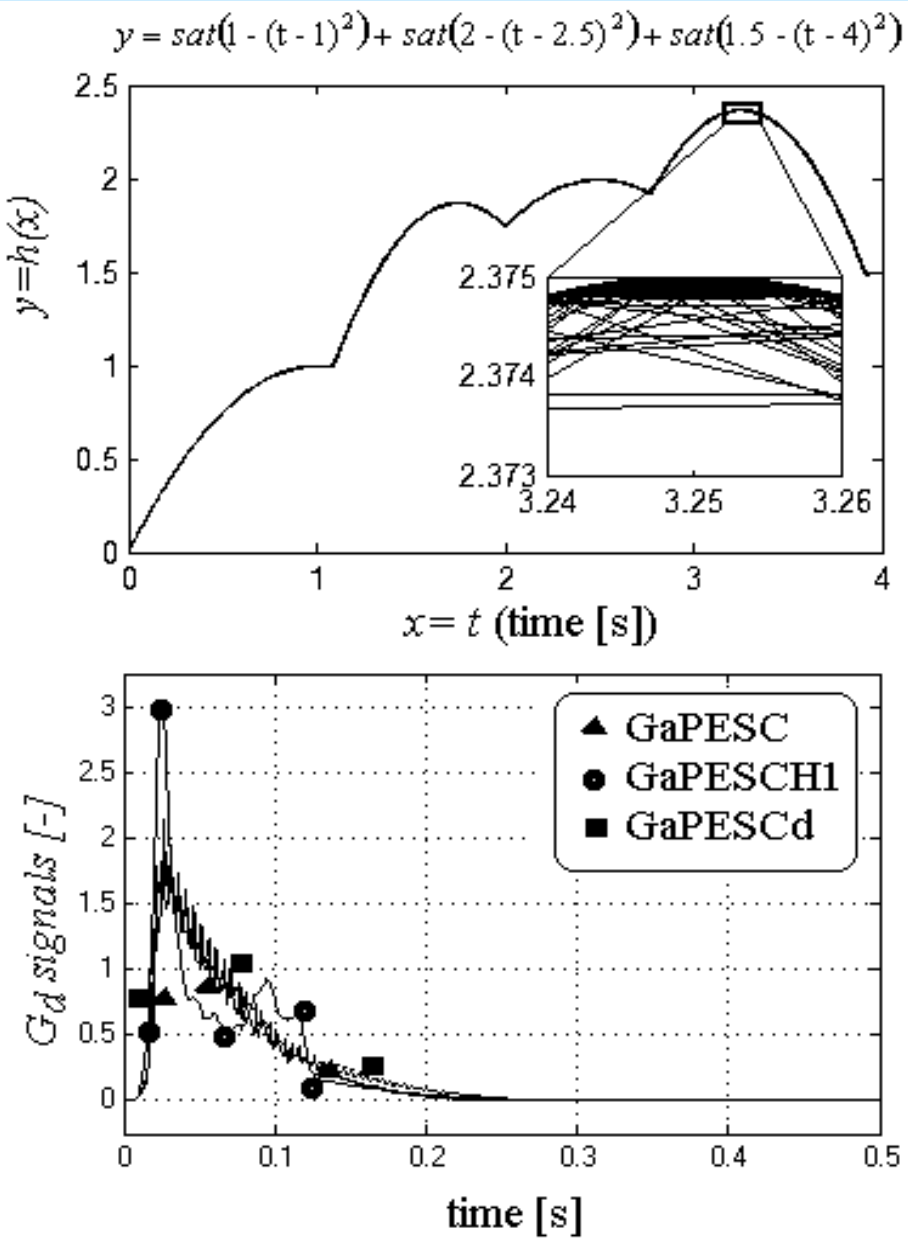

Figure 5. The G_d signals during the GMPP search based on the GaPESC scheme

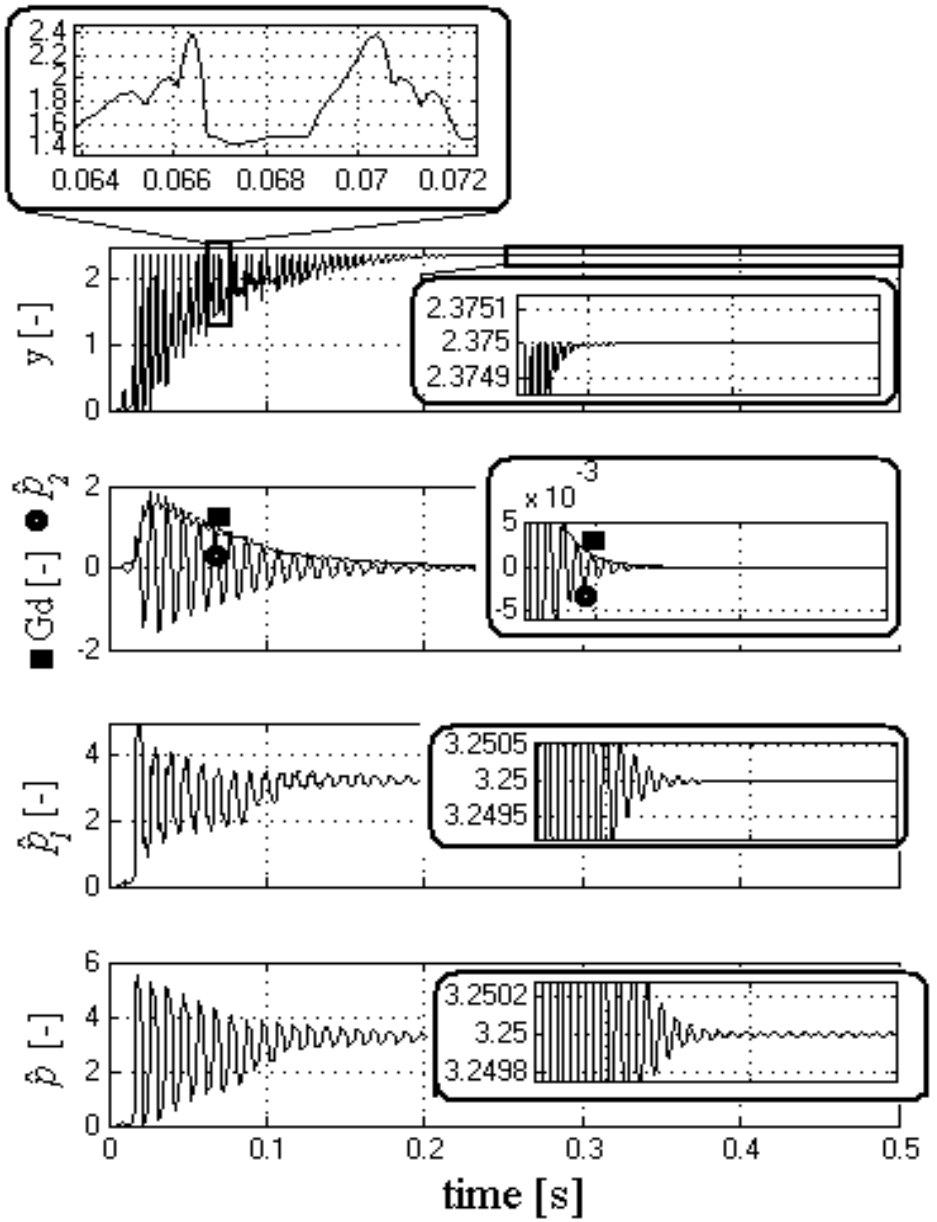

Figure 6. The GMPP search based on the GaPESC scheme

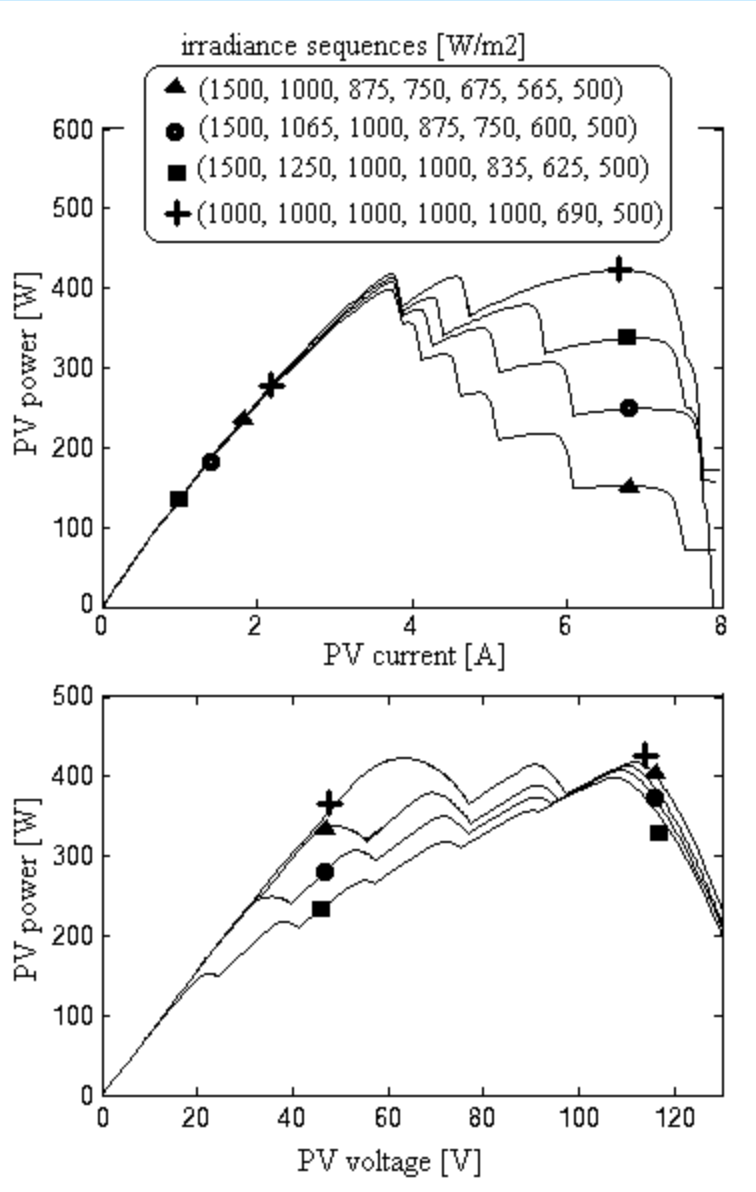

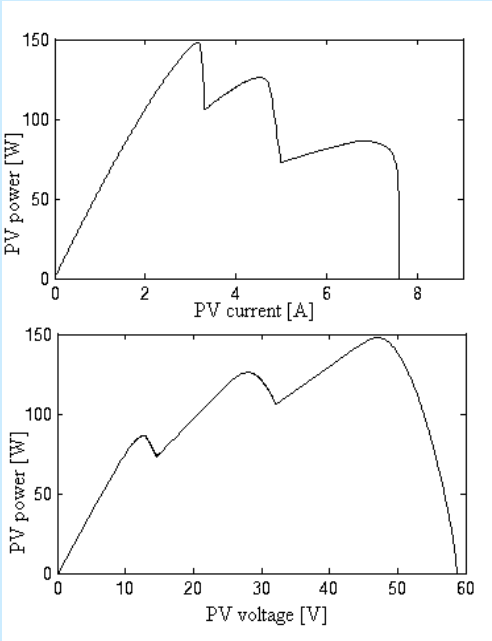

- **PV characteristics for the 1Px3S PV array**

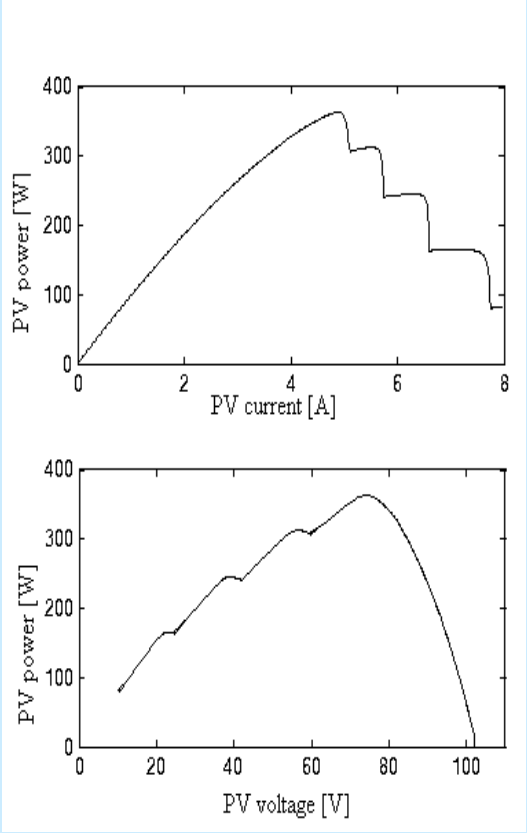

- **PV characteristics for the 1Px5S PV array**

Figure 8. The PV characteristics for the 1Px7S PV array under different irradiance sequences

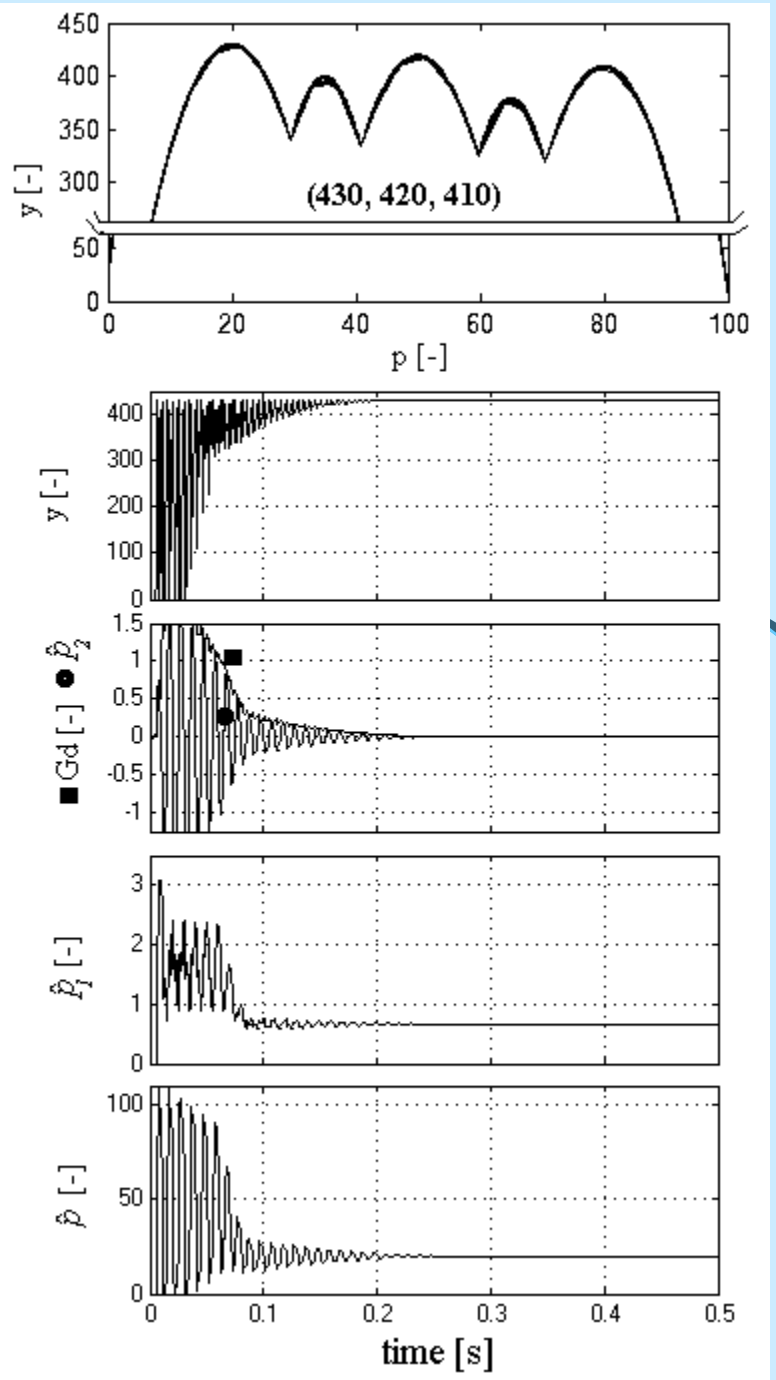

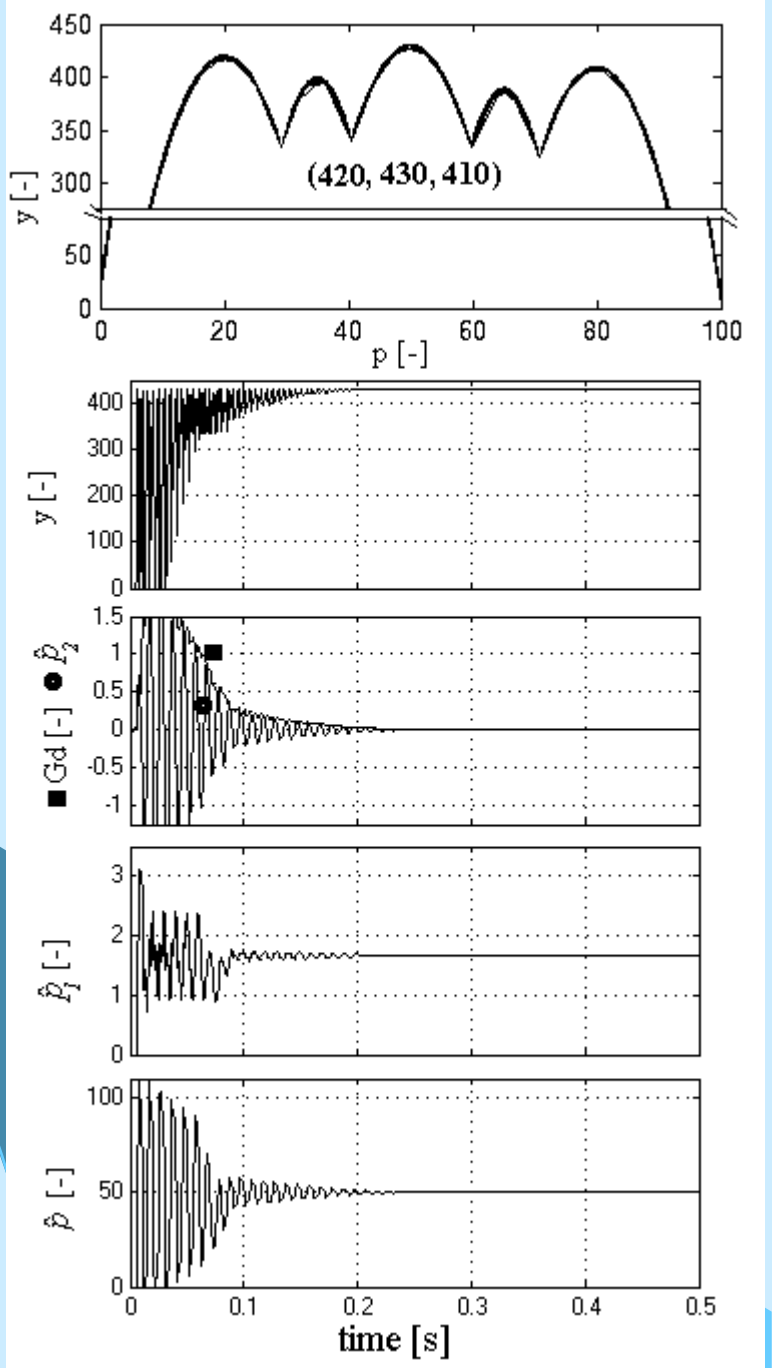

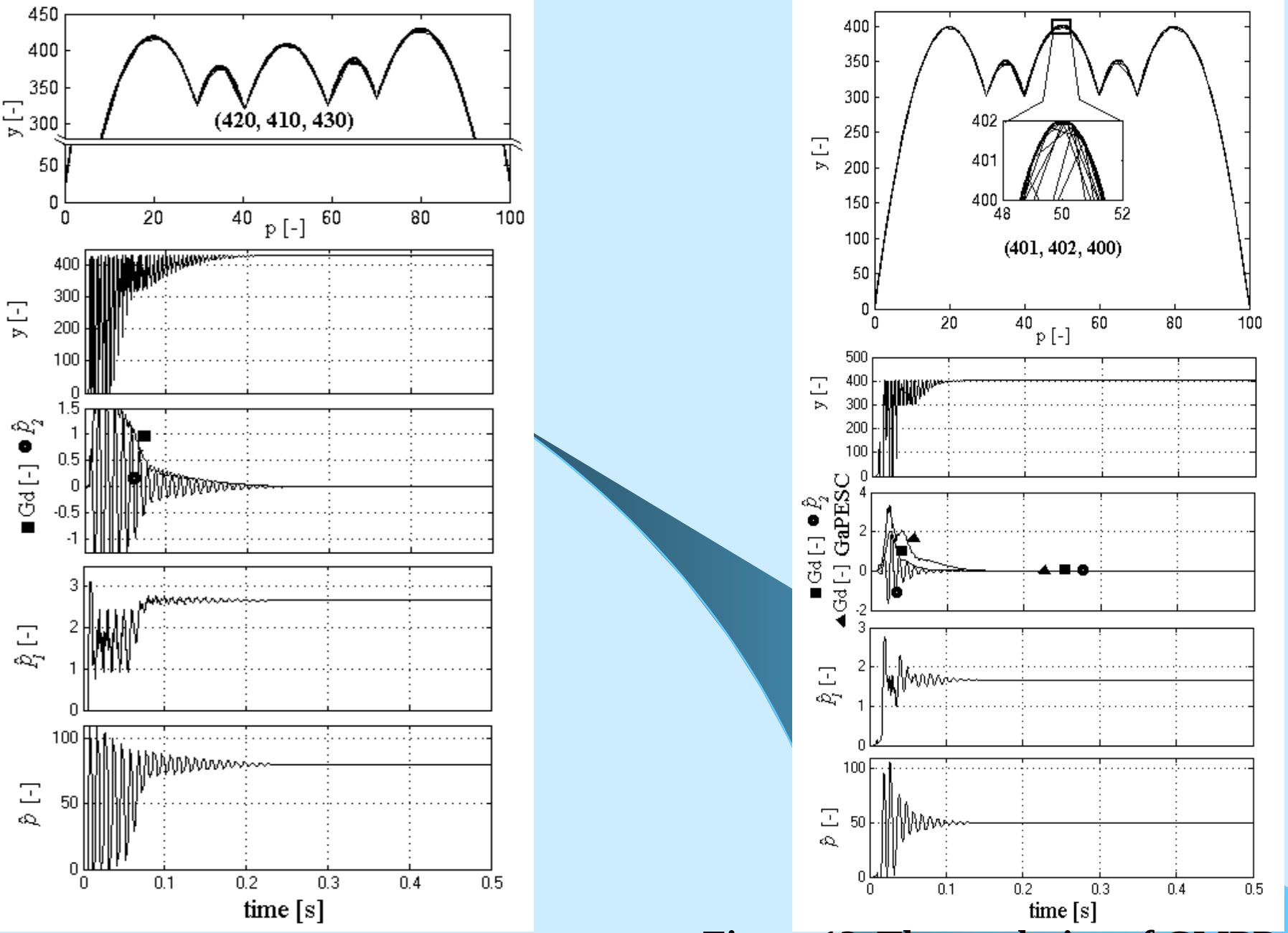

Figure 12. The resolution of GMPP searching for the GaPESCH1 scheme

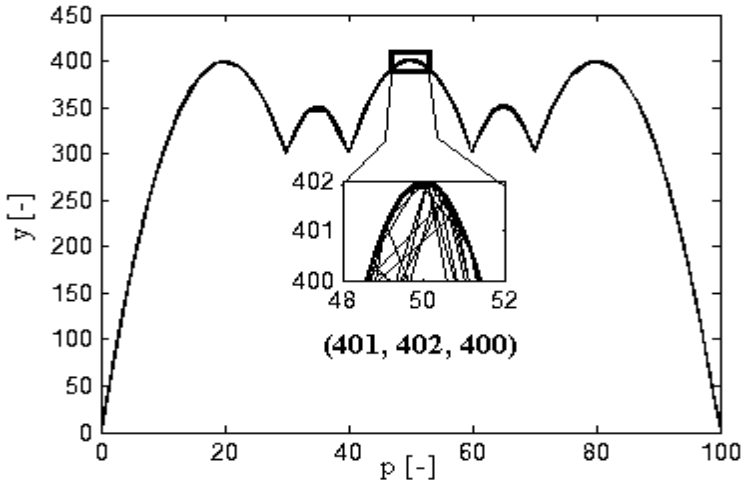

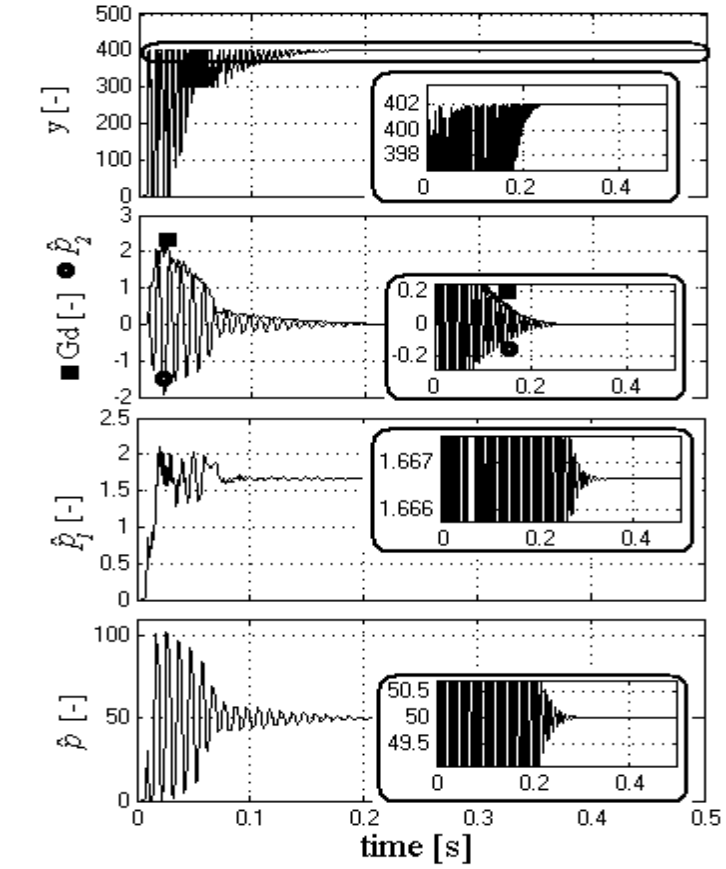

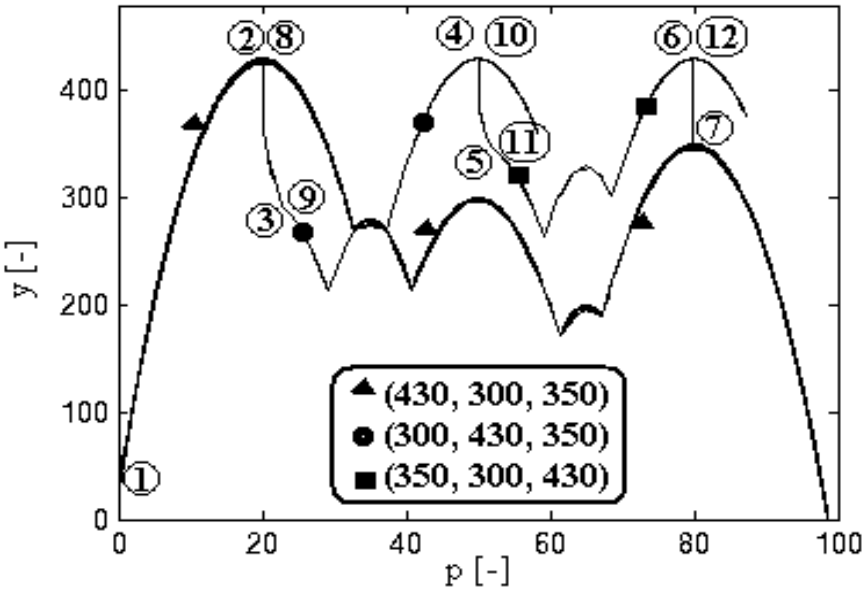

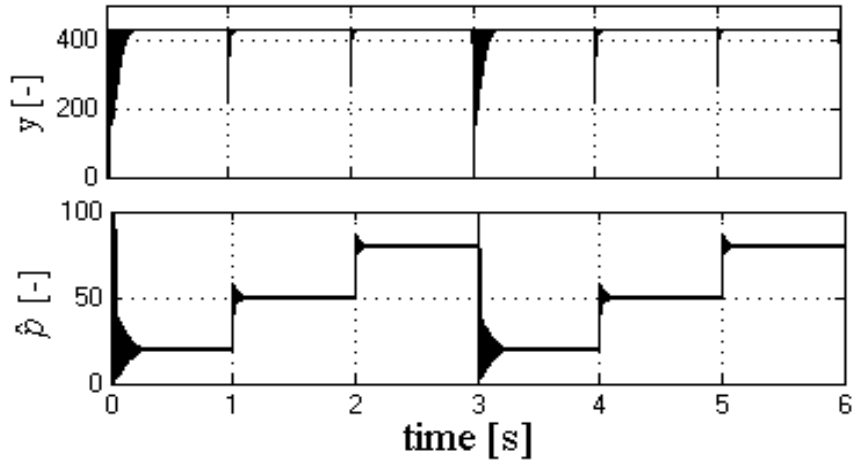

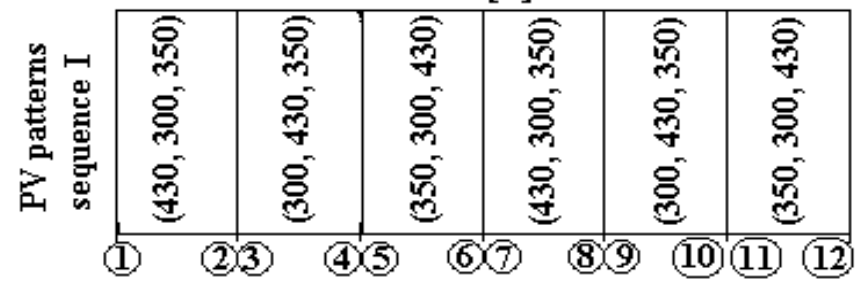

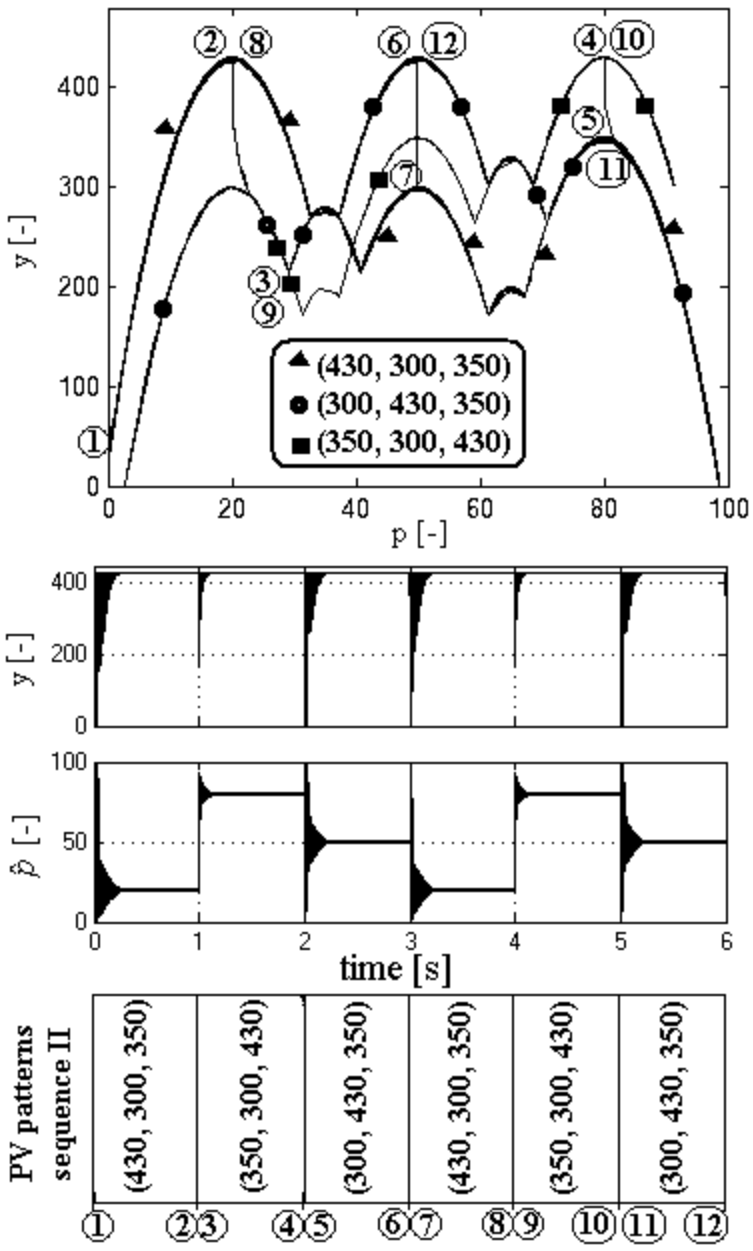

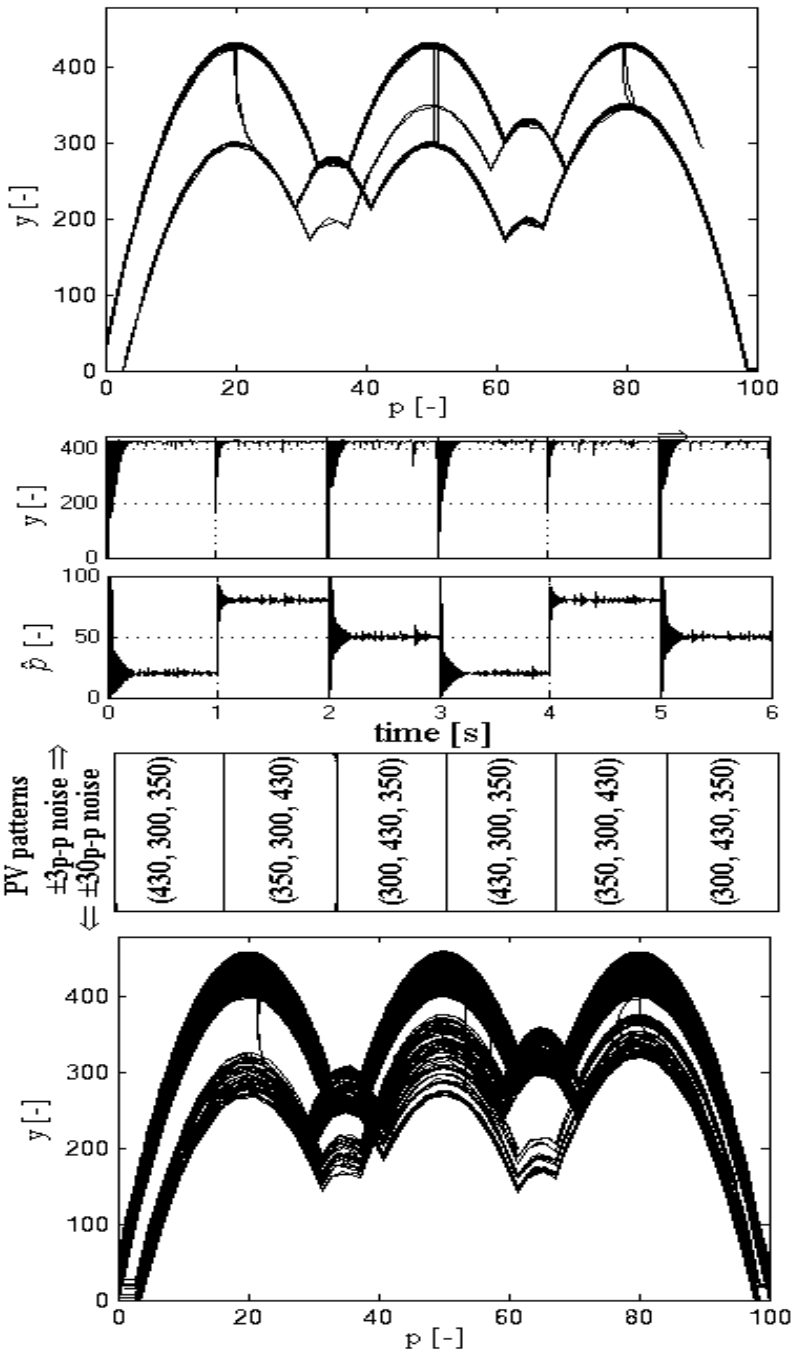

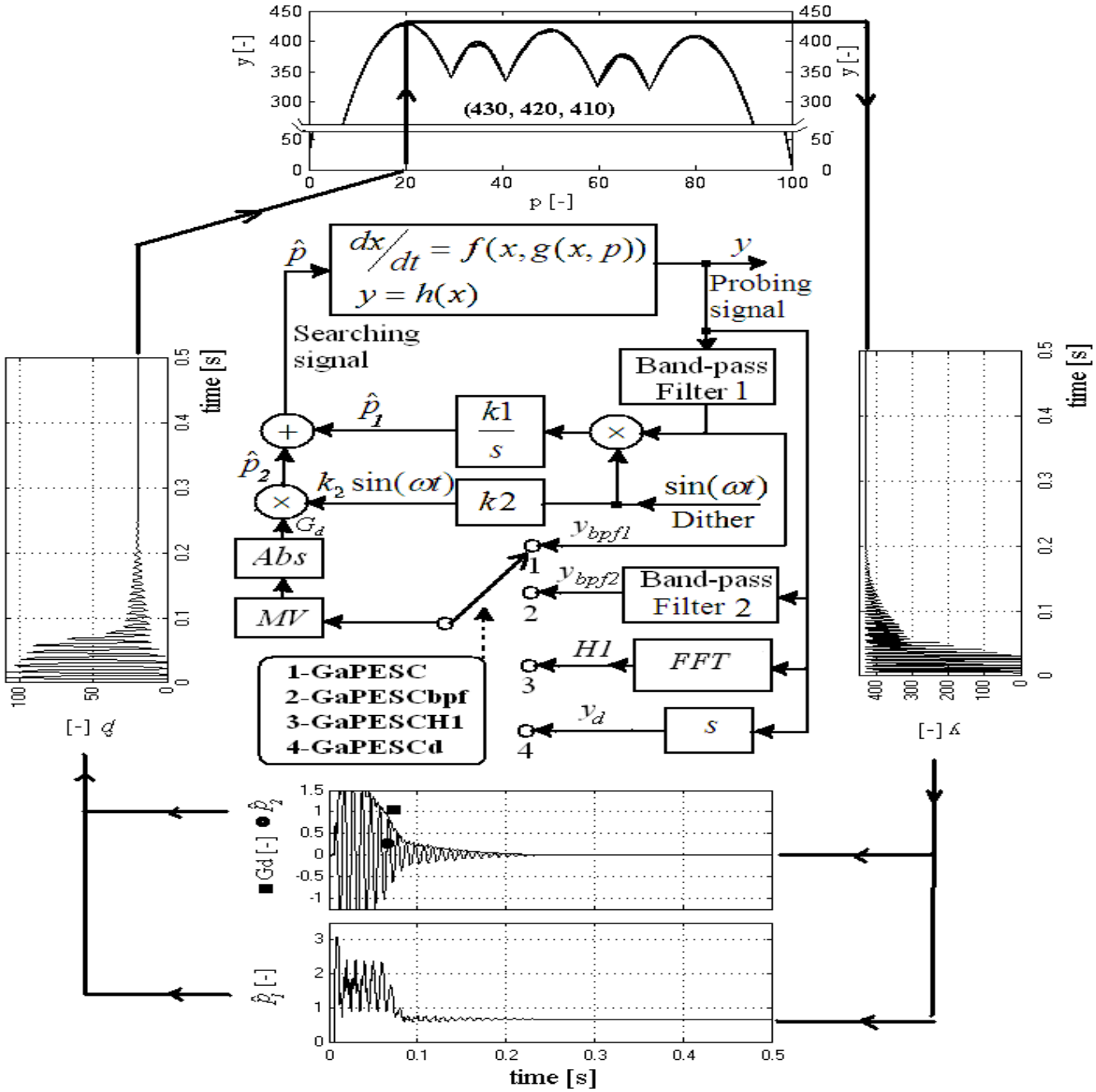

Conclusions

- The maximum, minimum and average value of the tracking accuracy reported for GaPESC scheme is of 99.99%, 99.95% and 99.97%
- The tracking efficiency of 99.97%
- The resolution of all schemes is lower than 0.25% (≅1/402).
- The robustness of the GMPP searching was tested for two PV patterns' sequences
- Each time the GMPP of the PV pattern from the noiselessly sequence was accurately tracked.
- The level of GMPP of the PV pattern from the noisy sequence is changed randomly at each 10 milliseconds. Therefore, the GaPESC scheme searches continuously the current GMPP.
- Based on the performance shown and its simplicity of implementation, the GaPESC scheme is competitive with similar techniques to scan the GMPP or other advanced GMPP algorithms proposed.
- Furthermore, the tuning ranges for the design parameters are relatively large because the GaPESC scheme is based on adaptive control of ESC type.

This presentation is mainly based on following copyrighted materials:

- **N. Bizon (Ed.), *Distributed Generation systems integrating Renewable Energy Resources*, 3 chapters written by N. Bizon, Nova Science Publishers Inc., USA, 2012, 978-1-61209-991-0 (hardcover), 978-1-61209-991-2 (ebook).**
- **N. Bizon, *Intelligent control of the Energy Generation System*, book chapter in: K. Metaxiotis (Ed.), Intelligent Information Systems and Knowledge Management for Energy: Applications for Decision Support, Usage and Environmental Protection, IGI Global, USA, 2009, chapter 2, pp. 40 - 96, ISBN 978-1-60566-737-9 (hardcover), ISBN 978-1-60566-738-6 (ebook).**
- **N. Bizon, Nonlinear control of fuel cell hybrid power sources: Part II –Current control, Applied Energy 88(7) (2011) 2574–2591, http://dx.doi.org/10.1016/j.apenergy.2011.01.044**
- **N. Bizon, Nonlinear control of fuel cell hybrid power sources: Part I –Voltage control, Applied Energy 88(7) (2011) 2559–2573, http://dx.doi.org/10.1016/j.apenergy.2011.01.030**
- **N. Bizon, A new Topology of Fuel Cell Hybrid Power Source for Efficient Operation and High Reliability, Journal of Power Sources 196(6) (2011) 3260–3270, http://dx.doi.org/10.1016/j.jpowsour.2010.11.049**

This presentation is mainly based on following copyrighted materials (continued):

- **N. Bizon, N. M. Tabatabaei and Hossein Shayeghi (Ed.), Analysis, Control and Optimal Operations in Hybrid Power Systems - Advanced Techniques and Applications for Linear and Nonlinear Systems, Springer Verlag London Limited, London, UK, 2013. 978-1-4471-5538-6, 978-1-4471-5537-9.**

http://dx.doi.org/10.1007/978-1-4471-5538-6,
http://www.springer.com/engineering/control/book/978-1-4471-5537-9

- **N. Bizon and N. M. Tabatabaei (Ed.), Advances in Energy Research: Energy and Power Engineering, Nova Science Publishers Inc., USA, 2013 978-1-62257-534-3 (hardcover), 978-1-62257-546-6 (ebook).**

https://www.novapublishers.com/catalog/product_info.php?products_id=36315&osCsid=cce0dd5ced12df6ba9340d8c9d71142b

- **N. Bizon (Ed.), Advances in Energy Research: Distributed Generation systems integrating Renewable Energy Resources, 3 chapters by N. Bizon, Nova Science Publishers Inc., USA, 2012, 978-1-61209-991-0 (hardcover), 978-1-61209-991-2 (ebook). 692 pp**
- **N. Bizon, Global Maximum Power Point Tracking (GMPPT) of Photovoltaic array using the Extremum Seeking Control (ESC): A review and a new GMPPT ESC scheme, Renewable & Sustainable Energy Reviews 57 (may 2016), 524–539, 10.1016/j.rser.2015.12.221**

http://www.sciencedirect.com/science/article/pii/S1364032115016044

- **N. Bizon, Global Extremum Seeking Control of the Power Generated by a Photovoltaic Array under Partially Shaded Conditions, Energy Conversion and Management, 10.1016/j.enconman.2015.11.046**

http://www.sciencedirect.com/science/article/pii/S0196890415010663

ACKNOWLEDGMENT
The support from the Ministry of EU Affairs Turkish National Agency under the Project Code: 2015-1-TR01-KA203-021342 is acknowledged.

Thank!
Questions?

- Nicu Bizon
- University of Pitesti,
- 1 Targu din Vale, Arges, 110040 Pitesti, Romania
- nicubizon@yahoo.com; nicu.bizon@upit.ro;
- http://www.upit.ro/index.php?page=nicu-bizon-personal-fecc
- https://www.researchgate.net/profile/Nicu_Bizon